UNIVERSITY
OF TASMANIA

Carbonaceous Nanoparticles and Carbon on Carbon Composite Materials: Preparation, Properties and Application in Adsorption

By Emer Duffy
B.Sc. (Hons), B.S.
School of Physical Sciences

Submitted in fulfillment of the requirements for the degree Doctor of Philosophy
University of Tasmania, August 2015

Declaration

This thesis contains no material which has been accepted for a degree or diploma by the University or any other institution, except by way of background information and duly acknowledged in the thesis, and to the best of my knowledge and belief no material previously published or written by another person except where due acknowledgement is made in the text of the thesis, nor does the thesis contain any material that infringes copyright.

The publishers of the papers comprising Chapters 2 to 5 hold the copyright for that content, and access to the material should be sought from the respective journals. The remaining non-published content of the thesis may be made available for loan and limited copying and communication in accordance with the Copyright Act 1968.

Emer Duffy

Statement of Co-Authorship

The following people and institutions contributed to the publication of the work undertaken as part of this thesis:

Paper 1 *Candidate (60%), Dimitar Mitev (5%), Pavel Nesterenko (15%), Artaches Kazarian (5%), Brett Paull (15%).*

Paper 2 *Candidate (40%), Dimitar Mitev (20%), Ashley Townsend (5%), Brett Paull (15%), Pavel Nesterenko (15%).*

Paper 3 *Candidate (60%), Xiaoyun He, Ekaterina Nesterenko, Dermot Brabazon, Avishek Dey, Satheesh Krishnamurthy (10%) Pavel Nesterenko (15%), Brett Paull (15 %).*

Paper 4 *Candidate (65%), Xiaoyun He (5%), Pavel Nesterenko (15%), Brett Paull (15%).*

Details of the author roles:

All authors contributed to experiment design, concepts, and final corrections.

We the undersigned agree with the above stated "proportion of work undertaken" for each of the above published (or submitted) peer-reviewed manuscripts contributing to this thesis:

Signed:

Date: 2/Sept/15 2 Sep 15

Prof. Brett Paull,	*Prof. John Dickey*
Supervisor,	*Head of School,*
School of Physical Sciences	*School of Physical Sciences*
University of Tasmania	University of Tasmania

Name and school	Emer Duffy, Australian Centre for Research on Separation Science, School of Physical Sciences (UTAS) = **Candidate**
Name and institution	Prof. Brett Paull, Australian Centre for Research on Separation Science, School of Physical Sciences (UTAS) and ARC Centre for Excellence in Electromaterials Science, School of Physical Sciences (UTAS) = **Author 1**
Name and institution	Prof. Pavel Nesterenko, Australian Centre for Research on Separation Science, School of Physical Sciences (UTAS) = **Author 2**
Name and institution	Dr. Dimitar Mitev, Australian Centre for Research on Separation Science, School of Physical Sciences (UTAS) **= Author 3**
Name and institution	Dr. Artaches Kazarian, Australian Centre for Research on Separation Science, School of Physical Sciences (UTAS) = **Author 4**
Name and institution	Dr. Ashley Townsend, Central Science Laboratory (UTAS) = **Author 5**
Name and institution	Dr. Xiaoyun He, Irish Separation Science Cluster, Dublin City University, Ireland = **Author 6**
Name and institution	Dr. Satheesh Krishnamurthy, Department of Engineering and Innovation, The Open University, Milton Keynes, UK = **Author 7**
Name and institution	Dr. Ekaterina Nesterenko, Irish Separation Science Cluster, Dublin City University, Ireland = **Author 8**
Name and institution	Dr. Dermot Brabazon, Irish Separation Science Cluster, Dublin City University, Ireland = **Author 9**
Name and institution	Avishek Dey, Department of Engineering and Innovation, The Open University, Milton Keynes, UK = **Author 10**

List of Publications from this Thesis

1. Duffy, E., Mitev, D.P., Nesterenko, P.N., Kazarian, A.A., Paull, B. Separation and Characterisation of Detonation Nanodiamond by Capillary Zone Electrophoresis. *Electrophoresis* 35 (2014) 1864-1872.

2. Duffy, E., Mitev, D.P, Townsend A.T., Paull, B., Nesterenko, P.N. (2015) Assessing the Extent, Stability, Purity and Properties of Silanised Detonation Nanodiamond, *accepted article, Applied Surface Science*

3. Duffy, E., He, X., Nesterenko, E.P., Brabazon, D., Dey, A., Krishnamurthy, S., Nesterenko, P.N., Paull, B. (2015) Thermally Controlled Growth of Carbon Onions Within Porous Graphitic Carbon-Detonation Nanodiamond Monolithic Composites. *RSC Advances* 5 (2015) 22906-22915.

4. Duffy, E., He, X., Nesterenko, P.N., Paull, B. (2015) Hierarchical Porous Graphitic Carbon Monoliths With Detonation Nanodiamonds: Synthesis, Characterisation and Adsorptive Properties. *Journal of Materials Science* 19 (2015) 6245-6259.

Conference Presentations

Oral presentations

1. Duffy, E., He, X., Nesterenko, E.P., Krishnamurthy, S., Brabazon, D., Nesterenko, P.N., Paull, B. Porous Graphitic Carbon Monoliths Embedded With Detonation Nanodiamonds and Other Temperature-Induced Nanocarbons. *12th International Conference on Frontiers of Polymers and Advanced Materials, 2013, Auckland, New Zealand.*

2. Vazquez M., Duffy, E., He, X., Vereschagina, E., Ducrée, J., Nesterenko, E.P., Brabazon, D., Nesterenko, P.N., Paull B. Solid Phase Micro-Extraction Centrifugal Microfluidic Disc Integrating Carbon Monolithic Stationary Phases. *20th International Symposium on Electro- and Liquid-Phase Separation Techniques (ITP 2013), Tenerife, Spain.*

3. Duffy, E. Krishnamurthy, S., He, X., Nesterenko, E.P., Nesterenko P.N., Brabazon, D., Paull, B. Preparation and Properties of Porous Graphitic Carbon Monoliths Embedded With Detonation Nanodiamonds and Other Temperature-Induced Nanocarbons. *Materials Research Society Spring Meeting 2014, San Francisco, USA.*

Poster presentations:

1. Duffy, E., Mitev, D.P, Nesterenko, P.N., Paull, B. Capillary Zone Electrophoresis for the Characterisation and Separation of Detonation Nanodiamond. *40th International Symposium on High Performance-Liquid-Phase-Separations and Related Techniques, 2013, Hobart, Tasmania, Australia.*

2. Vazquez M., Duffy, E., He, X., Vereschagina, E., Ducrée, J., Nesterenko, E.P., Nesterenko, P.N., Brabazon, D., Paull B. Centrifugal Microfluidic Disc Integrating Carbon Monoliths for Solid Phase Micro-Extraction. *39th International Symposium on High Performance-Liquid-Phase Separations and Related Techniques, 2013, Amsterdam, The Netherlands.*

3. Paull, B., Duffy, E., Mitev, D.P, Nesterenko, P.N. Separation and Characterisation of Purified and Surface Modified Detonation Nanodiamond by Capillary Zone Electrophoresis. *40th International Symposium on Capillary Chromatography, 2014, Riva del Garda, Italy.*

4. Duffy, E., He, X., Nesterenko, E.P., Krishnamurthy, S., Nesterenko, P.N., Paull, B. Adsorption of Aqueous Dyes by Hierarchical Porous Carbon Monolithic Composites Containing Detonation Nanodiamonds and Thermally Induced Nano-Carbons. *7th Biennial Australian Colloid & Interface Symposium, 2015, Hobart, Tasmania, Australia.*

5. Wei, Z., Duffy, E., Nesterenko, P.N., Paull, B. Surface Modification of Synthetic Diamond by Adsorption of Aluminium and 1-Pyrenecarboxylic Acid to Increase its Aqueous Suspension Stability. *7th Biennial Australian Colloid & Interface Symposium, 2015, Hobart, Tasmania, Australia.*

Abstract

The inclusion of carbonaceous nanoparticles (CNPs) in composite materials is an area of significant research interest. Their addition is expected to result in differing properties, and a possible transfer of the CNP's favourable properties to the final composite. Detonation nanodiamond (DND) has emerged as an interesting CNP, offering an array of attractive properties, including mechanical stability, thermal conductivity and a flexible surface chemistry, that make it an ideal candidate for integration in composite materials. This material still requires further characterisation in order to fully understand its colloidal stability, aggregation behaviour and batch-to-batch variability. The aim of the present thesis was to investigate DND as a new candidate for inclusion in the synthesis of novel carbon monolithic composite materials suitable for potential application in analytical chemistry, separation and adsorption processes, sensors or electrode materials. To address the variable nature of this CNP, new approaches for its characterisation and modification have been investigated.

Capillary electrophoresis (CE) was shown to provide an insight into the onset of particle aggregation and offered the capability of separating DND from different sources or purification processes. Surface modification with silanes resulted in hydrophobisation and improved DND colloidal stability. After a detailed characterisation of these different DND materials, a commercial suspension of single-digit DND particles was selected for preparation of carbon on carbon composites. Hierarchical porous graphitic carbon-nanodiamond monoliths (CND) were prepared by adding DND to a resorcinol formaldehyde copolymer, with silica gel as a hard template. The influence of DND was systematically studied and for the first time it has been shown that altering DND content can allow for facile tuning of surface areas, pore sizes, and graphitic nature of carbon monoliths. The first controlled production of novel structures resulting from DND inclusion within the composite monoliths, such as carbon onions, has been achieved. Properties of CND composites

including graphitic character, surface area, morphology, pore structures and adsorption performance for organic dyes were studied in detail. CND materials embody an interesting new group of carbon on carbon composite materials with potential for application in areas including adsorption, extraction, catalysis and electrode materials.

Acknowledgements

I would like to take this opportunity to express my immense gratitude to my supervisors Prof. Brett Paull and Prof. Pavel Nesterenko for their continuous guidance, support and advice, and for assisting me in each step towards completing this thesis. It's undoubtedly an exciting time to work in the area of nano-carbon research and I am grateful to have had the opportunity to share in their enthusiasm for this field.

I would also like to express my gratitude to the collaborators within ACROSS and the CSL at the University of Tasmania (UTAS), at Dublin City University and the Open University, for their valuable contributions to this research, the resultant publications, and to their respective research centres for access to facilities. This includes Dr. Dimitar Mitev for his work on modification of nanodiamonds and his contributions to their analysis, and Dr. Ashley Townsend for his expertise and guidance on ICP-MS. My thanks also go to Dr. Xiaoyun He, Dr. Ekaterina Nesterenko and Dr. Dermot Brabazon for their advice on carbon monolith synthesis, to Dr. Artaches Kazarian for his contribution to the CE paper draft, to Dr. Satheesh Krishnamurthy and Avishek Dey for providing XPS analysis and access to TEM, and to the CSL for SEM access.

My thanks also go to UTAS and the Australian Government for financial support and to Graduate Research for awarding me a postgraduate travel grant to attend and give an oral presentation at the Materials Research Society spring meeting in San Francisco, USA April 2014.

I would like to thank my family for always supporting me in life, this thesis is dedicated to them - to my dad John, my mum Bernie, and my sister Gill, for their enduring love, help and support from the other side of the world throughout this huge undertaking. To my wonderful partner Matt, thank you for always being there for me, I couldn't have done this without you!

Table of Contents

List of Figures

List of Tables

List of Equations

List of Abbreviations and Symbols

3DOM, Three-dimensionally ordered macroporous materials

AC, Activated carbon

BASD, Beads-assisted sonic disintegration

BET, Brunauer-Emmett Teller

BGE, Background electrolyte

BJH, Barret-Joyner-Halenda

CE, Capillary electrophoresis

CZE, Capillary zone electrophoresis

CM, Carbon monolith

CND, Carbon monolith with nanodiamond

CNP, Carbon nanoparticle

CNT, Carbon nanotube

CVD, Chemical vapour deposition

DAD, Diode array detector

DLS, Dynamic light scattering

DMODCS, Dimethyloctadecylchlorosilane

DND, Detonation nanodiamond

DS, Detonation soot

EDX, Energy dispersive X-ray electron spectroscopy

EOF, Electroosmotic flow

FE-HR-SEM, Field emission high-resolution scanning electron microscopy

FTIR, Fourier transform infrared spectroscopy

GO, Graphene oxide

HF, Hydrofluoric acid

HMDS, Hexamethyldisilazane

HPHT, High pressure high temperature

ICP-MS, Inductively coupled plasma mass-spectrometry

LOD, Limit of detection

MB, methylene blue

MWCNT, Multi-walled carbon nanotube

ND, Nanodiamond

NR, Neutral red

NSFPA, Detonation nanodiamond purified using a mixture of nitric acid, sulphuric acid, perchloric acid and hydrofluoric acid

PMMA, Poly(methyl methacrylate)

RF, Resorcinol formaldehyde

SEM, Scanning electron microscopy

SDND, Single digit nanodiamond

SWNT, Single-walled carbon nanotube

TEM, Transmission electron microscopy

TGA, Thermogravimetric analysis

TMCS, Trimethylchlorosilane

TOF-MS, Time-of-flight mass spectrometry

Tris, Tris(hydroxymethyl)aminomethane

XPS, X-ray photoelectron spectroscopy

Chapter 1.

Introduction

1.1 Introduction

Composite materials can be tailored to suit particular applications by selecting their components and appropriately tuning their structural properties and morphology. Composites are hybrid materials commonly made up of a continuous matrix phase, a filler phase, and an interface between these two phases. These phases are combined with the aim of preparing a multifunctional material with exceptional properties. A large number of composite materials comprise of a polymer, metal, carbon or ceramic matrix that is reinforced with carbon fibres, glass fibres or other micrometre-scale materials. Carbon fibre carbon-matrix composites are often referred to as carbon-carbon composites wherein the carbon fibre reinforcement results in a stronger material that is more resistant to thermal shock compared to graphite, and the coefficient of thermal expansion is near zero [1].

The emergence of nanocomposite materials has generated significant research interest due to the favourable properties of nano-materials themselves, and due to the promise offered by the unique combinations of properties that can be achieved through their inclusion in a composite material. The term nano-composite refers to a composite material with some nanometer-scale structure such as the filler size or the pore size. A nano-filler should be in the nanometer size range, typically 1-100 nm, and can take the form of nanoparticles or clusters, nanotubes, nanofibres, nano-sheets and other shapes. In nano-composite synthesis, the uniform distribution, and dispersion quality of the nano-filler are important factors to consider [2], where the distribution refers to the placement of nano-filler within the matrix and, a high dispersion quality refers to a stable suspension of small aggregate-free nanoparticles.

Maintaining high quality dispersions is a non-trivial challenge facing scientists in the field of nano-composite synthesis. For example, in the case of carbonaceous nanoparticle (CNP) fillers, there can be a variety of strong interactions between the nanoparticles themselves. Carbon nanotubes (CNTs) can undergo van der Waals interactions to form bundles or ropes, and detonation

nanodiamond (DND) has a strong propensity to form aggregates thought to be due to electrostatic and van der Waals interactions between the primary particles. DND can form aggregates between 100-200 nm, and greater in size [3-4], which could significantly affect the quality of the resultant composite. The primary focus within this thesis is on the investigation of detonation nanodiamond (DND) materials, specifically their properties and surface modification, and their suitability as a new candidate for inclusion in novel carbon composite materials. CNPs are therefore reviewed within this introductory Chapter where there is a particular emphasis on DND, as well as its incorporation in porous carbon materials towards preparation of novel carbon monolithic composites for application in adsorption. There has been a recent surge of interest in DND particles as it is expected that their surface which provides a variety of reactive functionalities, can be combined with the beneficial properties of macroscopic diamonds (such as their extreme hardness, chemical stability, biocompatibility, thermal conductivity and electrical resistivity [5]), making them a highly attractive nano-filler for development of new composite materials.

The properties of composites containing DND particles will be highly dependent on the dispersion stability of the particles themselves, as well as on their surface reactivity. Understanding the dispersion quality and improving particle stability of DND with the aim of obtaining monodisperse or “single-digit” particles is a challenge yet to be resolved. The properties of DND, including suspension stabilities and aggregation tendencies, are described in further detail in Section 1.3, and will be a major focal point within Chapters 2 and 3, where new strategies for characterisation, modification and improving dispersion quality of DND are investigated. Following the characterisation and modification of different DND materials, a commercial suspension of single-digit nanodiamond particles was selected as a nano-filler for incorporation in novel carbon composite materials, namely porous graphitic monolithic composites. Porous carbon materials will be introduced in Section 1.4 as a prelude to Chapters 4 and 5, which report on the synthesis, characterisation and adsorptive properties of novel porous carbon-nanodiamond monoliths or

"carbon on carbon" composites.

1.2 Carbon at the Nanoscale

Carbon is a tetravalent element that can undergo tetrahedral bonding with neighbouring atoms (sp^3 bonding), or it can take the form of a planar (sp^2) or a linear (sp) configuration. This flexibility in configuration comes from the small electronic "core" and the corresponding ability of the outer valence electrons to hybridise and form linear and one-dimensional (1D), planar (2D) and tetrahedral (3D) structures with the electrons of neighbouring atoms. Carbon can even undergo intermediate bonding e.g. between sp^2 and sp^3 hybridisation, as seen in the case of fullerenes. The best-known allotropes of carbon are graphite (sp^2) and diamond (sp^3). The non-crystalline form of amorphous carbon contains both sp^2 and sp^3 hybridisation. As a result of these variable hybridisation states, there are considerable differences among carbon's bulk forms. The chemical and electronic properties of carbonaceous nanomaterials are often determined by the dominant hybridisation state of the C-C bonds [6] (Figure 1.1).

In 1985 the discovery of fullerenes [7] was often considered as the uncovering of the third allotropic form of this element and since then, there has been an intense research focus on new forms of carbon where the ability of carbon to exist in different allotropic forms has resulted in a variety of interesting nanostructures. This fascinating element continues to surprise us, with the discovery of new nanostructures such as nanodiamonds, nanohorns, nanotori, nano buds, graphenes, and nano-onions emerging in recent decades.

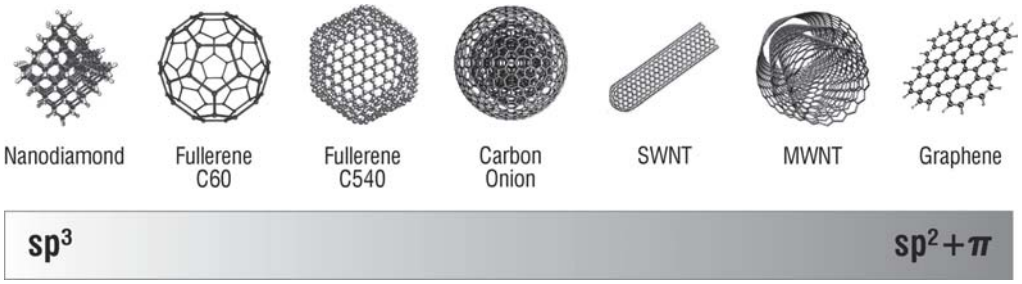

Figure 1.1 Nanocarbons and their hybridisation states. Reproduced from [8].

The thermodynamically stable bonding configuration of carbon at normal temperature and pressure is hexagonal graphite, while diamond is metastable according to the equilibrium phase diagram of bulk carbon [9]. The energy difference between these two phases is 0.02 eV/ atom. The high activation barrier for a transition of ~0.4 eV/atom requires the use of high temperatures/pressures and/or the use of a catalyst to induce the phase transformation [10]. Understanding the stability of carbon at the nanoscale has been the focus of many researchers since the 1990s. The importance of size-dependent phase stabilities has been established [11], since the Gibbs free energy depends on surface energy, which alters the phase diagram as shown in Figure 1.2. In the bulk form, graphite is stable (at low pressure and temperature), and diamond is stable at high temperature and pressure [12]. Both phases undergo (pressure dependent) melting above temperatures of 4500 K. The phase diagram for nanoscale carbon is overlaid in Figure 1.2, showing that the liquid phase is found at lower temperatures. Point A marks the Jouget point that is reached during detonation synthesis of nanodiamond, where pressure and temperature suddenly rise. As temperature and pressure decrease along the red line the carbon atoms condense into nanoclusters, which then form larger liquid droplets and crystallise [13]. The diamond-graphite equilibrium line marks the pressure threshold, below which, the growth of diamond is replaced by the formation of graphite. This accounts for the sp^2 surface layers associated with DND.

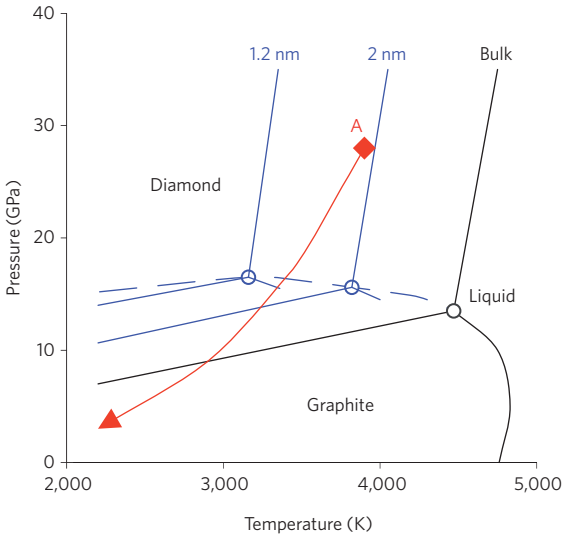

Figure 1.2 Phase diagram for carbon. Reproduced from [12].

CNPs possess remarkable properties and as a result, their potential applications appear unlimited. Some applications include the use of CNPs in coatings for protective purposes or for wear resistance, dispersions for medical applications, high surface area materials particularly for energy storage and drug delivery applications, within composite materials as an additive to improve strength or electrical properties, and in functional nanostructures [10]. Some of the most intensely studied CNPs are broadly reviewed herein, in terms of their discovery, synthesis, properties and applications, followed by a more detailed examination of detonation nanodiamond as potential new nano-filler for synthesis of carbon on carbon monolithic composites.

1.2.1 Fullerenes

The closed cage spherical molecules that are fullerenes (as shown in Figure 1.1) were first found to consist of 60 carbon atoms (C_{60} - named Buckminsterfullerene) [7] and have since then been shown to exist in a variety of forms (e.g. C_{70} is a another common form, but fullerenes with 76, 84 and up to 100 carbon atoms are also commonly obtained). Fullerenes have been produced

using several different synthesis methods, such as the method involving arc-discharge between graphite rods in an atmosphere of helium (Hüfmann-Krätschmer procedure), the combustion of benzene in an oxygen-deficient atmosphere, or the condensation of polycyclic aromatic hydrocarbons by pyrolytic dehydrogenation or dehydrohalogenation [14]. Following synthesis, fullerenes undergo isolation and purification procedures, which requires considerable effort in order to obtain materials of adequate purity to ensure their successful application. Endohedral fullerenes have additional non-carbon atoms, ions or clusters enclosed within their inner spheres and they have been prepared with a variety of different metals, noble gases and other atoms [15]. Fullerenes have been used in numerous biomedical applications [16], including imaging (as MRI contrast agents), drug delivery applications [17], and biosensors [18], in the preparation of composite materials [19], and solar cells [20].

1.2.2 Graphene

Graphene is a 2-dimensional sheet structure consisting of six-membered rings of sp^2-hybridised carbon atoms, often referred to as a "honeycomb" structure (Figure 1.1). The first isolation of a single layer of graphene from graphite was achieved in 2004 by Geim and co-workers [21], which led to intense interest and continued research in the scientific community. This has shown graphene to possess extraordinary electronic and mechanical properties, as well as interesting electrochemical properties. The top-down approach of mechanical exfoliation is still in use for preparation of graphene, however, it is not a high-throughput method and does not result in a high-yield. As a result, there have been efforts to produce graphene chemically in solution, to grow it directly from organic precursors, and to catalyse its growth on a substrate for *in situ* synthesis [22]. Nanodiamond (ND) can also be converted to multi-layer graphene by annealing at 1650 °C or higher in a helium atomsphere, however, the product has been shown to also have onion-like particles present [23], and these can form by the thermal annealing of ND as described further in Section 1.2.5. The

properties of different grades of graphene and their suitability for specific applications are highly dependent on the method of production used. Different applications require different grades of material, for example, liquid phase exfoliation of graphite is used industrially to prepare large volumes of graphene [24], for applications in composite materials, coatings, electrodes and energy storage. Other applications such as electronics and bio-applications including drug delivery and imaging require a higher grade of graphene that can be prepared by CVD [25].

1.2.3 Carbon Nanotubes

In 1991 Sumio Iijima first described the preparation of a new type of carbon nanostructure, which he referred to as "helical microtubules of graphitic carbon". They were produced from a cathode by a carbon-arc discharge method similar to that used in the preparation of fullerenes [26]. Carbon Nanotubes (CNTs) can be considered as molecular scale tubes of graphene sheets with a range of diameters (up to tens of nanometers) and lengths (up to centimetres), or as the one-dimensional analogues of zero-dimensional fullerene molecules, and their ends are typically capped with a fullerene-like structure. They can exist in different forms, i.e. single walled carbon nanotubes (SWCNT), and multi-walled carbon nanotubes (MWCNT), which contain two or more concentric graphitic tubes (Figure 1.1). The arc discharge method can be used to produce high quality SWCNTs and MWCNTs, and this involves evaporation of carbon atoms by helium plasma generated by a high current between anode and cathode. By controlling the arc discharge synthesis conditions, it is possible to prepare MWCNTs up to 10 μm in length with 5-10 nm diameter [10]. Laser ablation and chemical vapour deposition (CVD) are also commonly used methods of synthesis for CNTs.

CNTs are known to have extraordinary thermal and mechanical properties, including a high tensile strength, high thermal conductivity and stability. Interestingly, their electronic properties vary as a function of the arrangement of the graphene layers; they can either function as a conductor

or a semi-conductor [27]. Furthermore, their chemical modification with a variety of moieties has been reported, and is an important step in realising their promise in terms of applications. Application areas include biosensors, nano-electronics and electrode materials [28], gas sensors [29], and separation science [30-31].

1.2.4 Nanodiamonds

Diamond is an exceptional material in many respects, and nanodiamond (ND) is a nanoscopic version of sp^3 carbon (Figure 1.1) with unique properties originating from its lattice structure and its interesting surface chemistry [32]. It is emerging as an important material for a variety of applications. Attractive properties of ND include a high Young's modulus, biocompatibility, optical properties, high thermal conductivity and electrical resistivity. It has a high chemical stability despite its varied surface chemistry, which is dependent on both the synthesis and purification methods used in its production. The term ND is used to refer to a variety of diamond-based materials at the nanoscale and these range from single nano-sized diamond clusters to bulk nanocrystalline diamond films, and some of these interesting materials are described below. The synthesis, properties, surface chemistry and applications of detonation nanodiamond (DND) will be reviewed in more detail within Section 1.3.

ND was first discovered in the 1960s in Russia where scientists were studying the detonation of carbonaceous material in sealed chambers. Research interest grew in the 1980s in both Russia and the USA, where synthesis and purification methods were further developed [33]. There are a number of methods currently in use for the production of nanoscale diamond. The milling of both natural and synthetic diamond microcrystals is a relatively simple production method and the resulting diamonds can be fractionated based on size [32]. Detonation synthesis involves the detonation of explosives (the carbon source) in an oxygen-deficient atmosphere in a special detonation chamber, and this is one of the more common

methods of synthesis used on an industrial scale today. The resulting detonation soot contains nanodiamond particles, which must undergo subsequent purification due to the graphitic layer coating them, and due to other impurities such as non-carbon materials from the detonation chamber itself [34]. Shockwave synthesis has also proven to be a popular choice industrially, and it involves the direct phase transformation of graphite into diamond crystallites caused by an external detonation shockwave [35]. The size of nanodiamond particles is dependent on the method of production used. For example, depending on the precursor material, nanodiamonds between 4 and 25 nm can be synthesised via shockwave methods, whereas those produced by mechanical milling can have a larger size distribution up to 50 nm [32]. Nanodiamond produced by CVD methods can have a variety of sizes, properties and morphologies [36], but they tend to have less functionalities and a more simple structure when compared to DND [37]. Some of the major applications of diamond-based nanostructures are within composite materials, wear-resistant coatings, polishing, chromatographic and drug delivery applications [10].

1.2.5 Carbon Onions

Carbon onions (also referred to as “onion like carbon”) belong to a class of concentric fullerenes or curved concentric graphitic sheets (Figure 1.1) [38]. Sumio Iijima first discovered them in 1980, while studying a sample of carbon black by TEM [39]. Ugarte subsequently proposed the mechanism of their formation in 1992 based upon a study using a focused electron beam on amorphous carbon, which caused graphitisation and curling until closure to minimise surface energy [38]. Carbon onions may be produced (on the scale of several grams) by the thermal annealing of ND particles in a vacuum [40], and interestingly, the reverse transformation has also been reported. The electron irradiation of carbon onions resulted in formation of ND particles [41].

Annealing ND causes the particles to undergo graphitisation, which proceeds from the outer more reactive surface regions inwards, in a layer-by-layer fashion (Figure 1.3). The size of the

resultant carbon onions is dependent on the ND precursor material. Onions between 5-10 nm in diameter can be produced from 5 nm diameter ND materials. Other methods for the synthesis of carbon onions have been reported, including the arc discharge method between two graphite electrodes in water, laser excitation of ethylene in air to convert the hydrocarbon into a solid carbon onion, and CVD using an iron catalyst to decompose acetylene at 400 °C yielding much larger carbon onions (~50 nm) [42].

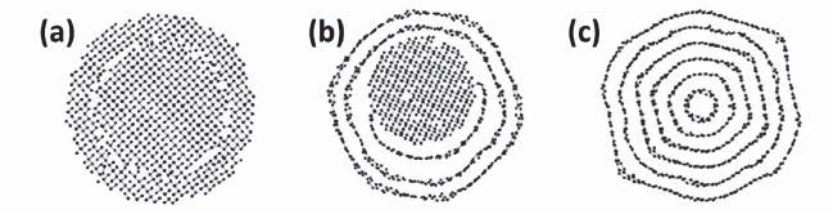

Figure 1.3 Molecular dynamics simulation of ND (A) annealed at a temperature of 1400 °C with graphitisation evident at the surface (also called a bucky-diamond) (B) and annealed at 2000 °C, where there is complete graphitisation of the ND particle resulting in formation of a carbon onion. Reproduced from [42].

The structural properties of carbon onions vary depending on the synthesis conditions and for the purpose of this thesis the focus will herein be on those derived from a DND precursor. There have been extensive studies carried out on the annealing of ND under different conditions to obtain carbon onions because of their wide potential applications and to improve understanding of the transition process. Xu *et. al.* demonstrated the effect annealing ND in different atmospheres could have on the properties of the resultant material. They reported that the onset of graphitisation occurred at 670 °C in argon and continued to proceed from the surface regions inwards up to a temperature of 1100 °C, during which time the ND underwent significant micro-structural and morphological changes [43]. They also reported the onset of oxidation of ND occurring at 496 °C,

affecting the reactive surface regions first. Butenko *et. al.* have further explored the physical and chemical characteristics of carbon onions produced by annealing ND in a vacuum at temperatures of ~800-1800 °C using photoemission spectroscopy to probe the structural properties [44]. It was found that carbon onions displayed higher binding energies than ND, which was explained by the curvature of graphitic layers that accumulate different types of defects during annealing of ND. The intermediate structures encountered during this annealing process are referred to as bucky-diamonds and they contain a diamond-like core and single or multiple cage-like shells (Figure 1.3) [45].

Carbon onions derived from ND display high surface areas, between 400-600 m^2/g. They are not inherently porous materials (i.e. there is no accessible internal porosity in carbon onions), however, pores may be formed by the space between multiple onions and these are typically in the mesopore size range. They have high electrical conductivities and relatively easy dispersibility compared to nanotubes and graphene, making them promising materials for electrochemical applications. They have been shown to be ideal additives to battery and supercapacitor electrodes for high power applications due to their excellent capacitance retention at high current densities [42, 46]. Carbon onions have also found application in composite materials, electromagnetic devices [47], lubricants, and environmental applications in remediation [48].

1.3 Detonation Nanodiamond: Synthesis and Properties

1.3.1 Synthesis

DND is produced by detonation of carbon-containing explosives (e.g. A 60:40 mixture of 2-methyl-1,3,5-trinitrobenzene and hexogen) with a negative oxygen balance in a closed detonation chamber filled with an inert gas or water coolant, where the explosives provide both a source of carbon and energy for the conversion. This is followed by the collection and purification of the detonation soot. Primary DND particles are typically small (4-5 nm diameter) with a narrow size

distribution as a direct result of the experimental conditions in their synthesis, such that the upper size limit for growing DND particles is set by the duration of the detonation shock wave within the detonation chamber when the pressure is sufficient for DND formation [49]. The detonation chamber is then subjected to a rapid cooling step to reduce formation of graphitic soot, which can form at the high temperatures present when the pressure drops following detonation. The carbon yield is 4-10% of the weight of the explosive precursor, and the detonation soot can contain up to 80 wt.% of the diamond phase [33, 49]. DND particles typically comprise of a diamond core of sp^3 carbon, partially coated with a graphitic shell with dangling bonds that are terminated by functional groups. The existence of disordered graphitic shells on the surface of DND particles can be attributed to the structural instability of the diamond surface having carbon atoms with no terminating species [10, 50]. As well as containing graphitic carbon, the raw detonation soot can contain metals, metal oxides and other impurities that come from the detonation chamber and the explosives used, therefore, purification of the detonation soot is a vital step in preparation of DND.

1.3.2 Purification

Impurities may fundamentally alter thermal and mechanical characteristics, as well as aggregation behaviour and physicochemical properties of DND. Purification procedures commonly employ wet chemistry techniques such as harsh oxidising treatments (e.g. nitric acid, or a mixture of sulfuric, and nitric acid, or nitric acid and hydrogen peroxide) that can have a significant impact on the surface chemistry of DND. They typically display oxygen-containing groups on the surface resulting from the oxidative treatment and the use of water as a cooling medium following detonation synthesis [51-52]. Surface functionalities can include hydroxyl, carboxylic, anhydride, ketone and lactone groups [53], and there can be some graphitic carbon remaining on the surface even after purification.

There are a variety of other purification procedures currently in use and under development

in an effort to improve DND quality. These include microwave-assisted acid oxidation [54], catalyst-assisted oxidation, ozone-enriched air oxidation, selective oxidation in air [5], ultrasonic, magnetic and electrolysis methods [55]. Establishment of a standardised purification procedure is necessary to ensure a less variable material and for the successful application of DND. Moreover, the dis-aggregation of DND particles is crucial in order to benefit fully from their advantageous properties, and many applications (e.g. biomedicine, nanocomposites) require a high dispersion quality.

1.3.3 Aggregation

DND particles have a strong tendency to form aggregates 100-200 nm in size, some of which are unbreakable even by intensive sonication [56]. These aggregates form as a result of the high surface area to volume ratio associated with nanoparticles where surface forces contribute to interparticle attractions, as well as the surface chemistry contribution coming from the DND surface functionalities. There has been a significant effort towards understanding the interactions between DND particles that causes such strong aggregation, and the underlying mechanism for their formation has been heavily debated.

Recent research suggests that electrostatic interactions are the main cause of aggregation in DND materials, where strong inter-particle electrostatic interactions result in the formation of agglutinates (~60 nm) and agglomerates (~100-200 nm) as put forward by Barnard and Osawa based upon the density functional theory model [3-4]. Van der Waals forces have also been proposed as the underlying mechanism for DND agglomerate formation. Xu and Zhao have recently demonstrated the possibility that interactions between DND particles could be dominated by van der Waals forces [57]. Strong bonding in the sp^2 matrix has also been linked with aggregation tendencies in DND, whereby it is thought that graphitic shells can engulf a number of primary DND particles and hold them together resulting from the detonation synthesis conditions.

However a full understanding of aggregation mechanisms of DND remains a fundamental research question.

1.3.4 Towards Producing Stable Suspensions of Single Digit DND

Despite the uncertainty over agglomeration mechanisms in DND materials, the goal of producing a suspension of single digit or monodisperse DND particles remains unchanged, and a number of de-aggregation routes have been established. Milling methods with ceramic microbeads and beads-assisted sonic disintegration (BASD) have been developed by Osawa and co-workers [56, 58], and have more recently been utilised for the de-agglomeration and surface functionalisation of DND to obtain stable functionalised particles in colloidal solution [59]. Microbead milling can lead to contamination of the DND with bead material, however, dry milling has shown promise as an alternative method that does not introduce contaminants, using readily available milling materials such as sugars or salts [60].

A number of other methods for DND de-aggregation have been proposed, including graphitisation and subsequent oxidation of the thin graphitic layer formed on the DND, resulting in reduced particle sizes for 50% of the particles in suspension to below 50 nm [61]. Hydrogenation at 500 °C has also been shown to successfully break aggregates down to a monodisperse suspension of core-sized DND (4 nm) with a high dispersion stability over extended periods [62]. Centrifugation can be used to separate DND particles into size-based fractions as demonstrated by Larionova *et. al.* where fractions containing aggregates of different sizes were isolated and Fourier transform infrared spectroscopy (FTIR) analysis showed them to display some differences in surface chemistry (in relation to number of oxygen-containing groups on the surface) [63].

The variable surface of DND can also display a very wide range of zeta (ζ) potentials, ranging from as low as −100 mV up to +70 mV. This affects the colloidal stability of the particles, and potentials above 30 mV or below −30 mV are typically observed for stable nanoparticle

suspensions. The ζ potential refers to the value of electric potential at the shear surface (cloud of ions surrounding a charged colloidal particle in an electrolyte), and it can be studied by laser Doppler electrophoresis since ζ potential is related to electrophoretic mobility of the particles [64]. This relationship will be discussed in further detail in Chapter 2, where the electrophoretic parameters of different DND materials are investigated by capillary electrophoresis, a potential new method for their characterisation and separation/fractionation.

1.3.5 Surface Chemistry and Functionalisation Strategies

The flexibility offered by the functionalised DND surface allows for sophisticated modifications without affecting the attractive properties of the diamond core, and for many applications a suitable surface termination is required. The surface functional groups enable the immobilisation of different moieties such as polymer chains, biomolecules or drug molecules, and this is achieved through adsorption or covalent attachment. This also presents an opportunity to impart a high colloidal stability to the particles by tailoring the surface functionalities appropriately. Control over the surface chemistry of DND requires a purified sample, ideally with only one kind of functional group present, to ensure high reproducibility of any further reactions it is subjected to. Although the various functional groups can be used directly for covalent functionalisation, a popular approach has been to firstly ensure maximum oxidation of the DND so that the surface is carboxylated.

This can be achieved through the use of harsh oxidising acids (e.g. a mixture of hydrochloric, nitric and sulfuric acids) or an acid piranha (sulfuric acid and hydrogen peroxide) which will oxidise the surface, and remove non-diamond carbon and some metal impurities, while improving the purity of the DND which is an inherent advantage of this approach [53]. Surface oxidation has also been achieved in air at carefully selected elevated temperatures [5]. The use of microwave-assisted acidic oxidation has produced a highly pure and oxygenated DND material that would be

suitable for further surface functionalisation [54], using various mixtures of acids (nitric, sulfuric, hydrochloric, perchloric and hydrofluoric acids) for removal of non-carbon contaminants resulting in 99.95% purity compared with detonation soot. Oxidised DND materials display hydrophilicity and negative zeta potentials, and are suitable for dispersion in polar solvents.

The hydroxylation of the DND surface also provides a suitable surface for further functionalisation, and has proven to be a popular approach for surface homogenisation alongside carboxylation. The formation of hydroxyl groups can be achieved by subjecting oxygen-terminated DND to reduction reactions using the Fenton reagent (mixture of hydrogen peroxide and iron sulfate) [65], borane, or lithium aluminium hydride. Krueger and co-workers applied both borane and lithium aluminium hydride reduction to DNDs to achieve surface hydroxylation prior to attachment of silane moieties acting as a linker between the DND and peptides in developing a material suitable for biological applications [66]. Mechanochemical treatment of DND particles in water has proven to be a facile method of introducing -OH groups to the surface and it involves using BASD or milling procedures on the particles. Based on increases in -OH related bands in the FTIR spectrum, it was concluded that these milling methods resulted in stable suspensions of -OH terminated particles [53].

The surface of oxidised DND can then be modified using wet chemistry techniques, or high-temperature gas treatment. Heating carboxylated DND in the presence of hydrogen can result in the reduction of the carboxyl group to an alcohol, with the formation of additional C-H groups on the surface. The remaining oxygen can be removed by increasing the temperature (up to 700 °C) [67]. Heating in ammonia can lead to the formation of a number of new surface functional groups (e.g. NH_2, C≡N, and groups containing C=N), and the amination of DND surfaces is attractive for further binding of biomolecules. Heating in chlorine will produce acylchloride groups on the surface [12]. The annealing of DND in an inert gas, or under vacuum, will lead to removal of functional groups and graphitisation of the diamond to form carbon onions as discussed in Section

1.2.5.

Covalent modification of the surface has also been demonstrated using wet chemistry techniques, such as halogenation (usually with fluorine) followed by nucleophilic substitution for grafting of ethers, amines and C-C single bonds on DND. This represents a useful method for direct DND alkylation or amination, however, the mechanism of nucleophilic substitution is under further investigation [53]. Formation of amides on carboxylated DND has been achieved through reaction of an acid chloride modified surface with amines. The formation of ester linkages has also been demonstrated using the carboxylic group through reaction with suitable alcohols using acid catalysis or acid chlorides [53]. Furthermore, hydroxylated DND has proven suitable for covalent modification. Esters were formed on the surface through reaction with carboxylic acid chlorides. The -OH functionality can also be used for reaction with silanising reagents as commonly carried out on glass, silica and other surfaces which is attractive for the production of hydrophobic DND particles, ideal for dispersion in non-polar media provided the applied silane reagents impart hydrophobicity to the DND.

Modification of the surface of DND allows for more precise control over the behaviour of these variable nanoparticles, and has the potential to dramatically reduce aggregation and improve particle stability towards the ultimate goal of obtaining single digit particles. It provides a homogeneous platform for further functionalisation, allowing for development of DND applications, and some examples of applications include polishing in electronics and machinery-finishing [68], biological applications such as the development of drug delivery systems [69-70], the high-affinity capture of proteins [71], and as a fluorescent marker for biological moieties [66]. Nanodiamonds can be added to motor oil as a lubricant [10]. They are used in the production of nanocomposites to improve the mechanical strength and wear resistance of polymers [12], their tunable electronic properties make them ideal for use in electronic applications and they have been used in coating electrodes [37, 55]. The specific

application of ND as a nano-filler within composite materials is examined in further detail below.

1.3.6 Applications in Nanocomposite Materials

The flexible surface chemistry combined with the excellent mechanical and thermal properties of ND materials make them a promising nano-filler material for composites. There have been numerous reports on the incorporation of DND in polymer-based composite materials and the resulting improvement in certain properties. Considerable changes in mechanical strength have been achieved for electrospun polymer fibres containing high loadings of DND for application in protective coatings [72], and for ND-epoxy composites with 3 times greater hardness when the DND was covalently bound to the matrix through amino groups [73]. The incorporation of ND in polymer matrices has been widely studied and other enhancements in properties have been detailed, including improved thermal conductivity [74], wear resistance [75] and electromagnetic shielding [76]. The combination of two different nanocarbons in a polymer composite has been shown to result in superior properties such as the addition of binary combinations of ND, few-layer graphene and single-walled CNTs to reinforce polyvinyl alcohol where significant changes in mechanical properties were achieved (stiffness and hardness improved up to 400%) compared to composites that were reinforced with a single nanocarbon [77]. Inorganic-based ND composites have mainly focused on CVD techniques for diamond deposition in the production of hard carbide- or nitride-containing coatings, and this is of interest to the composite and coatings communities due to the improved hardness that can be achieved through addition of ND [55]. Electrodeposition of inorganic ND composite coatings has also been used with chromium and silicon for reduction of brittleness [78].

The incorporation of DND within carbonaceous composites is an expanding area of research that has not yet been explored in great depth. There are only a small number of

existing reports on the preparation of this new type of composite available. Gordeev and co-workers have bonded ND into a composite using a graphite matrix demonstrating immobilisation of biomolecules in 2003 and 2015 [79-80] for potential application in drug delivery. The electrical and magnetic properties of a similar ND-pyrocarbon composite were also investigated for semiconductor applications [81-82]. Improvements in BET surface area (up to 58%) have resulted from incorporation of ND within a carbon fibre composite prepared using covalent attachment of ND modified with hydroxyl and amino groups to the carbon fibre's surface [83]. Another class of nanocarbon-based composites containing ND are produced by coupling various nanocarbons with NDs. This has been accomplished through the CVD deposition of diamond nanocrystallites on CNTs [84-85], and by heating aqueous suspensions of graphene oxide (GO) and ND to 100 °C over a period of 2 days forming a GO-ND composite that displayed good electrochemical performance [86].

There is evidently a growing interest in ND-containing composite materials within the materials, coatings, energy storage, and biomedical communities due to its outstanding properties. This low-cost nanocarbon also has the advantage of low thermal expansion, which renders it suitable for incorporation in composites requiring a thermal treatment step in their synthesis such as polymers or carbonaceous composites. An interesting study from Shi and co-workers showed that annealing GO-ND composites at 1200 °C resulted in their transformation to flexible mesoporous graphene-carbon onion composite films with high surface areas and conductivities [87]. Synthesis of carbon composite materials can often involve an annealing/pyrolysis step. A DND nano-filler has the potential to improve the thermal conductivity or thermal stability of a material, and this should have a temperature-dependent effect on the properties of the final composite. With the investigation of DND as a nano-filler within porous carbon monolithic composites in this work, it is anticipated that the pyrolysis process involved in preparation of carbon monolithic composites will be affected by DND's

thermal properties. At high temperatures, the graphitisation of DND to form carbon onions could occur, whereas at lower temperatures, the thermal stability of DND may play a role.

Finally it is important to consider the dispersion quality of the nano-filler in used nanocomposite synthesis. The purity and stability of a DND nano-filler should be optimised to ensure a high quality final material with improved properties. Degradation in properties is likely to occur if the DND is unstable, poorly dispersed, aggregated, or high in impurities. Therefore, careful consideration was taken when selecting a DND material for incorporation in carbon monolithic composites. A commercial DND material available from PlasmaChem Gmbh (Berlin, Germany) in the form of a stable suspension of “single-digit nanodiamonds” produced by chemical disintegration of aggregates was selected due to its good dispersibility in a variety of solvents, good stability, and small particle size (5-15 nm by dynamic light scattering with a diamond crystallite size of 3.5-5.2 nm) and purity (free from additives and milling impurities).

1.4 Porous Materials: Carbon Monoliths for Application in Adsorption

1.4.1 Classification of Porous Materials

Porous materials continue to attract significant interest within science and technology fields due to their numerous applications in catalysis, gas storage, chemical separations, and energy storage to name a few. They are classified according to their pore sizes, which are outlined by the IUPAC as follows: macropores are pores with an internal width greater than 50 nm; mesopores have an internal pore width between 2 and 50 nm; and micropores have an internal pore width of less than 2 nm.

Sorption behaviour of fluids in macropores is different to that in meso- and micropores. Micropores have a high adsorption potential due to their small width, and adsorption within them (micropore filling) is dominated by interactions between the pore walls and fluid molecules. In

contrast, macropores are relatively large and adsorption within them is dependent both on the interaction between fluid molecules and the interaction between the fluid and the pore walls. This leads to capillary condensation wherein a gaseous adsorbate condenses to a liquid-like phase in pores at a pressure below saturation pressure of the bulk fluid [88].

The shape of an adsorption isotherm depends on the strength of interaction between the sorbent walls and the adsorbate, as well as the effects of confined pore space. Figure 1.4 shows the six types of adsorption isotherm based upon the IUPAC classification. Type I is a reversible isotherm and can be generated when adsorption is limited to only one or a few molecular layers of adsorbate. The amount adsorbed approaches a limiting value as the relative pressure (P/P_0) nears 1. This is commonly observed for chemisorption and can also be seen for physisorption on microporous materials where the high uptake at low relative pressures is due to micropore filling which takes place here due to the high adsorption potential of the small pores. Type II isotherms indicate that monolayer-multilayer adsorption has occurred, and they are commonly observed for macroporous adsorbents. Point B is marked on the isotherm in Figure 1.4 and this is often referred to as the knee. It shows the point at which multilayer adsorption begins, following adsorption of a monolayer. The type III isotherm is also reversible and it demonstrates a weak adsorbent-adsorbate interaction throughout the range of relative pressures, with the notable absence of a knee in the isotherm [88].

Type IV isotherms are commonly seen for mesoporous materials and they have a characteristic hysteresis loop indicative of capillary condensation occurring in the mesopores. The type IV isotherm shown in Figure 1.4 has a limiting step at high relative pressures and this suggests that complete pore filling has taken place. Type V isotherms also display a hysteresis loop suggesting capillary condensation, however the concave shape of the isotherm at low relative pressures (similar to type III) shows a weak adsorbent-adsorbate interaction. Finally, the type VI isotherm shows multilayer adsorption, which occurs in a step-by-step process on a uniform, non-porous material [88].

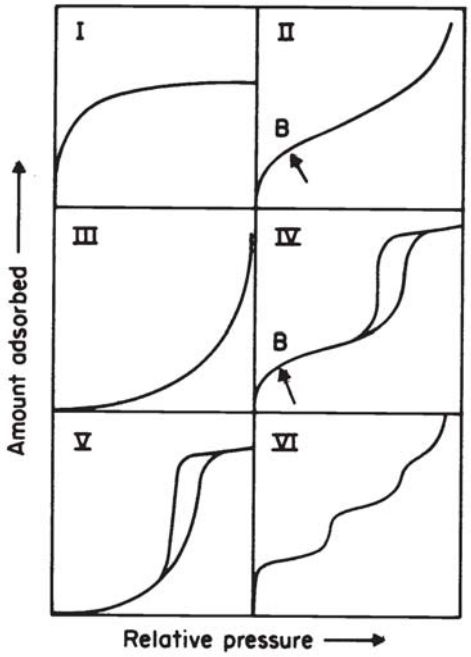

Figure 1.4 Types of physisorption isotherms based on IUPAC classification. Reproduced from [89].

1.4.2. Development of Carbon Monoliths and their Application in Adsorption

Tailoring the structural and chemical properties of porous materials including pore size, shape, surface reactivity and connectivity is a key step in furthering their application. Porous carbon materials are highly topical for use in supercapacitors and as an electrode material [90-91], as adsorbents for environmental remediation and gas separation and storage [92-93]. One novel route to the production of porous carbons is by synthesis of a carbon monolith, which typically exhibits a hierarchical pore network. Hierarchical porous carbon materials should have a combination of macro- meso- or micro-pores. Tri-modal porous materials contain all three levels of pores. Carbon monoliths offer the advantage of a tuneable 3D interconnected pore network, high surface area, and good thermal and chemical stability, which gives them some advantages in terms of high flow-through permeability, good electronic conductivity, and high rates of mass and heat transfer. Their

high permeability and ease of handling lends them well to applications in electrochemistry or separation processes including chromatographic columns and filtration devices where improved electrolyte diffusion and electron conductivity are advantageous [94]. They can be fabricated in a variety of different shapes such as discs or rods thus offering more manageability and flexibility than porous carbon powders made up of fine carbon particles [95].

Monoliths can be defined as a continuous piece of material with a defined 3D shape that generally has an interconnected porous structure [96], and they have traditionally been prepared from silica or polymers for applications in separation science [97-98]. The first carbon monolith reported for use in separation science, specifically for high-performance liquid chromatography (HPLC), was prepared by Guichon and co-workers in 2003, where it was shown to be a promising alternative stationary phase to silica and polymer monoliths, due to the reduced swelling in organic solvents and improved resistance to hydrolysis [100]. The use of a spherical silica template was effective in creating a highly interconnected macropore network within this carbon monolith, and has proven to be an effective route for preparation of carbon monolithic materials for chromatographic or adsorptive applications [100-103].

In general, pore design is key to the synthesis of carbon monoliths and a variety of synthetic methods have been reported which allow for creation of controlled pores. The most common route of fabrication is to use a templating approach to facilitate the creation of a tailored pore structure. Templates are classified as either hard templates (inorganic colloids, preformed porous inorganic structures, such as silica spheres or monoliths) or soft templates (such as polymers or surfactants). The template is combined with a carbon precursor, which undergoes polymerisation and carbonisation followed by template removal (Figure 1.5). In the case of a hard template this requires the use of strong acid or base for template removal, whereas solvent washing, or thermal decomposition more easily removes soft templates [99]. After template removal, a negative carbon replica of the original template structure is produced. Selection of an appropriate precursor material

can also allow for tuning the structure and morphology of the carbon itself, which can be prepared by thermal polymerisation or drying methods such as freeze drying or evaporation, followed by carbonisation.

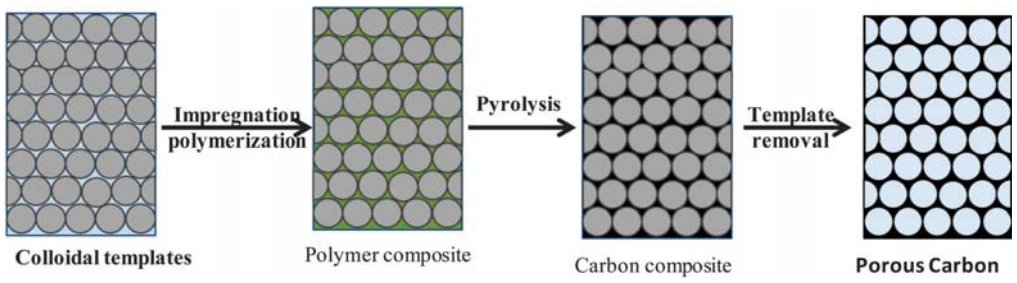

Figure 1.5 Scheme representing the synthesis of porous carbon monolithic materials based on the colloidal templating approach using hard or soft templates to facilitate the creation of a controlled pore network (e.g. silica colloids or polymeric colloids can be used as templates). Reproduced from [99].

The use of silica spheres as a hard template was reported by Knox and Gilbert in 1979 for the production of commercially available porous graphitic carbon stationary phases (Hypercarb®) wherein highly porous silica gel was used as a template, with phenol formaldehyde resin as the carbon precursor [105], and template removal was achieved using hot potassium carbonate before graphitisation at 2340 °C. Synthesis of carbon monoliths by Guichon *et. al.* and later by our group followed the same fashion using a spherical silica template for creation of uniform macropores [100-103]. This synthesis was based on the polymerisation of a resorcinol formaldehyde (RF) precursor infiltrating a packed spherical silica template. An iron catalyst was used to achieve localised graphitisation at relatively low temperatures, and this was followed by HF removal of the silica template. The orientation of the silica spheres was dependent on gravity, which can lead to a lack of order in the macropores. Silica monoliths have also been utilised as a hard template for preparation of carbon monoliths (Figure 1.6), often with glucose, sucrose or furfuryl alcohol as the

carbon precursor, and this nanocasting approach allows for a high degree of control over the final porosity where a more ordered structure can be achieved [106-107].

Other hard templating methods that have been explored include colloidal crystal templating (using templates such as colloidal silica or polymeric spheres) for preparation of inverse opal or three-dimensionally ordered macroporous materials (3DOM) [108]. The colloidal template should self-assemble into an ordered structure with tightly packed particles, and following template removal, the resultant carbon monolith should have a high degree of periodicity in three dimensions [109]. The synthesis of tailored 3DOM materials is limited by the diameter of the colloidal template, which is generally 0.1-1 μm [109], however, ordered microporous and mesoporous carbons can be synthesised to have smaller pore diameters, well below 10 nm, using zeolites or mesoporous silicas [110].

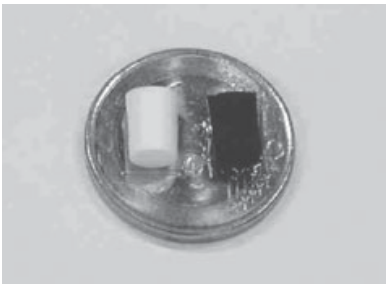

Figure 1.6 Photograph showing bimodal silica monolith (meso- and macro-pores) used as a mould (left) for synthesis of nano-cast carbon monolith replica (right). Reproduced from [106].

Soft templating synthesis can offer a less time consuming alternative procedure to the multistep hard templating methods described above. However, the production of highly ordered carbon monoliths by soft templating procedures is challenging. The carbon precursor should form a highly cross-linked polymer within which the soft templates can be sacrificed as a porogen during the carbonisation step. It is important that there is a matching interaction between the carbon precursor and the porogen, and the porogen should be stable enough to survive the drying or curing process,

but should decompose during carbonisation, or be easily removed by solvent washing. Soft templates can be surfactants that form micelles, single molecules, small molecules that will self-assemble, or high molecular weight molecules such as dendrimers or polymers [111]. Polymer colloids such as poly(methyl methacrylate) (PMMA) and polystyrene colloids are often used as soft templates, and RF resins are commonly used as the carbon precursor. The polymeric templates can easily be removed with solvent washing or during carbonisation as reported for PMMA colloidal templates with RF carbon precursor where the template was removed by carbonisation up to 900 °C [112].

Surfactant assemblies have also been widely used in fabrication of carbon monoliths, where ampiphilic triblock copolymers and surfactants are used as soft templates and RF carbon precursors. Following thermal polymerisation of the RF precursor around the soft template, the template is removed and the remaining material carbonised to produce a mesoporous carbon, typically displaying 3-10 nm wide pores. Liang and Dai reported the preparation of a bimodal carbon monolith using a polymerisation-induced phase separation method for preparation of macroporous polymers. Bicontinuous macroporous morphologies with microdomains from 0.5-6 μm diameter were fabricated and the materials were subsequently carbonised to produce a meso-macroporous carbon monolith by decomposition of the triblock co-polymer soft template (poly(ethylene oxide)-poly(propylene oxide)-poly(ethylene oxide) [113]. Triblock co-polymers are often used as a template in carbon monolith synthesis in conjunction with RF resins, as similarly described by Huang *et. al.* in 2008 where two Pluronic® triblock co-polymers were used as double soft templates with RF as a carbon precursor, for a one-step base-catalysed hydrothermal polymerisation, resulting in a uniform distribution of ~3 nm mesopores with an irregular macroporous network [114]. Yuan and co-workers also demonstrated the synthesis of an ordered mesoporous carbon monolith using a Pluronic® triblock co-polymer and RF resin with a low temperature autoclave step at 50 °C over a period of 3 days [115]. Other methods of soft templating synthesis of carbon monoliths include

emulsion templating for preparation of templated porous polymers using a high internal phase emulsion along with carbon rich monomers that are then pyrolysed to produce porous carbon monoliths [116], or by ice templating where a suspension or emulsion is frozen, and the frozen solvent is removed by lyophilisation to produce a highly interconnected macroporous network [117-118].

The properties of carbon monoliths can be further tuned using a surface functionalisation approach to allow for improvements in the material at the bulk or interface level. This can be achieved through direct incorporation of heteroatoms in the synthesis step, activation or oxidation of the surface following synthesis, or attachment of moieties to the surface such as nanoparticles or polymer coatings [119]. The incorporation of non-carbonaceous nanoparticles into the framework of carbon monoliths during synthesis or as a post-synthesis modification has received considerable research interest. More recently, the addition of carbonaceous nanoparticles, specifically fullerenes, was explored as a route to tailor the carbon monolith's properties and has resulted in improved properties such as greater surface areas, more uniform pore size distributions, and changes in electrochemical performance [104]. With the effective preservation of the CNPs during the graphitisation step, there is likely to be a transfer of their unique properties to the composite monolith. The favourable properties associated with DND make it a promising candidate for inclusion in such a composite as outlined in Section 1.3.6.

1.5 Conclusions

Carbon is a remarkable element, with its unique electronic structure and size, allowing it to form various bonds with other carbon atoms leading to an array of interesting structures. A number of CNPs were introduced within this Chapter and there was a specific focus on DND, which has emerged in recent decades as an outstanding material in terms of its unique properties and potential applications. However, there is a great degree of variability associated with DND resulting from the different explosive precursors used in its synthesis and the different purification routes, as well as the diverse surface functionalities, particle sizes and and aggregation tendencies, all of which necessitate further attention from scientists. These issues must be addressed in order to ensure the continued success of DND-based applications, and in the case of composite materials specifically, a nano-filler should be aggregate-free and have a good colloidal stability. The biocompatibility, mechanical strength, thermal stability and conductivity, and large accessible surface area presenting readily tailorable functional groups of DND make it an exciting candidate for inclusion in composite materials. Its incorporation in the production of carbon on carbon composite materials is an area of research that has not yet been explored in great depth, but offers the potential for development of novel materials with exceptional properties.

1.6 Aims

The overall goal of this research was to investigate detonation nanodiamond (DND) as a nano-filler for synthesis of novel carbon on carbon composite monoliths. This required a prior understanding of the properties of DND such as their size, zeta potential, dispersibility, agglomeration tendencies and other variable aspects of this nanomaterial. Therefore, the following aims were identified towards achieving this goal:

- Characterise of a variety of DND materials from different sources and purification routes with the goal of improving understanding of their respective properties including colloidal stability, agglomeration tendencies, particle size distributions, zeta potentials and factors that affect the onset of agglomeration
- Explore strategies for the modification of DND surface chemistry through silanisation with the intention of producing a highly stable hydrophobic particle with reduced agglomeration, and to perform a detailed characterisation this newly functionalised DND material
- Select a DND nano-filler for incorporation in a porous graphitic carbon monolith, and explore the composite material's properties and potential application as an adsorbent material
- Characterise the effects of DND inclusion on the properties of the composite monoliths, with a particular focus on the thermal properties of DND and how they affect the material during pyrolysis

References

1. Chung, D.L. *Composite Materials: Science and Applications*, Springer-Verlag, London, 2010.
2. Hu, Y., Shenderova, O., Hu, Z., Padgett, C.W., Brenner, D.W. Carbon Nanostructures for Advanced Composites, *Rep. Prog. Phys*, 69 (2006) 1847-1895.
3. Barnard, A.S. Self-Assembly in Nanodiamond Agglutinates, *J. Mater Chem.* 18 (2008) 4038–4041.
4. Chang, L.-Y., Osawa, E., Barnard, A.S. Confirmation of the Electrostatic Self Assembly of Nanodiamonds, *Nanoscale* 3 (2011) 958–962.
5. Osswald, S., Yushin, G., Mochalin, V., Kucheyev, S.O., Gogotsi, Y. Control of sp2/sp3 Carbon Ratio and Surface Chemistry of Nanodiamond Powders by Selective Oxidation in Air, *J. Am. Chem. Soc.* 128 (2006) 11635-11642.
6. Setton, R., Bernier, P., Lefrant, S. Carbon Molecules and Materials, Taylor and Francis, London, 2002.
7. Kroto, H.W., Heath, J.R., O'Brien, S.C., Curl, R.F., Smalley, R.E. C_{60}: Buckminsterfullerene, Nature 318 (1985) 162-163.
8. Mauter, M.S., Elimelech, M. Environmental Applications of Carbon-Based Nanomaterials, *Environ. Sci. Technol.* 42 (2008) 5843–5859.
9. Bundy, F.P., Bassett, W.A., Weathers, M.S., Hemley, R.J., Mao, H.K., Goncharov, A.F. The Pressure–Temperature Phase and Transformation Diagram for Carbon; Updated Through 1994, *Carbon* 34 (1996) 141–53.
10. Shenderova, O.A., Zhirnov, V.V., Brenner, D.W. Carbon Nanostructures, *Crit. Rev. Sol. State Mater. Sci.* 27 (2002) 227-356.
11. Jiang, Q., Chen, Z.P., Thermodynamic Phase Stabilities of Nanocarbon, *Carbon* 44 (2006) 79-83.

12. Mochalin, V.M., Shenderova, O., Ho, D., Gogotsi, Y. The Properties and Applications of Nanodiamonds, *Nat. Nanotech.* 7 (2012) 11-23.
13. Danilenko, V.V. Synthesis, Properties and Applications of Ultrananocrystalline Diamond, D. Gruen, O. Shenderova, A. Vul' (Eds.) *Proceedings of NATO Advanced Research Workshop*, 181-198, Springer 2005.
14. Langa, F., Nierengarten, J.-F. *Fullerenes: Principles and Applications*, RSC Publishing, Cambridge, UK, 2007.
15. Akasaka, T., Nagase, S. *Endofullerenes: A New Family of Carbon Clusters*, Kluver Academic Publishers, Dordrecht, The Netherlands, 2002.
16. Yang, X., Ebrahami, A., Li, J., Cui, Q. Fullerene-Biomolecule Conjugates and their Biomedicinal Applications, Int. J. Nanomedicine, 9 (2014) 77-92.
17. Panchuk, R.R., Prylutska, S.V., Chumak, V.V., Skorokhyd, N.R., Lehka, L.V., Evstigneev, M.P., Prylutskyy, Yu.I., Berger, W., Heffeter, P. Scharff, P., Ritter, U., Stoika, R.S. Application of C60 Fullerene-Doxorubicin Complex for Tumour Cell Treatment *in vitro* and *in vivo*, *J. Biomed. Nanotechnol*. 11 (2015) 1139-1152.
18. Afreen, S., Muthoosamy, K., Manickam, S., Hashim, U. Functionalized Fullerene (C60) as a Potential Nanomediator in the Fabrication of Highly Sensitive Biosensors, *Biosens. Bioelectron.* 63 (2015) 354-364.
19. Xu, J.Z., Zhong, G.J., Hsiao, B.S., Fu, Q., Li, Z.M. Low-Dimensional Carbonaceous Nanofiller Induced Polymer Crystallization, *Prog. Polym. Sci*. 39 (2014) 555-593.
20. Lai, Y.Y., Cheng, Y.J., Hsu, C.S. Applications of Functional Fullerene Materials in Polymer Solar Cells, *Energy Environ. Sci.* 7 (2014) 1866-1883.
21. Novoselov, K.S., Geim, A.K., Morozov, S.V., Jiang, D., Zhang, Y., Dubonos, S.V., Grigorieva, I.V., Firsov, A.A. Electric Field Effect in Atomically Thin Carbon Films, *Science* 306 (2004) 666-669.

22. Allen, M.J., Tung, V.C., Kaner, R.B. Honeycomb Carbon: A Review of Graphene, *Chem. Rev.* 110 (2010) 132-145.

23. Subrahmanyam, K.S., Vivekchand, S.R.C., Govindaraj, A., Rao, C.N.R. A Study of Graphenes Prepared by Different Methods: Characterization, Properties and Solubilization, *J. Mater. Chem.* 18 (2008) 1517-1523.

24. Segal, M. Selling Graphene by the Ton, *Nature Nanotechnol*. 4 (2009) 612–614.

25. Novoselov, K.S., Fal'ko, V.I., Colombo, L., Gellert, P.R., Schwab, M.G., Kim, K. A Roadmap for Graphene, *Nature* 490 (2012) 192–200.

26. Iijima, S. Helical Microtubules of Graphitic Carbon, *Nature* 354 (1991) 56-58.

27. Dai, H., Wong, E.W., Lieber, C.M. Probing Electrical Transport in Nanomaterials: Conductivity of Individual Nanotubes, *Science* 272 (1996) 523-526.

28. Trojanowicz, M. Analytical Applications of Carbon Nanotubes: A Review, *TrAC* 25 (2006) 480-489.

29. Dai, L.M., Soundarrajan, P., Kim, T. Sensors and Sensor Arrays Based on Conjugated Polymers and Carbon Nanotubes. *Pure Appl. Chem.* 74 (2002) 1753-1772.

30. Herrera-Herrera, A.V., Gonzalez-Curbelo, M.A., Hernández-Borges, J., Rodríguez-Delgado, M.A. Carbon Nanotubes Applications in Separation Science: A Review, *Anal. Chim. Acta* 734 (2012) 1–30.

31. Ravelo-Pérez, L.M., Herrera-Herrera, A.V., Hernández-Borges, J., Rodríguez-Delgado, M.A. Carbon Nanotubes: Solid-Phase Extraction, *J. Chromatogr. A*. 1217 (2010) 2618-2641.

32. Krueger, A. The Structure and Reactivity of Nanoscale Diamond, *J. Mater. Chem.* 18 (2008) 1485-1492.

33. Danilenko, V.V. On the History of the Discovery of Nanodiamond Synthesis, *Phys. Solid State* 46 (2004) 595–599.

34. Dolmatov, V.Y., Veretennikova, M.V., Marchukov, V.A., Sushchev, V. G. Currently Available Methods of Industrial Nanodiamond Synthesis, *Phys. Solid State* 46 (2004) 611–615.

35. Shenderova, O.A., Vlasov, I. I., Turner, S., Van Tendeloo, G., Orlinskii, S.B., Shiryaev, A.A., Khomich, A.A., Sulyanov, S.N., Jelezko, F., Wrachtrup, J. Nitrogen Control in Nanodiamond Produced by Detonation Shock-Wave-Assisted Synthesis, *J. Phys. Chem. C* 115 (2011) 14014–14024.

36. Butler, J. E., Sumant, A.V. The CVD of Nanodiamond Materials, *Chem. Vap. Deposition* 14 (2008) 145–160.

37. Krueger, A. Diamond Nanoparticles: Jewels for Chemistry and Physics, *Adv. Mater.* 20 (2008) 2445–2449.

38. Ugarte, D. Curling and Closure of Graphitic Networks Under Electron-Beam Irradiation, *Nature* 359 (1992) 707-709.

39. Iijima, S. Direct Observation of the Tetrahedral Bonding in Graphitised Carbon Black by High Resolution Electron Microscopy, *J. Cryst. Growth* 50 (1980) 675-683.

40. Kuznetsov, V.L., Chuvilin, A.L., Butenko, Y.V., Malkov, I.Y., Titov, V.M. Onion-Like Carbon from Ultra-Disperse Diamond, *Chem. Phys. Lett.* 222 (1994) 343-348.

41. Banhart, F., Ajayan, P.M. Carbon Onions as Nanoscopic Pressure Cells for Diamond Formation, *Nature* 382 (1996) 433-435.

42. McDonough, J.K., Gogotsi, Y. Carbon onions: Synthesis and Electrochemical Applications, *Electrochem. Soc. Interface*, 3 (2013) 61-66.

43. Xu, N.S., Chen, J., Deng, S.Z. Effect of Heat Treatment on the Properties of Nano-Diamond Under Oxygen and Argon Ambient, *Diam. Relat. Mater*. 11 (2002) 249-256.

44. Butenko, Y., Krishnamurthy, S., Chakraborty, A., Kuznetsov, V. Dhanak, V., Hunt, M., Šiller, L. Photoemission Study of Onion Like Carbons Produced by Annealing Nanodiamonds, *Phys. Rev. B* 71 (2005) 075420.

45. Xu, Q., Zhao, X. Bucky-Diamond Versus Onion-Like Carbon: End of Graphitisation, *Phys. Rev. B* 86 (2012) 155417.

46. Portet, C., Yushin, G., Gogotsi, Y. Electrochemical Performance of Carbon Onions, Nanodiamonds, Carbon Black and Multiwalled Carbon Nanotubes in Electrical Double Layer Capacitors, *Carbon* 45 (2007) 2511-2518.

47. Shenderova, O. Jones, C., Borjanovic, V., Hens, S., Cunningham, G., Moseenkov, S., Kuznetsov, V., McGuire, G. Detonation Nanodiamond and Onion-Like Carbon: Applications in Composites, *Phys. Status Solidi A,* 205 (2008) 2245–2251.

48. Seymour, M.B., Su, C., Gao, Y. Lu, Y. Li, Y. Characterization of Carbon Nano-Onions for Heavy Metal Ion Remediation, *J. Nanopart. Res*. 14 (2012) 1087.

49. Shenderova, O.A., Gruen, D.M. *Ultrananocrystalline Diamond*, William Andrew Publishing, Norwich, N.Y. 2006.

50. Barnard, A.S. Theory and Modeling of Nanocarbon Phase Stability, *Diam. Relat. Mater.* 15 (2006) 285-291.

51. Petrov, I., Shenderova, O., Grishko, V. Grichko, V., Tyler, T., Cunningham, G. McGuire, G. Detonation Nanodiamonds Simultaneously Purified and Modified by Gas Treatment, *Diam. Relat. Mater.* 16 (2007) 2098–2103.

52. Mochalin, V., Osswald, S., Gogotsi, Y. Contribution of Functional Groups to the Raman Spectrum of Nanodiamond Powders, *Chem. Mater*. 21 (2009) 273–279.

53. Krueger, A., Lang, D. Functionality is key: Recent Progress in the Surface Modification of Nanodiamond, *Adv. Funct. Mater.* 22 (2012) 890–906.

54. Mitev, D.P., Townsend, A.T., Paull, B., Nesterenko, P.N. Microwave-Assisted Purification of Detonation Nanodiamond, *Diam. Relat. Mater.* 48 (2010) 37-46.

55. Kharisov, B.I., Kharissova, O.V., Cháávez-Guerrero, L. Synthesis Techniques, Properties and Applications of Nanodiamonds, *Synth. React. Inorg. M.* 40 (2010) 84-101.

56. Ozawa, M. Inakuma, M., Takahashi, M., Kataoka, F., Krueger, A., Osawa, E. Preparation and Behaviour of Brownish, Clear Nanodiamond Colloids, *Adv. Mater.* 19 (2007) 1201-1206.

57. Xu, Q., Zhao, X., Electrostatic Interactions Versus Van der Waals Interactions in the Self-Assembly of Dispersed Nanodiamonds, *J. Mater. Chem*. 22 (2012) 16416-16421.

58. Krueger, A., Kataoka, F., Ozawa, M., Fujino, T., Suzuki, Y., Aleksenskii, A.E., Vil, A.Y., Osawa, E. Unusually Tight Aggregation in Detonation Nanodiamond: Identification and Disintegration, *Carbon* 43 (2005) 1722-1730.

59. Liang, Y., Ozawa, M., Krueger, A. A General Procedure to Functionalise Agglomerating Nano Particles Demonstrated on Nanodiamond, *ACS Nano* 3 (2009) 2288-2296.

60. Pentecost, A., Gour, S., Mochalin, V., Knoke, I., Gogotsi, Y. Deagglomeration of Nanodiamond Powders Using Salt- and Sugar-Assisted Milling, *ACS Appl. Mater. Interfaces* 2 (2010) 3289-3294.

61. Xu, L., Xue, Q.J.A. New Method for Deaggregation of Nanodiamond from Explosive Detonation: Graphitization-Oxidation Method, *Phys. Solid State* 46 (2004) 649–650.

62. Williams, O.A., Hees, J., Dieker, C., Jäger, W., Kirste, L., Nebel, C.E. Size-Dependent Reactivity of Diamond Nanoparticles, *ACS Nano* 4 (2010) 4824–4830.

63. Larionova, I., Kuznetsov, V., Frolov, A., Shenderova, O., Moseenkov, S., Mazov, I. Properties of Individual Fractions of Detonation Nanodiamond, *Diam. Relat. Mater*. 15 (2006) 1804–1808.

64. Overbeek, J.T.G., Wiersema, P.H., in: Bier, M. (Ed.), *Electrophoresis: Theory, Methods and Applications*, Vol. II, Academic Press, New York 1967, 1-52.

65. Martín, R., Álvaro, M., Herance, J.R., García, H. Fenton-Treated Functionalized Diamond Nanoparticles as Gene Delivery System, *ACS Nano* 4 (2010) 65-74.

66. Krueger, A., Liang, Y., Jarre, G., Stegk, J. Surface Functionalisation of Detonation Nanodiamond Suitable for Biological Investigations, *J. Mater. Chem.* 16 (2006) 2322-2328.

67. Arnault, J.-C., Petit, T., Girard, H., Chavanne, A., Gesset, C., Sennour, M. Chaigneau, M. Surface Chemical Modifications and Surface Reactivity of Nanodiamonds Hydrogenated by CVD Plasma, *Phys. Chem. Chem. Phys*. 13 (2011) 11481.

68. Dolmatov, V.Y. Detonation Synthesis Ultradispersed Diamonds: Properties and Applications, *Russ. Chem. Rev.* 70 (2007) 607–626.

69. Li, Y., Zhou, X., Wang, D., Yang, B., Yang, P. Nanodiamond Mediated Delivery of Chemotherapeutic Drugs, *J. Mater. Chem*. 21 (2011) 16406-16412.

70. Zhu, Y., Li, J., Li, W., Zhang, Y., Yang, X., Chen, N., Sun, Y. Zhao, Y., Fan, C., Huang, Q. The Biocompatibility of Nanodiamonds and their Application in Drug Delivery Systems, *Theranostics* 2 (2012) 302–312.

71. Kong, X.L., Huang, L.C.L., Hsu, C.M., Chen, W.H., Han, C.C., Chang, H.C. High-Affinity Capture of Proteins by Diamond Nanoparticles for Mass Spectrometric Analysis, *Anal. Chem*. 77 (2005) 259–265.

72. Behler, K.D., Stravato, A., Mochalin, V., Korneva, G. Yushin, G., Gogotsi, Y. Nanodiamond-Polymer Composite Fibers and Coatings, *ACS Nano* 3 (2009) 363–369.

73. Mochalin, V. N., Neitzel, I., Etzold, B.J.M., Peterson, A., Palmese, G., Gogotsi, Y. Covalent Incorporation of Aminated Nanodiamond into an Epoxy Polymer Network, *ACS Nano* 5 (2011) 7494–7502.

74. Nietzel, I., Mochalin, V., Knoke, I., Palmese, G.R., Gogotsi, Y. Mechanical Properties of Epoxy Composites with High Contents of Nanodiamond, *Compos. Sci. Technol*. 71 (2011) 710-716.

75. Lee, J.Y., Lim, D.P., Lim, D.S. Tribological Behaviour of PTFE Nanocomposite Films Reinforced with Carbon Nanoparticles, *Composites B* 38 (2007) 810-816.

76. Shenderova, O., Jones, C., Borjanovic, V., Hens, S., Cunningham, G., Moseenkov, S., Kuznetsov, V., McGuire, G. Detonation Nanodiamond and Onion Like Carbon: Applications in Composites, *Phys. Stat. Sol. A* 205 (2008) 2245–2251.

77. Prasad, K.E., Das, B., Maitra, U. Ramamurty, U., Rao, C. Extraordinary Synergy in the Mechanical Properties of Polymer Matrix Composites Reinforced with 2 Nano Carbons *Proc. Natl. Acad. Sci.* 106 (2009) 13186–13189.

78. Vinokurov, E.G., Orlova, L.A., Stepko, A.A., Bondar, V.V. Synthesis and Properties of Inorganic Composite Coatings Containing Detonation Nanodiamonds, *Prot. Met. Phys. Chem. Surf.* 50 (2014) 480–483.

79. Ostrovidova, G.U., Makeev, A.V., Biryukov, A.V., Gordeev, S.K. Carbon Nanocomposite Materials as Medicinal Depot, *Mater. Sci. Eng. C* 23 (2003) 377–381.

80. Gordeev, S.K. Carbon Nano Structured Drug Containers Based on a Nanodiamond Composite Material, Met, *Sci. Heat. Treat*. 56 (2015) 559–563.

81. Kiselev, N.I., Velikanov, D.A., Korchagina, S.B., Petrakovskaya, E.A., Vasil'ev, A.D., Solov'ev, L.A., Balaev, D.A., Bayukov, O.A., Denisov, I.A., Tsegel'nik, S.S., Eremin, E.V., Znak, D.A., Shaikhutdinov, K.A., Shubin, A.A., Shestakov, N.P., Volkov, N.V., Gordeev, S.K., Belobrov, P.I. Electrical and Magnetic Properties of Nanodiamond and Pyrocarbon Composites, *Russ. J. Gen. Chem*. 83 (2013) 2173–2181.

82. Gordeev, S.K., Konopleva, R.F., Chekanov, V.A., Korchagina, S.B., Belyaev, S.P., Golosovskii, I.V., Denisov, I.A., Belobrov, P.I. Specific Features in the Change of Electrical Resistivity of Carbon Nanocomposites Based on Nanodiamonds Under Neutron Irradiation, *Phys. Solid State* 55 (2013) 1480–1486.

83. Zhao, F., Liu, R., Yu, X., Ding, H., Qu, X., Zhang, Q. Carbon Fiber Grafted with Nanodiamond: Preparation and Characterisation, *J. Nanosci. Nanotechnol*. 15 (2015) 5807-5815.

84. Terranova, M.L., Orlanducci, S., Fiori, A., Tamburri, E., Sessa, V., Rossi, M., Barnard, A.S. Controlled Evolution of Carbon Nanotubes Coated by Nanodiamond: The Realisation of a New Class of Hybrid Nanomaterials, *Chem. Mater.* 17 (2005) 3214–3220.

85. Varga, M., Vretenar, V., Izak, T., Skakalova, V., Kromka, A. Carbon Nanotubes Overgrown and Ingrown with Nano Crystalline Diamond Deposited by Different CVD Plasma Systems, *Phys. Stat. Sol. B* 251 (2014) 2413–2419.

86. Wang, Q., Pylahan, N., Shelke, M.V., Deverapalli, R.R., Li, M., Subramanian, P., Djenizian, T., Boukherroub, R., Szunerits, S. Nanodiamond Particles/Reduced Graphene Oxide Composites as Efficient Supercapacitor Electrodes, *Carbon* 68 (2014) 175-184.

87. Sun, Y., Wu, Q., Xu, Y., Bai, H., Li, C., Shi, G. Highly Conductive and Flexible Mesoporous Graphitic Films Prepared by Graphitizing the Composites of Graphene Oxide and Nanodiamond, *J. Mater. Chem*. 21 (2011) 7154-7160.

88. Lowell, S., Shields, J.E., Thomas, M.A., Thommes, M. *Characterization of Porous Solids and Powders: Surface Area, Pore Size and Density*. Kluwer Academic Publishers, London, 2004.

89. Sing, K.S., Everett, D.H., Haul, R.A.W., Moscou, L., Pierotti, R.A., Rouquérol, J., Siemieniewska, T. Reporting Physisorption Data for Gas/Solid Systems, *Pure Appl. Chem.* 57 (1985) 603–619.

90. Ruo-wen, F.U., Zheng-hui, L.I., Ye-ru, L., Feng, L.I., Fei, X.U., Ding-cai, W.U. Hierarchical Porous Carbons: Design, Preparation and Performance in Energy Storage, *New Carbon Mater.* 26 (2011) 171–179.

91. Dutta, S., Bhaumik, A., Wu, K.C.-W. Hierarchically Porous Carbon Derived from Polymers and Biomass: Effect of Interconnected Pores on Energy Applications, *Energy Environ. Sci*. 7 (2014) 3574–3592.

92. Sevilla, M., Fuertes, A.B. Sustainable Porous Carbons with a Superior Performance for CO2 Capture, *Energy Environ. Sci*. 4 (2011) 1765-1771.

93. Gupta, V.K., Saleh, T.A. Sorption of Pollutants by Porous Carbon, Carbon Nanotubes and Fullerene - An Overview, *Environ. Sci. Pollut. Res*. 20 (2013) 2828–2843.

94. Garcia-Gomez, A., Miles, P., Centeno, T.A., Rojo, J.M., Why Carbon Monoliths are Better Supercapacitor Electrodes than Compacted Pellets, *Electrochem. Solid State Lett.* 13 (2010) 112-114.

95. Sevilla, M., Fuertes, A.B., Fabrication of Porous Carbon Monoliths with a Graphitic Framework, *Carbon* 56 (2013) 155-166.

96. Švec, F., Tennikova, T.K., Deyl, Z. (Eds.), *Monolithic Materials, Preparation, Properties and Applications*, Elsevier, The Netherlands, 2003.

97. Švec, F., Porous Polymer Monoliths: Amazingly Wide Variety of Techniques Enabling their Preparation, *J. Chromatogr. A* 1217 (2010) 902-924.

98. Guichon G., Monolithic Columns in High-Performance Liquid Chromatography, *J. Chromatogr. A* 1168 (2007) 101-168.

99. Roberts, A.D., Li, X., Zhang, H. Porous Carbon Spheres and Monoliths: Morphology Control, Pore Size Tuning and their Applications as Li-Anode Battery Materials, *Chem. Soc. Rev.* 43 (2014) 4341-4356.

100. Liang, C., Dai, S., Guiochon, G. A Graphitized-Carbon Monolithic Column, *Anal. Chem.* 75 (2003) 4904–4912.

101. Eltmimi, A.H., Barron, L., Rafferty, A., Hanrahan, J.P., Fedyanina, O., Nesterenko, E., Nesterenko, P.N., Paull, B. Preparation, Characterisation and Modification of Carbon-Based Monolithic Rods for Chromatographic Applications, *J. Sep. Sci*. 33 (2010) 1231–1243.

102. He, X., Nesterenko, E.P., Nesterenko, P.N., Paull, B., Omamogho, J., Glennon, J.D., Luong, J.H.T. Porous Graphitized Carbon Monolith as an Electrode Material for Probing Direct

Bioelectrochemistry and Selective Detection of Hydrogen Peroxide, *Anal. Chem*. 84 (2012) 2351-2357.

103. He, X., Male, K.B., Nesterenko, P.N., Brabazon, D., Paull, B., Luong, J.H.T. Adsorption and Desorption of Methylene Blue on Porous Carbon Monoliths and Nanocrystalline Cellulose, *ACS Appl. Mater. Interfaces* 5 (2013) 8796–8804.

104. He, X., Nesterenko, E.P., Nesterenko, P.N., Brabazon, D., Zhou, L., Glennon, J.D., Luong, J.H.T., Paull, B. Fabrication and Characterization of Nanotemplated Carbon Monolithic Material, *ACS Appl. Mater. Interfaces* 5 (2013) 8572-8580.

105. Knox, J.H., Gilbert, M.T. US Patent 4263268, 1979.

106. Taguchi, A., Smått, J.H., Lindén, M. Carbon Monoliths Possessing a Hierarchical Fully Interconnected Porosity, *Adv. Mater.* 15 (2003) 1209-1211.

107. Shi, Z.G., Feng, Y.Q., Xu, L., Da, S.L., Zhang, M., Synthesis of a Carbon Monolith with Trimodal Pores, *Carbon* 41 (2003) 2677-2679.

108. , Liu, A.-H., Zhao, D., Wan, Y. (Eds.), *Nanocasting: A Versatile Strategy for Creating Nanostructured Porous Materials*, RSC Publishing, UK, 2010.

109. Stein, A., Li, F., Denny, N.R., Morphological Control in Colloidal Crystal Templating of Inverse Opals, Hierarchical Structures and Shaped Particles, *Chem. Mater*. 20 (2007) 649-666.

110. Ma, T.-Y., Liu, L., Yuan, Z.-Y. Direct Synthesis of Ordered Mesoporous Carbons, *Chem. Soc. Rev.* 42 (2013) 3977-4003.

111. Pal, N., Bhaumik, A., Soft Templating Strategies for the Synthesis of Mesoporous Materials: Inorganic, Organic-Inorganic Hybrid and Purely Organic Solids, *Adv. Coll. Interface Sci.* 189-190 (2013) 21-41.

112. Vu, A., Qian Y., Stein, A., Porous Electrode Materials for Lithium-Ion Batteries – How to Prepare Them and What Makes Them Special, *Adv. Energy Mater*. 2 (2012) 1056–1085.

113. Liang, C., Dai, S., Dual Phase Separation for Synthesis of Bimodal Meso-/Macroporous Carbon Monoliths, *Chem. Mater.* 21 (2009) 2115-2124.

114. Huang, Y., Cai, H., Feng, D., Gu, D., Deng, Y., Tb, B., Wang, H., Webley, P.A., Zhao, D., One-Step Hydrothermal Synthesis of Ordered Mesostructured Carbonaceous Monoliths with Hierarchical Porosities, *Chem. Comm*. (2008) 2641-2643.

115. Liu, L., Wang, F.Y., Shao, G.S., Yuan, Z.-Y., A Low Temperature Autoclaving Route to Synthesize Monolithic Carbon Materials with an Ordered Mesostructure, *Carbon* 48 (2010) 2089-2099.

116. Asfaw, H.D., Roberts, M.R., Tai, C.-W., Younesi R., Valvo, M., Nyholm, L., Edström, K. Nanosized $LiFePO_4$-Decorated Emulsion-Templated Carbon Foam for 3D Micro Batteries: A Study of Structure and Electrochemical Performance, *J. Mater. Chem. A* 1 (2013) 13750–13758.

117. Qian L., Zhang, H., Controlled Freezing and Freeze Drying: A Versatile Route for Porous and Micro-/Nano-Structured Materials*, J. Chem. Technol. Biotechnol*. 86 (2011) 172–184.

118. Qiu, L., Liu, J.Z., Chang, S.L.Y., Wu Y., Li, D., Biomimetic Superelastic Graphene-Based Cellular Monoliths, *Nat. Commun*. 3 (2012) 1–7.

119. Stein, A., Wang, Z., Fierke, M.A., Functionalization of Porous Carbon Materials with Designed Pore Architecture, *Adv. Mater.* 21 (2009) 265-293.

Chapter 2.

Separation and Characterisation of Detonation Nanodiamond by Capillary Zone Electrophoresis

This chapter has been removed for copyright or proprietary reasons.

Published as: Duffy, E., Mitev, D. P., Nesterenko, P. N., Kazarian, A. A., Paull, B., 2014. Separation and characterisation of detonation nanodiamond by capillary zone electrophoresis. Electrophoresis, 35 (12-13), 1864-1872

Chapter 3.

Assessing the Extent, Stability, Purity and Properties of Silanised Detonation Nanodiamond

Abstract

The functionalisation of nanodiamond is a key step in furthering its application in areas such as surface coatings, drug delivery, bio-imaging and other biomedical avenues. Accordingly, analytical methods for the detailed characterisation of functionalised nano-materials are of great importance. This work presents an approach for the elemental analysis of zero-dimensional nanocarbons, specifically detonation nanodiamond (DND) following purification and functionalisation procedures. There is a particular emphasis on the presence of silicon, both for the purified DND, and after its functionalisation with silanes. Five different silylation procedures for purified DND were explored and assessed quantitatively using inductively coupled plasma-mass spectrometry (ICP-MS) for analysis of dilute suspensions. A maximum Si loading of 29,300 μg/g on the DND was achieved through a combination of two silylating reagents. The presence of 28 other elements in the DND materials was also quantified by ICP-MS. The characterisation of Si-O bond formation was supported by an FTIR evaluation of relevant functional groups. The thermal stability of the silylated DND was examined by thermogravimetric analysis. Improved particle size distribution and dispersion stability resulted from the silylation procedure, as confirmed by dynamic light scattering and capillary zone electrophoresis.

3.1 Introduction

There is a growing interest in the properties and applications of ultra-dispersed matter, specifically nanodiamonds (ND), which are produced by a variety of synthetic methods. Some popular production methods include cavitation and laser production, chemical vapour deposition, crushed high-pressure high-temperature (HPHT) diamond, and detonation synthesis for the production of detonation nanodiamond (DND) [1]. The method of production can have a significant impact on the resultant diamond's properties, and DND is known to have higher impurity levels than those present in other synthetically derived diamonds [2]. The type and level of impurities present in DND can vary dramatically, as they depend on both the production and purification methods utilised [3].

DND has shown significant promise for application in a wide variety of areas, including materials synthesis within polymer and carbon-based nano-composites [4-6], coating technologies [7], separation science/chromatography [8], and biomedical applications such as drug delivery and bio-imaging [9-12]. The purity of DND is of the utmost importance in biomedical applications due to the ultimate goal of using these nanoparticles in human patients. It is therefore vital that reliable methods of elemental analysis and evaluation for DND are available. Furthermore, the control of DND surface properties and functionalities will be a key step in ensuring their continued progress in real world applications. It is imperative that there is full understanding and control over the surface chemistry of DND to allow its dispersion in solvents, or bonding to solid matrices, while simultaneously preventing the problem of agglomeration. Silylation can be very useful as a tool to tailor diamond nanoparticles for use as composite ingredients [13-15], or to adjust the surface properties of prospective diamond-based sorbents for chromatography [8, 16-17]. It offers a method for surface homogenisation prior to conjugation with biomolecules for bio-applications. It is important to note that the de-agglomeration of primary DND particles is critical before proceeding with surface modification, and silylation has proven to be an effective route to enhance dispersion

stability and reduce aggregate size as demonstrated by Krueger *et. al.* where the silylation of nanodiamond with (3-aminopropyl)trimethoxysilane and further with biotin was carried out for biological applications including labeling and drug delivery [18]. Liang *et. al* utilised 3-acryloxypropyl(trimethoxysilane) in combination with beads-assisted sonication for improving dispersion quality and stability [19]. Jeong *et. al.* also reported on the silylation of ND for improving dispersion stability, prior to its inclusion in development of transparent composites where aggregate size directly affected the composite material's performance [20]. Dolmatov described a silylation procedure for nanodiamonds aimed at composites based on elastomer and polymer matrices, however there was no characterisation of the actual degree of silylation in the ND materials produced [21].

In the preparation of such stabilised, homogenised or modified particles, it is also vital that there are reliable characterisation methods allowing an understanding of the surface chemistry and impurities present in DND, as well as evaluating the stability of such particles under different conditions. Until as recently as 2013, there was a lack of comprehensive information on the presence of metal and non-carbon impurities in DND as a whole [22]. Controlling and quantifying the heteroatom content in DND is a key step towards fully understanding and ensuring a high degree of purity before applying this variable material. There was an absence of suitable reliable analytical methods for this specific nanocarbon; an issue that was recently addressed in our laboratories. The direct aspiration of very dilute DND suspensions into a sector field inductively coupled plasma mass spectrometer (ICP-MS) has proven to be a reliable and sensitive method for the determination of impurities in DND [22-23]. Herein we demonstrate the application of this method to the quantification of purposefully introduced elements (like silicon) to the surface of DND. This analysis was performed on silylated DND, Si-contaminated DND, and purified DND, in order to clearly assess the extent of silylation achieved. While this method requires expensive instrumentation and experienced operators, it is relatively fast and reduces the reliance on more

time-consuming and less informative methods such as thermogravimetric analysis (TGA), FTIR, and others [24-26], which are generally better suited to qualitative rather than quantitative characterisation. In this instance, TGA and FTIR were used to further characterise the surface chemistry and thermal stability of the modified DND. In addition, the stability of modified DND was investigated using capillary zone electrophoresis (CZE), which has proven to be an informative technique with regard to nanoparticle size distributions, dispersion quality, which is reflected in the peak shape obtained by a voltage-induced separation [27].

3.2 Experimental Methods

3.2.1 Materials and Reagents

The DND was obtained from YTM ARGE A.S. (Istanbul, Turkey; product code NDG.11.02.28.01). Additionally, raw detonation soot (DS) was supplied by the same producer; in the form of a black-coloured powder. A 1% w/v aqueous suspension of the DS had a pH of 9.43.

Milli-Q® deionised water (Millipore, Bedford, MA, USA) with resistivity 18.5 MΩ.cm (at 25 °C) was used throughout this work. All reagents used were of analytical grade quality: 95-97% sulfuric acid, 48% hydrofluoric acid, and 70% nitric acid were all obtained from Chem-Supply, Gillman, SA, Australia. In addition, 37% hydrochloric acid from Merck, Kilsyth, Australia, and 70% perchloric acid from Univar, Ingleburn, Australia were used. The silylation reagents: trimethylchlorosilane (TMCS), dimethyloctadecylchlorosilane (DMODCS), hexamethyldisilazane (HMDS), and toluene were of analytical grade quality, and were purchased from Sigma Aldrich, Castle Hill, NSW, Australia. Sodium tetraborate (99.998%) and NaOH were used in the preparation of background electrolytes (BGE) for CZE, and were also obtained from Sigma Aldrich, Castle Hill, NSW, Australia. Buffers were prepared by dilution of a stock solution of sodium tetraborate, and the pH was adjusted using 1 *M* NaOH.

3.2.2 Modification of Detonation Nanodiamond

3.2.2.1 Initial Purification Procedures

The raw DS obtained from YTM ARGE A.S. had been purified by the supplier prior to shipment, whereby a sulphuric acid/potassium dichromate wet graphite digestion method was utilised [19]. This material was additionally purified on-site using a procedure previously described by our research group [28] for preparation of NSFPA type of purified DND. Briefly, NSFPA was purified from the DS using acidic oxidation with a mixture of nitric, sulphuric, perchloric and hydrofluoric acids (where % ratio was 44:44:6:6). Subsequent washing steps were performed to reduce the digested impurities and residual acids. It is important to note that Si contamination of DND can occur through everyday processing of DND materials in borosilicate glassware [28] and as a precaution, special attention was paid to handling procedures for DND within this study wherein only polypropylene containers were used for storage of DND samples.

3.2.2.2 Hydrophobisation of Detonation Nanodiamond Using Silanisation

The NSFPA type of purified DND was used in all experiments on hydrophobisation.

Sample 1

0.451 g of DND, and 5 mL TMCS were added to 45 mL of wet toluene in a triple-neck flat-bottomed flask. The reaction was kept under constant magnetic stirring and the reaction flask was fitted with a reflux condenser and a thermometer. The temperature was set to 103 °C, at which time an additional 1 mL of TMCS was added to the flask. The mixture was then stirred at 103 °C for 21 hours. 2 mL of TMCS and 2 mL pyridine were then added to the reaction flask, and the reaction was allowed to continue for a further 5 hours.

Sample 2

DND was firstly dried under vacuum at 400 °C overnight. Then 0.218 g of dried DND and 0.207 g DMODCS were added to 50 mL of anhydrous toluene in a triple-neck flat-bottomed flask.

The reaction flask was fitted with a reflux condenser and a thermometer, as above, and was kept under constant magnetic stirring. The temperature was then set to 100 °C, at which time an additional 0.313 g DMODCS dissolved in 5 mL of toluene was added. The reaction mixture was refluxed under stirring for 19 hours.

Sample 3

0.264 g of dried DND (vacuum dried, 400 °C overnight), 4 mL of HMDS and 8 mL of TMCS were added to 188 mL of anhydrous toluene in a triple-neck flat-bottomed flask. The reaction mixture was refluxed under magnetic stirring for 19 hours.

Sample 4

0.189 g of dried DND (vacuum dried, 400 °C overnight), 0.534 g DMODCS and 2.2 mL of HMDS were added to 58 mL anhydrous toluene in a triple-neck flat-bottomed flask. The reaction mixture was held under the same conditions as described above for Sample 3.

Sample 5

0.220 g of dried DND (vacuum dried, 400 °C overnight) and 10 mL TMCS were added to 50 mL anhydrous toluene in a triple-neck flat-bottomed flask. The reaction mixture was held under the same conditions as described above for Sample 3.

3.2.3 Instrumentation

An Element 2 sector field ICP-MS spectrometer (Thermo Fisher, Bremen, Germany) was employed for ICP-MS analysis of DND. Aqueous suspensions of DND were diluted to 0.1 mg g^{-1} prior to direct analysis by ICP-MS according to the procedure described in [22]. This approach was applied for multi-element detection, and results are reported for elements that were present in DND at concentrations higher than 10^{-5} mass % in the dry DND, or 10^{-8} mass % in suspension. Multiple spectral resolutions were employed to allow commonly encountered polyatomic interferences to be

clearly resolved from analytes of interest. We note that non-metal impurities like O, N and Cl are excluded from consideration here, as they are not quantifiable by ICP-MS.

Surface area measurements were performed using a surface area analyser (Tristar II 3020, Micromeritics, Gemini, GA, USA) by the nitrogen adsorption/desorption method.

FTIR analysis was performed using a Spectrum 100 FT-IR Spectrometer fitted with Universal ATR Accessory (PerkinElmer, Waltham Massachusetts, USA). The scanning range was 650-4000 cm^{-1} and the resolution was 1 cm^{-1}.

A Zetasizer Nano ZS particle analyser (ATA Scientific, Taren Point, NSW, Australia) fitted with 632.8 nm red laser and 175 ° backscatter detector was used to estimate zeta potential and particle size distributions of derived samples. DND suspensions in isopropanol and water were analysed after 1 minute of sonication in an ultrasonic bath (Bransonic 5510E-DTH, Branson, Danbury, USA).

TGA data were obtained with a Labsys Evo instrument (Setaram, Caluire, France) under nitrogen flow (50 mL/min). DND samples were placed in alumina crucibles for analysis, where a heating rate of 2.5 °C/min was applied from 30 to 900 °C. CZE experiments were performed on an Agilent 7100 CE system (Agilent Technologies, Germany) equipped with a photodiode array detector. Adsorption was monitored at 230 nm at a data acquisition rate of 40 Hz. All reported results were obtained in triplicate. Fused silica capillaries (Polymicro, Phoenix, AZ, USA) with 75 μm i.d., 365 μm o.d. were used, with a total capillary length of 32.5 cm. Detection windows were burned 8.5 cm from the capillary end using a butane torch. Pre-conditioning of capillaries was performed using 1 *M* NaOH (15 min flush), followed by water (10 min) and finally with BGE (10 min). DND suspensions of 0.125 mg/mL were injected for 5 s at 5 kPa, and separated under an applied potential of +5 kV.

3.3 Results and Discussion

3.3.1 Purification and Refinement of Detonation Nanodiamond

It is important to consider the possible presence of impurities in DND materials, prior to modification of their surface, or incorporation into other materials. Ensuring an effective purification, and stable DND dispersion ensures reproducible functionalisation of DND for applications in biomedicine and composite materials. The presence of Si and other non-carbon impurities were assessed by ICP-MS, with the quantitative findings shown in Figure 3.1. As a consequence of the dichromate/acid-based purification that had been carried out on the YTM material prior to receiving it, this DND product was abundantly rich in impurities with an Si-level of 2870 μg/g for the sample in suspension (Figure 3.1). Prior to the controlled silylation of DND particles, a refinement procedure was applied to the materials to ensure contributions from Si impurities were minimised. Conventional handling of DND materials during production procedures and everyday laboratory work can actually significantly increase their Si-content [28]. Following the refinement procedure, the Si content was reduced to only 2.2 μg/g (Figure 3.1). The Brunauer-Emmett Teller (BET) surface area for DND materials was calculated from the nitrogen adsorption isotherms. This was found to be 260 ± 5 m^2/g for YTM. A higher surface area of 287 ± 8 m^2/g was obtained for the NSFPA treated DND which underwent additional purification resulting in further removal of surface impurities, and a reduction in contamination levels up to a factor of 6.5 [28]. Elevated Al and S contents for the refined DND were suggested to result from contaminated acid.

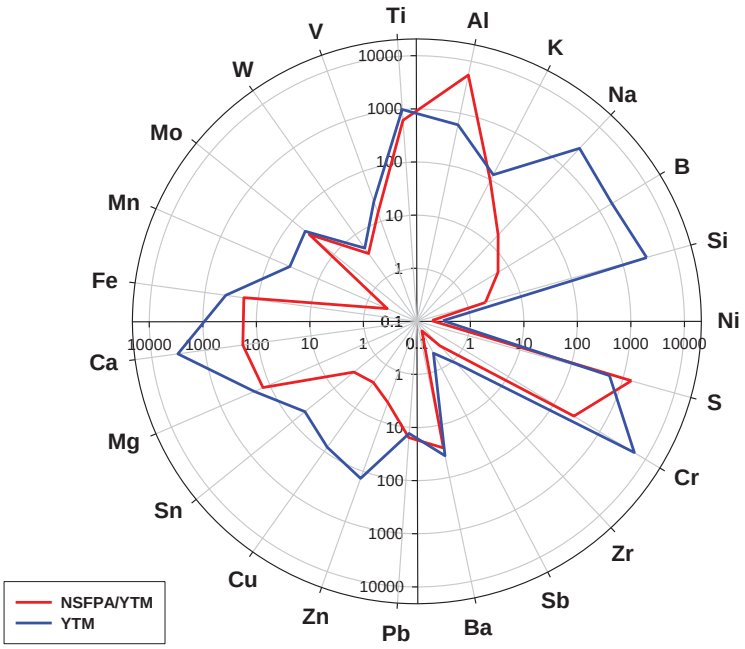

Figure 3.1 Impurity contents (µg/g, logarithmic scale) in the samples of commercial DND as received from YTM ARGE A.S. and after purification using NSFPA protocol (initial purification procedure as described in Experimental methods) [28].

3.3.2 Silylation

Surface hydroxyl and carboxyl groups of DND may be successfully derivatised by silylation, as is similarly performed on a range of chemical compounds, glass, silica and other surfaces. The application of the ICP-MS characterisation method [22] provided valuable quantitative information for comparison of the effectiveness of the different silylating agents, and their corresponding effects on DND impurity levels.

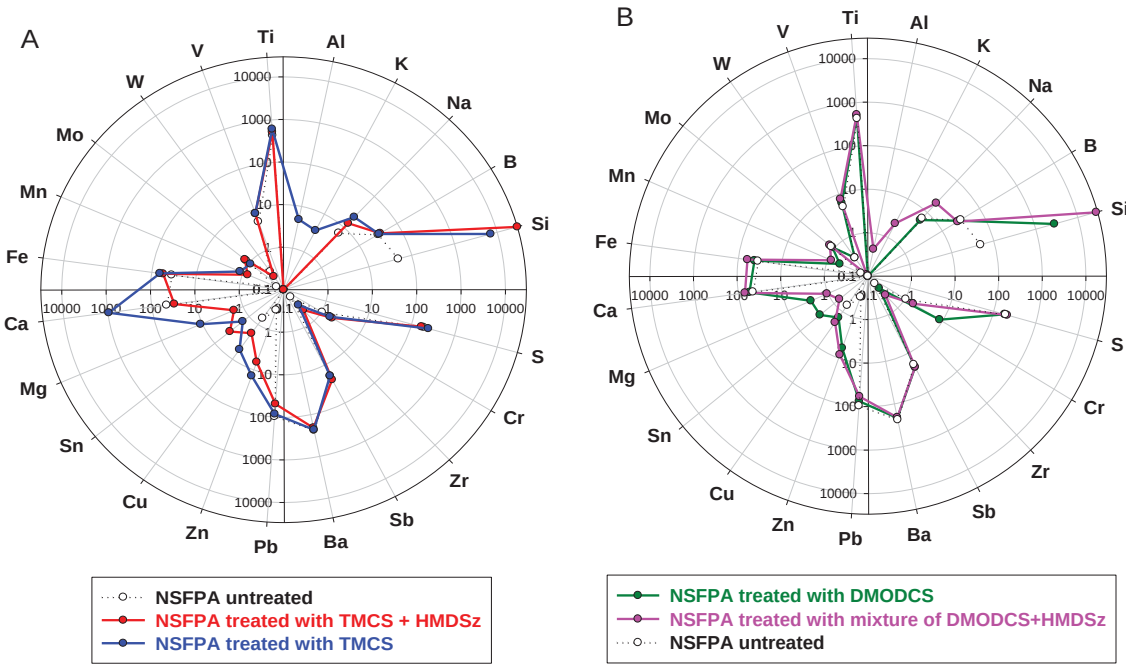

Figure 3.2 Composition of minor elements (µg/g, logarithmic scale) of original DND type NSFPA and the silylated products.

Silylation is highly sensitive to the presence of moisture in the reaction mixture. DND is a hygroscopic material (dry DND kept in air can retain up to 4.1% of water) [29], so all samples were dried under vacuum at 400 °C overnight prior to silylation. As a demonstration, the "as-stored" DND and toluene were not subjected to any drying steps to eliminate moisture (procedure outlined for Sample 1 above). The presence of moisture in toluene prevented silylation of the DND sample, despite the addition of pyridine which serves as a proton acceptor to base catalyse the silylation reaction [30]. The results shown in Figure 3.2 reveal that without an initial drying step, Sample 1 (TMCS treated) only showed a 5-fold increase in Si content up to 212 µg/g compared to the 48 µg/g originally found in the precursor DND (Table 3.1). There was a significant increase in the Si content to 7020 µg/g recorded for Sample 5, which was dried under vacuum at 400 °C overnight, and silylated with a higher concentration of TMCS in toluene dried over silica gel (see Figure 3.2(B)). This was achieved in the absence of organic bases, which are normally used to catalyse the

silylation reaction by absorbing HCl produced by the reaction, as shown in Equations 3.1-3.2. Other elemental impurities also present in the DND after each treatment were determined and are shown in Table 3.1. The addition of HMDS to the reaction (Sample 3) enhanced the degree of silylation on DND, and is related to the production of ammonia by the reaction described in Equation 3.4. This ammonia neutralises HCl produced by the reaction between TMCS and the protogenic groups at the surface of DND, (Equation 3.1-3.2). The Si-content increased dramatically to 29,300 μg/g in Sample 4, realising an increase of over 610 times as compared to the original DND.

Equation 3.1 $\equiv C\text{-}OH + ClSi(CH_3)_3 \rightarrow \equiv C\text{-}O\text{-}Si(CH_3)_3 + HCl\uparrow$

Equation 3.2 $\equiv C\text{-}C(=O)OH + ClSi(CH_3)_3 \rightarrow \text{-}C(=O)\text{-}O\text{-}Si(CH_3)_3 + HCl\uparrow$

Equation 3.3 $\equiv C\text{-}NHR + ClSi(CH_3)_3 \rightarrow \text{-}C\text{-}N^{+}HRSi(CH_3)_3\ Cl^{-}$

Equation 3.4 $2\equiv C\text{-}OH + (CH_3)_3SiNHSi(CH_3)_3 \rightarrow 2\equiv C\text{-}O\text{-}Si(CH_3)_3 + NH_3\uparrow$

(Where ≡C-OH, ≡C-C(=O)OH and ≡C-NHR are protogenic functional groups at the surface of DND).

A similar result was obtained when using another derivatisation reagent DMODCS, instead of TMCS. When applied as the sole silylating agent upon vacuum-dried DND in dry toluene, a significant increase in the Si-content to a level of 2770 μg/g was observed in Sample 2, which is 58 times higher than in NSFPA type DND. However, when DMODCS was combined with HMDS, it resulted in a further increase in Si content up to 27,400 μg/g, i.e. 570 times, as was similarly observed for the combination of silylating reagents discussed above for Sample 3. The maximum DND surface coating of 0.88 - 0.95 mmol/g, as calculated from the increase in Si-content after silylation, is 2-3 times higher than the coating of 0.3 - 0.4 mmol/g reported for the hydrophobic DND samples prepared by esterification with alkanoic acid chlorides [31].

It should be noted that serious contamination of DND by Si is possible during everyday processing of DND in glassware [28]. Figure 3.3 shows the kinetic of accumulation of Si during storage of aqueous suspension of DND in deionised water in borosilicate glassware (for both the DND suspension, and the water after filtration of the suspension) due to exposure to the glass. The maximum contamination could be as high as 2 - 3 mg/g as compared with 47 μg/g detected in NSFPA type DND. Special precautions were taken during modification processes of DND within this work as described in the purification and modification procedures.

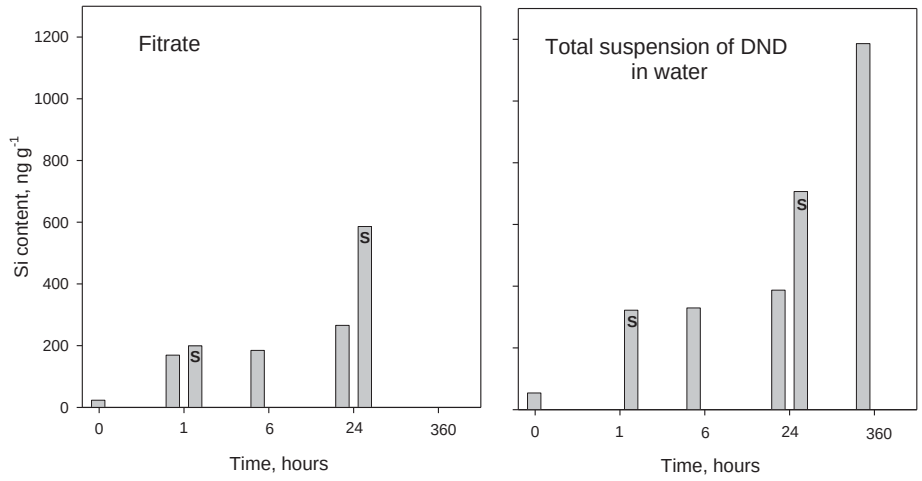

Figure 3.3 Kinetics of contamination of NSFPA by Si during storage (of aqueous suspension of DND (0.66 mg/g) and filtrate of the same DND suspension) in borosilicate laboratory glassware (S means sonication was applied to sample). Adapted from [28].

Table 3.1 Elemental concentrations* in dry DND samples by ICP-MS (μg/g)

	Sample						
	-	-	(1)	(5)	(2)	(4)	(3)
Element[a]	NSFPA	YTM powder	TMCS	TMCS	DMODCS	DMODCS +HMDS	TMCS +HMDS
B	31.1	6.4	36.8	32.8	28.1	25.6	35.3
Sr	0.1	9.1	0.3	1.0	0.2	0.2	0.2
Zr	0.2	0.5	0.3	0.3	0.2	0.4	0.5
Mo	1.2	44.3	1.9	0.9	1.1	1.4	1.3
Sn	0.0	36.9	1.4	1.5	2.6	0.7	3.6
Sb	19.3	0.4	28.2	19.0	22.7	22.5	24.0
Ba	234	49.9	238	229	214	208	206
W	0.3	4.0	0.7	0.1	0.3	0.1	0.2
Pb	96.5	11.3	81.9	84.5	76.3	59.3	49.1
Bi	0.0	0.1	0.0	0.0	0.0	0.0	0.0
Na	6.6	244	30.0	21.5	5.8	19.8	13.6
Mg	0.0	264	6.0	10.9	2.7	1.1	1.7
Al	0.0	460	8.3	4.8	0.0	0.4	0.0
Si	48.0	1430	212	7020	2770	27,400	29,230
P	0.0	3.5	0.4	5.1	0.0	3.0	0.7
S	189	764	254	244	180	208	168
Ca	45.5	3020	64.4	942[b]	54.9	69.7	30
Sc	0.0	0.0	0.0	0.0	0.0	0.0	0.0
Ti	429	1280	571	605	488	524	520
V	5.0	27.7	7.5	8.0	6.1	7.5	7.9
Cr	1.0	5110	1.5	1.7	8.5	1.7	1.9
Mn	0.2	49.3	0.6	1.2	0.5	0.8	0.8

Fe	35.0	328	41.8	64.9	41.9	60.9	54.6
Co[c]	0.0	0.3	0.1	277	655	950	888
Ni	0.0	3.4	0.2	0.0	0.8	1.4	0.9
Cu	0.7	74.9	1.9	5.2	1.5	2.0	1.8
Zn	0.3	61.9	32.1	14.0	5.7	8.3	6.4
K	0.0	207	0.0	3.7	0.0	2.3	0.0
As	0.0	0.0	0.0	0.0	0.0	0.0	0.0
Total	1142	13480	1621	9593	4565	29560	31310

* - excluding O, N, Cl *etc*. not determined by ICP-MS

a - in the order of instrument measurement

b - contamination of the sample

c - elevated concentration of Co in silylated DND originates from the silica gel used for drying of toluene, namely the “blue→red” moisture indicator)

3.3.3 Infrared Spectroscopy of Silylated Detonation Nanodiamonds

FTIR was used to further confirm derivatisation of the DND surface. Figure 3.4 shows several characteristic absorbance bands in the spectra of the purified and silylated DNDs. The line at 848 cm^{-1} is associated with rocking vibrations of CH_2-groups [32], and can also be linked directly with the Si-CH_3 moiety [33]. There was a gradual increase of hydrocarbon groups as the extent of silylation increased (samples 5→4→3) as confirmed by these vibrations, and by the C-H asymmetric stretch around 2960 cm^{-1} and stretches corresponding to Si-CH_3 bands in –Si$(CH_3)_2$O– groups within the silane structure at 1260 cm^{-1}. These observations support the increasing extent of silylation previously discussed in relation to ICP-MS characterisation. The broad spectral line at 1435 cm^{-1} is persistent for DND samples treated by the HMDS reagent, and according to Nascimento Filho *et. al.* [34] this spectral line can be attributed to physically adsorbed HMDS. Adsorption at 1707 cm^{-1} is characteristic for all silylated nanodiamond samples and may be attributed to the ν(C=O) band of trimethylsilyl-esters formed with carboxylic groups at the diamond surface [33]. It should be noted that carboxylic groups are more acidic and reactive as compared with hydroxyl-groups and residual water, so this band was noted for all samples independent of their respective modification conditions. The peak shift from 1110 cm^{-1} (NSFPA) to 1092 cm^{-1} for the silyl derivatives confirms the formation of Si-O bonds [35].

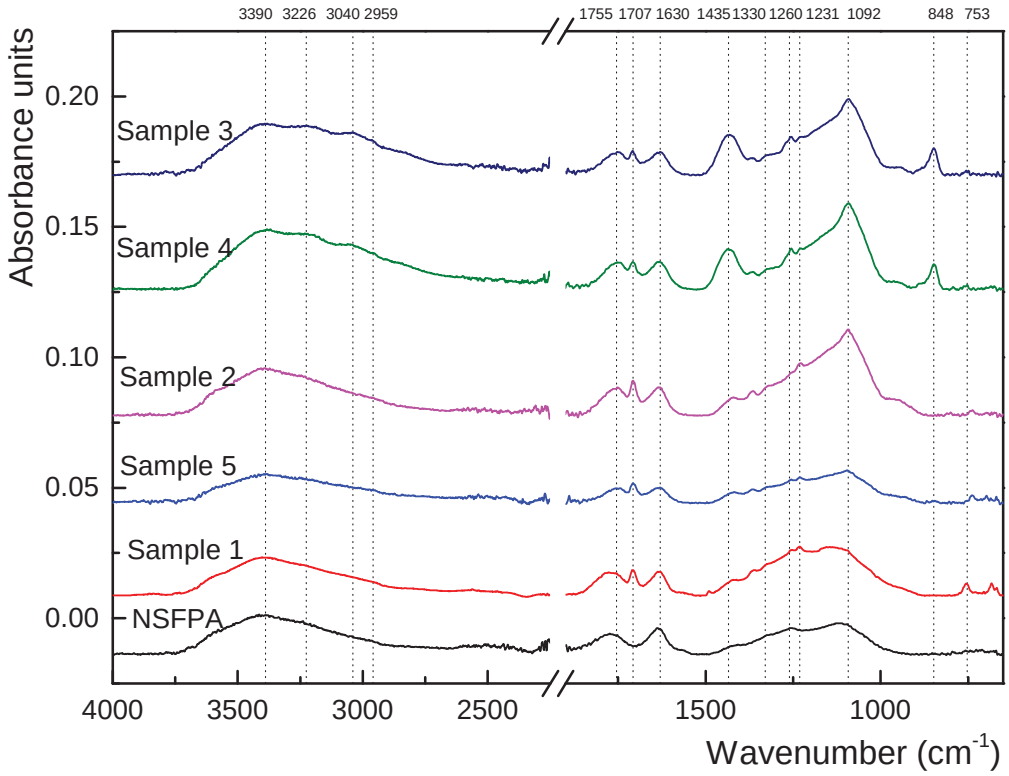

Figure 3.4 ATR-FTIR spectra of purified nanodiamond (NSFPA) and five silylated samples (Sample 1-5).

3.3.4 Suspension Stability

Silylated DNDs form stable suspensions after sonication in nonpolar solvents like dichloromethane. The suspensions remained stable for up to one week, and demonstrated effective light scattering due to the Tyndall effect (Figure. 3.5), thus confirming the suspension stability. This behaviour differs from that observed for unmodified DNDs, which do not usually form stable suspensions (e.g. YTM type DND shown in Figure 3.5 and results presented in [31]) and flocculate in less than an hour in dichloromethane.

Table 3.2 Average particle sizes (d_p, nm) of original and silylated DND measured by dynamic light scattering

Sample	YTM	NSFPA	(5)	(2)	(4)	(3)
Silylating agent	-	-	TMCS	DMODCS	DMODCS + HMDS	TMCS + HMDS
Aqueous suspension	264	100	-	-	143	124.3 (88)*
Isopropanol suspension	171*	83*	180* (78)**	115*	-	-

***** after ultra sonication for 1 min
****** after ultra sonication for 3 min

Particle size (d_p) measurements (by dynamic light scattering) (DLS) of the samples under investigation in both aqueous suspension and *iso*-propanol are presented in Table 3.2. There is a clear reduction in the average d_p when YTM type DND is subjected to further purification procedures to produce the NSFPA material. The tendency for aggregation has been reduced both in water and in *iso*-propanol solvents. As a result of silylation of NSFPA, the average d_p in aqueous suspension increased from 100 nm to 143 and 124 nm for Samples 3 and 4, respectively. Obviously, some aggregation between silanised particles occurred because of hydrophobic interactions between silylated nanoparticles in polar aqueous suspension. However, the reduction in average d_p to 88.6 nm for Sample 3 was achieved by ultrasonication of this suspension for one minute. A similar effect was observed for Samples 2 and 5 in *iso*-propanol. For example, average diameter of aggregates for Sample 5 dropped from 180 to 78 nm after sonication in *iso*-propanol.

A more dramatic increase in average d_p from 50 nm to 200 nm was reported by Krueger *et. al* for DND aggregates treated with (3-aminopropyl)trimethoxysilane [18]. Inter-molecule condensations can take place when using trimethoxysilanes for the modification of DND surface,

leading to the formation of siloxane bonds between DND nanoparticles and, ultimately, to the formation of bigger aggregates. However, such condensation reactions are not possible when trialkylmonochlorosilanes or HMDS are used as silylating reagents. Interestingly, suppression of the zeta potential on the DND samples was observed following silylation. The aqueous suspension of NSFA had a zeta potential of 29.6 mV, while the silylated samples 3 and 4 displayed lower values of 3.1 and 8.2 mV respectively.

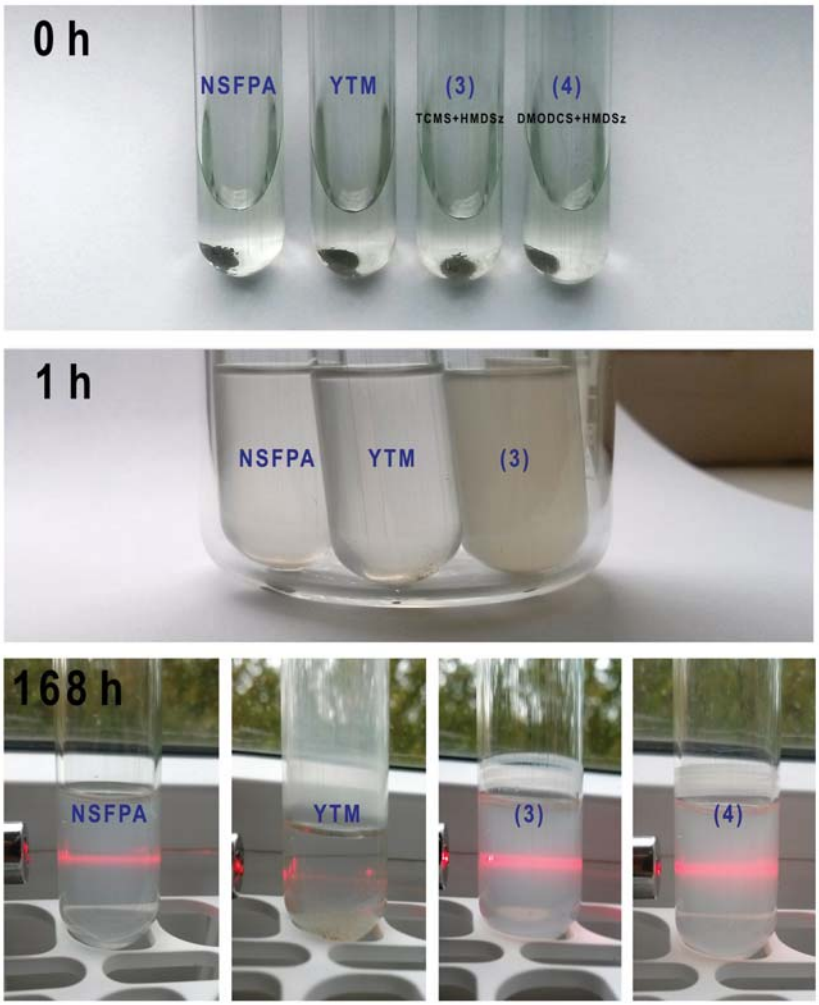

Figure 3.5 Suspension stability of DND type NSFPA, YTM and silylated (Sample 3) and (Sample 4) in dichloromethane: before sonication (above), an hour after sonication (middle) and a week after sonication (below, with shown Tyndall effect).

3.3.5 Capillary Zone Electrophoresis

CZE has recently been employed to characterise the dispersion quality and stability of DND, and was previously applied to the precursor NSFPA material [27]. In this earlier study, the NSFPA sample in sodium tetraborate buffer (pH 9.3) exhibited a well-defined broad peak followed by two smaller broad peaks, demonstrating the presence of stable agglutinates within a polydisperse sample (Figure 3.6; 20 sec injection of NSFPA at 5 kPa; + 15 kV applied voltage; effective capillary length 57.5 cm). Following silylation of NSFPA, the samples were studied under similar conditions by CZE (5 sec injection at 5 kPa, + 5 kV applied voltage, effective capillary length 24 cm). Figure 3.6 shows the typical electropherograms obtained for Samples 3 and 4 in 20 mM sodium tetraborate, where the DNDs were negatively charged at pH 9.3, and migrated after the electro-osmotic flow (EOF) (*iso*-propanol marker) in a single well-defined broad peak. The absence of any spikes within this broad peak demonstrates that the suspension is stable under these conditions, and that it is likely to be composed of small agglutinates as similarly observed for commercial DND samples in sodium tetraborate buffer [27]. This observation is in agreement with the particle size data obtained by DLS for these silylated DNDs in aqueous suspension (Table 3.2) as discussed above. Both silylated DND materials demonstrated a similar apparent mobility under the same conditions (calculated by $\mu_{sample} - \mu_{EOF}$ where $\mu = L_d.L_t/V.t_{migration}$ wherein L_d is capillary length to detection window, L_t is total capillary length, V is applied voltage and $t_{migration}$ is the migration time of the analyte). The apparent mobility of sample 3 and sample 4 were -2.58 x 10^{-8} m^2/Vs and -2.43 x 10^{-8} m^2/Vs respectively. These similar mobility values indicate the similarity in both size and charge of the silylated DND under these conditions.

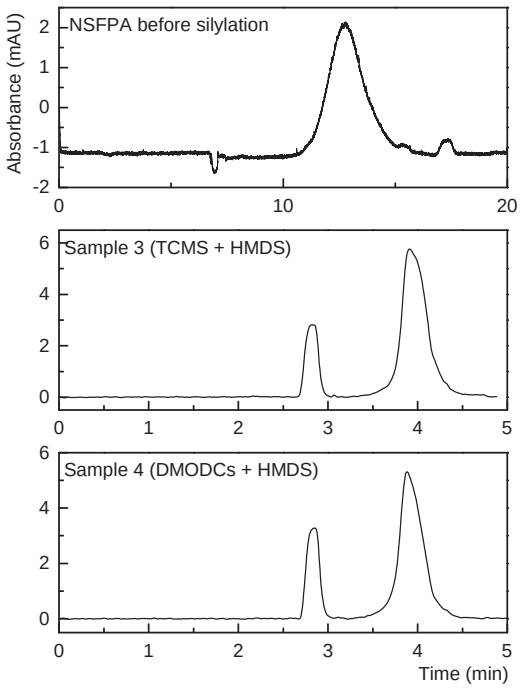

Figure 3.6 Electropherograms showing the separation of purified detonation nanodiamond NSFPA (purified from detonation soot using oxidising acids as outlined in Experimental Methods Section 3.2) and silylated nanodiamond Sample 3 (silanised with trimethylchlorosilane and hexamethyldisilazane) and Sample 4 (silanised with dimethyloctadecylchlorosilane and hexamethyldisilazane) in 20 mM sodium tetraborate buffer pH 9.3. Conditions: 5 second injection at 5 kPa, + 5 kV applied voltage.

3.3.6 Thermal Stability

The impact of vacuum annealing on the Si-content of the silylated DND was investigated. After careful washings with dry toluene and then acetone, three types of silylated DNDs were annealed under vacuum: namely Samples 3, 4 and 5, at 250 °C for 18 hours. After this continuous exposure, residues were deposited on the walls of sample tubes containing silylated DND (Samples 3 and 4), demonstrating that there was adsorption of HMDS on the surface of DND; whereas no residue was deposited onto the walls for Sample 5 when only TMCS was used for silylation (Figure 3.7). These results are in agreement with FTIR data showing an extra band at 1435 cm^{-1} for Samples 3 and 4.

Following annealing, there was a reduction in sample mass, and a notable reduction in Si-content was also observed, as determined by ICP-MS (Table 3.3).

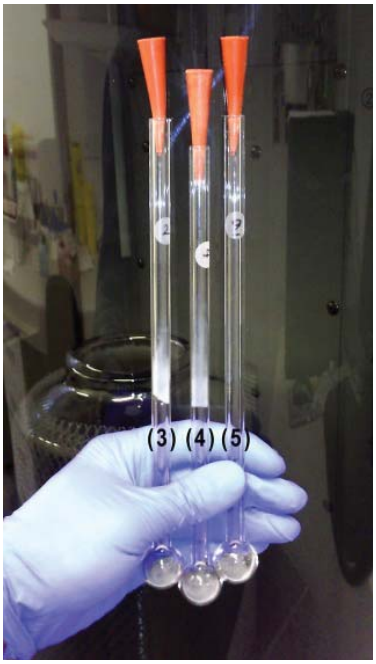

Figure 3.7 Sample tubes with heated silylated DND Samples 3, 4 and 5

It should be noted that the temperature of 250 °C used here is below the decomposition thermal limits of the correspondent silylation products, which is 300-350 °C for TMCS-derivatives [36]. Additionally, the effect of acid cleavage (excess 0.5M hydrochloric acid in *iso*-propanol overnight) on the annealed silylated DND was found to be a relatively slow, likely due to the elimination of water from the DND which prevents hydrolysis of the silylated surface.

Table 3.3 Silicon content variation in silylated DND measured by ICP-MS (μg/g)

Si in dry samples, μg g^{-1} *	Samples (silylating reagents)		
	Sample 3 (TMCS+HMDS)	Sample 4 (DMODCS/HMDS)	Sample 5 (TMCS)
Silylated DND	29300	27400	7020
Silylated and heated at 250°C DND	15600	14000	3950
Acid washed	7500	5200	1060

** Si-content in original NSFPA type of DND was 48 μg/g*

TGA can offer further insight into the effect of high temperatures on the degradation of silylated DND. Figure 3.8 shows the multi-step decomposition resulting from annealing of silylated DND (Sample 3 and 4) in nitrogen atmosphere. Following annealing to 900 °C, Sample 3 underwent ~18% weight loss and Sample 4 underwent ~23% weight loss, thus demonstrating the DMODCS/HMDS silylated ND had more physically adsorbed HMDS molecules, which are generally less thermally stable under these conditions, than TMCS/HMDS silylated DND. The initial rapid loss seen for Sample 3 can be attributed to residual solvent or volatiles (loss to temperatures of 100 °C). There is a slight gain in weight seen for Sample 4 within this temperature range (up to ~140 °C).

The two materials display different thermal behaviour from 200-500 °C, where surprisingly Sample 3 remains relatively stable with no significant changes in weight, and Sample 4 undergoes a steady decline in weight. The favourable thermal properties of ND may play a role in stabilising Sample 3, as the weight loss expected around 350 °C for TMCS degradation was not evident in the TGA curve. ND is known to have improved heat dissipation in composite systems and it has excellent thermal conductivity and low thermal expansion [17]. As seen in the TGA weight loss curve, Sample 3 was no longer stable above 500 °C, and it experienced continual weight loss

throughout the rest of the analysis. It is important to note that ND can undergo surface graphitisation in the temperature range 750-800 °C in an inert atmosphere, and above this temperature range graphitisation of ND continues to produce concentric curved graphitic sheets, known as carbon onions [37]. This conversion may result in weight losses which can account for the losses observed in Figure 3.8 above 750 °C.

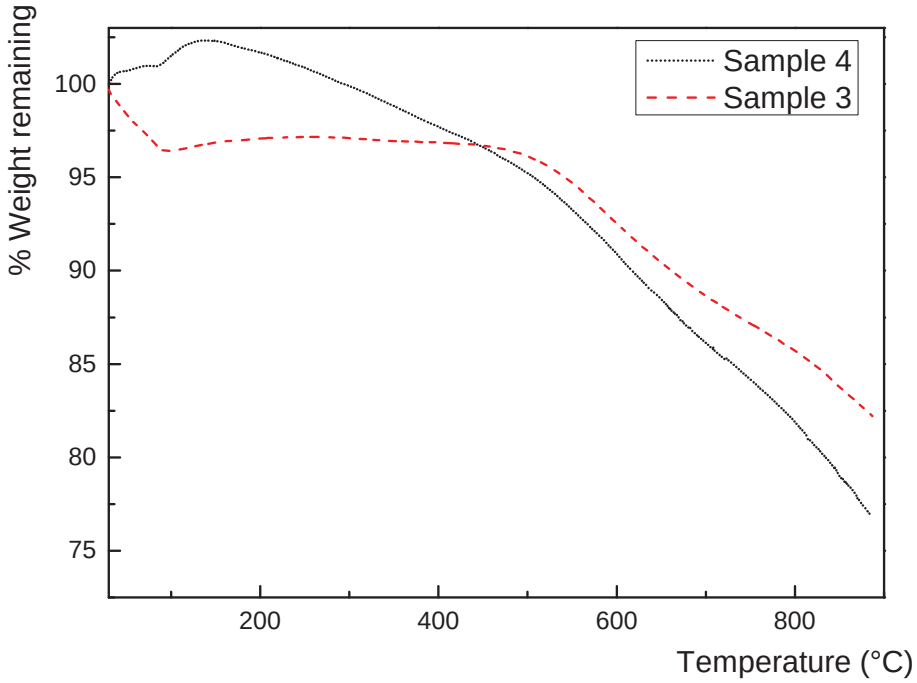

Figure 3.8 Thermogravimetric curve for silylated DND Samples 3 and 4 heated to 900 °C in an atmosphere of nitrogen (50 mL/min)

3.4 Conclusion

In this work the Si concentration profiles (along with other common non-carbon elements) of seven differently purified, refined and silylated DND samples were determined and compared using a direct ICP-MS approach. The efficiency of different silylation procedures, preliminary preparations and post-silylation treatments were assessed with respect to the changes in covalently bonded and adsorbed silicon, through ICP-MS, FTIR, TGA and CE analysis. The ICP-MS method

provided fast and accurate determinations of non-carbon elements present in various DND preparations. These elemental determinations were used to rationally improve DND purification and derivatisation procedures. This method for evaluating DND is expected to be essential for incorporating DND nano-materials in biomedicine, nano-composites and other fields.

References

1. Shenderova, O., Gruen, D. *Ultrananocrystalline Diamond: Synthesis, Properties, and Applications*, Elsevier, 2012, 133-164.
2. Shenderova, O., Gruen, D. *Ultrananocrystalline Diamond*, William Andrew, Norwich, NY, 2006.
3. Sakovich, G.V., Zharkov, A.S., Petrov, E.A. Results of Research into the Physicochemical Processes of Detonation Synthesis and Nanodiamond Applications, *Nanotechnol. Russ.* 8 (2013) 581–591.
4. Wang, D.H., Tan, L.-S., Huang, H., Dai, L., Osawa, E. In-Situ Nanocomposite Synthesis: Arylcarbonylation and Grafting of Primary Diamond Nanoparticles with a Poly(ether-ketone) in Polyphosphoric Acid, *Macromolecules* 42 (2009) 114-124.
5. Shenderova, O., Jones, C., Borjanovic, V., Hens, S., Cunningham, G., Moseenkov, S., Kuznetsov, V., McGuire, G. Detonation Nanodiamond and Onion-like Carbon: Applications in Composites*, Phys. Stat. Sol. (a)* 205 (2008) 2245-2251.
6. Duffy, E., He, X., Nesterenko, E.P., Dey, A., Krishnamurthy, S., Brabazon, D., Nesterenko, P.N., Paull, B. Thermally Controlled Growth of Carbon Onions within Porous Graphitic Carbon-Detonation Nanodiamond Monolithic Composites, *RSC Adv*. 5 (2015) 22906-2915.
7. Mazeheri, H., Allahkaram, S.R. Deposition, Characterization and Electrochemical Evaluation of Ni-P-Nano Diamond Composite Coatings, *App. Surf. Sci*. 10 (2012) 4574-4580.
8. Peristyy, A.A., Fedyanina, O.N., Paull, B., Nesterenko, P.N. Diamond Based Adsorbents and their Application in Chromatography, *J. Chromatogr. A* 1357 (2014) 68-86.
9. Kharisov, B., Kharissova, O., Chavez-Guerrero, L. Synthesis Techniques, Properties, and Applications of Nanodiamonds, *Synth. React. Inorg. Metal-Org. Nano-Metal. Chem*. 40 (2010) 84-101.

10. Mochalin, V., Shenderova, O., Ho, D., Gogotsi, Y., The Properties and Applications of Nanodiamonds, *Nat. Nanotechnol*. 7 (2012) 11-23.
11. Man, H.B., Ho, D. Diamond as a Nanomedical Agent for Versatile Applications in Drug Delivery, *Phys. Status Solidi A* 209 (2012) 1609–1618.
12. Krueger, A., Liang, Y., Jarre, G., Stegk, J. Surface Functionalisation of Detonation Nanodiamond Suitable for Biological Applications, J. Mater. Chem. 16 (2006) 2322-2328.
13. Dolmatov, V. Polymer-Diamond Composites Based on Detonation Nanodiamonds. Part 2, *J. Superhard Mater.* 29 (2007) 65-75.
14. Pramatarova, L., Radeva, E., Pecheva, E., Hikov, T., Krasteva, N., Dimitrova, R., Mitev, D. Montgomery, P., Sammons, R. *The Advangates of Polymer Composites with Detonation Nanodiamond Particles for Medical Applications*, L.D. Pramatarove (Ed.) On Biomimetics, Intech, 2011, 297-320.
15. Lu, J., Wang, Y.H., Zang, J.B., Li, Y.N. Protective Silicon Coating for Nanodiamonds Using Atomic Layer Deposition, *Appl. Surf. Sci.* 253 (2007) 3485-3488.
16. Nesterenko, P.N., Fedyanina, O.N., Volgin, Y.V. Microdispersed Sintered Nanodiamonds as a New Stationary Phase for High-Performance Liquid Chromatography, *Analyst* 132 (2007) 403-405.
17. Nesterenko, P.N., Haddad, P.R. Diamond-Related Materials as Potential New Media in Separation Science, *Anal. Bioanal. Chem*. 396 (2010) 205-211.
18. Krueger, A., Stegk, J., Liang, Y., Lu, L., Jarre, G. Biotinylated Nanodiamond: Simple and Efficient Functionalization of Detonation Nanodiamond, *Langmuir* 24 (2008) 4200-4204.
19. Liang, Y., Ozawa, M., Krueger, A. A General Procedure to Functionalize Agglomerating Nanoparticles Demonstrated on Nanodiamond, *ACS Nano* 3 (2009) 2288-2296.

20. Jeong, M.-G., Chun, Y.-S., Lim, D.-S., Kim, J. Y. Effect of a Silane Coupling Agent on the Optical and the Mechanical Characteristics of Nanodiamond/Acrylic Resin Composites, *J. Korean Phys. Soc.* 65 (2014) 1049–1053.
21. Dolmatov, V.Y. Composition Materials Based on Elastomer and polymer Matrices Filled with Nanodiamonds of Detonation Synthesis, *Nanotechnol. Russ.* 4 (2009) 556-575.
22. Mitev, D.P., Townsend, A.T., Paull, B., Nesterenko, P.N. Direct Sector Field ICP-MS Determination of Metal Impurities in Detonation Nanodiamond, *Carbon* 60 (2013) 326-334.
23. Mitev, D.P., Townsend, A.T., Paull, B., Nesterenko, P.N. Screening of Elemental Impurities in Commecrial Detonation Nanodiamond using Sector Field Inductively Coupled Plasma-Mass Spectrometry, *J. Mater. Sci*. 49 (2014) 3573-3591.
24. Gaspar, H., Pereira, C., Rebelo, S., Pereira, M., Figueiredo, J.L., Freire, C. Understanding the Silylation Reaction of Multi-Walled Carbon Nanotubes, *Carbon* 49 (2011) 3441-3453.
25. Cagnoli, M.V., Casuscelli, S.G., Alvarez, A.M., Bengoa, J.F., Gallegos, N.G., Crivello, M.E., Herrero, E.R., Marchetti, S.G. Ti-MCM-41 Silylation: Development of a Simple Methodology for its Estimation: Silylation Effect on the Activity and Selectivity in the Limonene Oxidation with H_2O_2, *Catal. Today* 107-108 (2005) 397-403.
26. Brieva, G., Campos-Martin, J., de Frutos, M., Fierro, J. Some Insights on the Negative Effect Played by Silylation of Functionalized Commercial Silica in the Direct Synthesis of Hydrogen Peroxide, *Catal. Today* 158 (2010) 97-102.
27. Duffy, E., Mitev, D.P., Nesterenko, P.N., Kazarian, A.A., Paull, B. Separation and Characteriation of Detonation Nanodiamond by Capillary Zone Electrophoresis, *Electrophoresis* 35 (2014) 1864-1872.
28. Mitev, D.P., Townsend, A.T., Paull, B., Nesterenko, P.N. Microwave-Assisted Purification of Detonation Nanodiamond, *Diam. Relat. Mater*. 48 (2014) 37-46.

29. Batsanov, S.S., Lesnikov, E.V., Dan'kin, D.A., Balakhanov, D.M. Water Shells of Diamond Nanoparticles in Colloidal Solutions, *Appl. Phys. Lett.* 104 (2014) 133105.
30. C. Sweeley, R. Bentley, M. Makita, W. Wells, Gas-Liquid Chromatography of Trimethylsilyl Derivatives of Sugars and Related Substances, *J. Am. Chem. Soc.* 85 (1963) 2497-507.
31. Krueger, A., Boedeker, T. Deagglometation and Functionalisation of Detonation Nanodiamond with Long Alkyl Chains, *Diam. Relat. Mater*. 17 (2008) 1367-1370.
32. Fruehauf, S., Streiter, I., Schulz, S.E. Brendler, E., Himcinschi, C., Friedrich, M., Gessner, T., Zahn, D.R.T. Advanced Metallization Conference, A. McKerrow, Y. Shacham-Diamand, S. Zaima, T. Ohba (Eds.) *Mater. Res. Soc. Conf. Proc. ULSI XVII, 2011 MRS*, Warrendale, PA, 287-294.
33. Harrison, P.G., Torr, A. FT-IR Study of the Gas Phase Thermolysis of Trimethylsilyl Acetate, *J. Organomet. Chem*. 538 (1997) 19-29.
34. Nascimento Filho, A.P., de Carvalho, A.T., da Silva, M.L.P., Demarquette, N.R. Preconcentration in Gas or Liquid Phases Using Adsorbent Thin Films, *Materials Research* 9 (2006) 33-40.
35. Oh, T., Lee, K., Choi, C. A Study on the Structure of Si-O-C Thin Films with Nano Size Pore by ICPCVD, Stud. *Surf. Sci. Catal*. 146 (2003) 387-390.
36. *GC Derivatization, Applications Handbook & Catalog*, Pierce Biotechnology, Inc., Rockford, IL, 2003.
37. Xu, N.S., Chen, J., Deng, S.Z. Effect of Heat Treatment on the Properties of Nano-Diamond Under Oxygen and Argon Ambient, *Diam. Relat. Mater*. 11 (2002) 249-256.

Chapter 4.

Thermally Controlled Growth of Carbon Onions Within Porous Graphitic Carbon-Detonation Nanodiamond Monolithic Composites

Abstract

Unique porous carbon monoliths containing thermally annealed carbon onions, were prepared from a resorcinol formaldehyde precursor rod, containing silica gel acting as a hard template, detonation nanodiamond, and Fe^{3+} as a graphitisation catalyst. Detonation nanodiamond was converted to carbon onions during controlled pyrolysis under N_2, where the temperature cycle reached a maximum of 1250 °C. Thermal characterisation and high resolution electron microscopy have confirmed the graphitisation of nanodiamond, and revealed the resulting quasi-spherical carbon onions with an average particle size of 5.24 nm. The bimodal porous composite contains both macropores (5 μm) and mesopores (10 nm), with a BET surface area of 214 m^2/g for a nanodiamond prepared monolith (0.012 wt.% nanodiamond in the precursor mixture), approximately twice that of blank monoliths, formed without the addition of nanodiamond, thus providing a new approach to increase surface area of such porous carbon rods. Raman spectroscopy and X-ray photoelectron spectroscopy also confirmed an enhanced graphitisation of the monolithic carbon skeleton resulting from the elevated thermal conductivity of the added nanodiamond. TEM imaging has confirmed the nanodiamond remains intact following pyrolysis at temperatures up to 900 °C.

4.1 Introduction

New porous materials continue to attract significant interest within the science and technology community due to their unique and versatile properties, and advanced applications [1]. In particular, the design of porous carbon materials with tailored chemical and structural properties has immense significance within the fabrication, coatings and coating and energy storage based industries, addressing key technological challenges. For porous carbons, these properties include high specific surface area, chemical inertness, thermal stability and electronic conductivity. The use of porous carbons as an electrode material [2] and indeed in electrochemical double layer capacitors, or super capacitors [3] is therefore currently very topical. In the area of environmental technology, there are reports demonstrating utility as catalyst supports, e.g. for gas separation or storage [4-5], and as adsorbents for separation or remediation processes [6].

Several excellent reviews on the subject of porous carbon production and applications have recently emerged [7-9]. One novel route to the production of porous carbon materials is the formation of so-called carbon monoliths. These typically exhibit a hierarchical porous structure, and are often produced through various templating methods, for example the use of hard and soft removable templates. Silica particles (including mesoporous silica or silica nanoparticles) are commonly used in the hard-templating synthesis of porous carbon monoliths, to facilitate creation of a controlled macroporous structure in the final material. The inorganic template is embedded in the carbon precursor, or the carbon precursor is introduced into the pores of the template. After undergoing carbonisation via pyrolysis, the template is removed, thus generating a porous material with isolated pores or an interconnected pore network. Mesopores may also be created by catalytic graphitisation and this is commonly achieved using a metal ion catalyst, or by the carbonisation of a polymer blend containing a carbon precursor polymer and a decomposable polymer that is removed to produce the pores. Reports on the production of such hierarchical porous carbons with bimodal pore structures (pore size distribution has two modes) have been published [7-10], several of which

are based on the polymerisation and carbonisation of silica particle embedded resorcinol formaldehyde (RF) resin, using Fe^{3+} as a catalyst to enhance graphitisation [10-11].

Porous carbon monoliths offer inter-connected channels within their pore network, with a high flow-through permeability, good thermal and electrical conductivity hence their potential application in adsorption or separation processes [10-12], and electrochemical energy storage applications [13]. Recently, the use of nanocarbons to form porous carbon monoliths or carbon-carbon composite materials has produced some exciting results, showing considerably enhanced electrochemical properties for potential applications in the above areas [14-15]. Indeed, changes to the physical, chemical and electrochemical properties of the nano-composite monoliths have been reported, when compared to simple carbon monoliths without embedded or surface exposed nanocarbons. Physical enhancements include higher specific surface area, greater mesopore volume and a narrower pore size distribution [16]. However, to-date such studies are limited in number, and controlled approaches to achieve substantially enhanced properties, e.g. surface area, for such monolithic substrates are rather limited.

It can be expected that with the inclusion of nanocarbons within porous carbon monoliths, there will be a transfer of unique physical-chemical properties to the final composite, provided the nanocarbon is preserved through any carbonisation process. These unique nanocarbon properties have seen them applied in a wide variety of ways in recent times, e.g. in environmental applications as sensors, filters, and sorbents [17], with fullerenes, carbon nanotubes and carbon onions having demonstrated high sorption capacities for organic pollutants and heavy metal contaminants [18]. Recently, nanodiamond (ND) has received renewed attention, primarily due to its biocompatibility and potential applications in drug delivery [19-20]. Nanoscale diamond (sp^3 carbon) may be produced by detonation synthesis, where the detonation soot is purified under oxidative acidic conditions to yield detonation nanodiamond (DND), which is known to have a high thermal conductivity, mechanical stability and surface chemistry readily amenable to functionalisation.

Carbon onions may be produced by the thermal annealing of ND [21] in an inert atmosphere or under vacuum. They too have a variety of interesting properties (such as high surface area and electrical conductivity), making them of interest for use in supercapacitors [22], lubrication, and in environmental remediation [18].

Therefore, herein is described a novel route for the preparation and characterisation of a new porous carbon monolith with significantly enhanced surface area and graphitic character, via embedded carbon onions produced through the controlled thermal annealing of DND during the carbonisation process. The new carbon on carbon composite material was formed by pyrolysis of a precursor rod containing a mixture of RF resin, silica particles and DND, with a Fe^{3+} catalyst used to increase localised graphitisation. The thermal conductivity of the DND was also expected to enhance the graphitisation process, and the precise thermal conversion of diamond particles to carbon onions during the pyrolysis (to a maximum temperature of 1250 °C) was explored.

4.2 Experimental Methods

4.2.1 Synthesis of Graphitic Carbon Monoliths with Thermally Annealed Carbon Onions

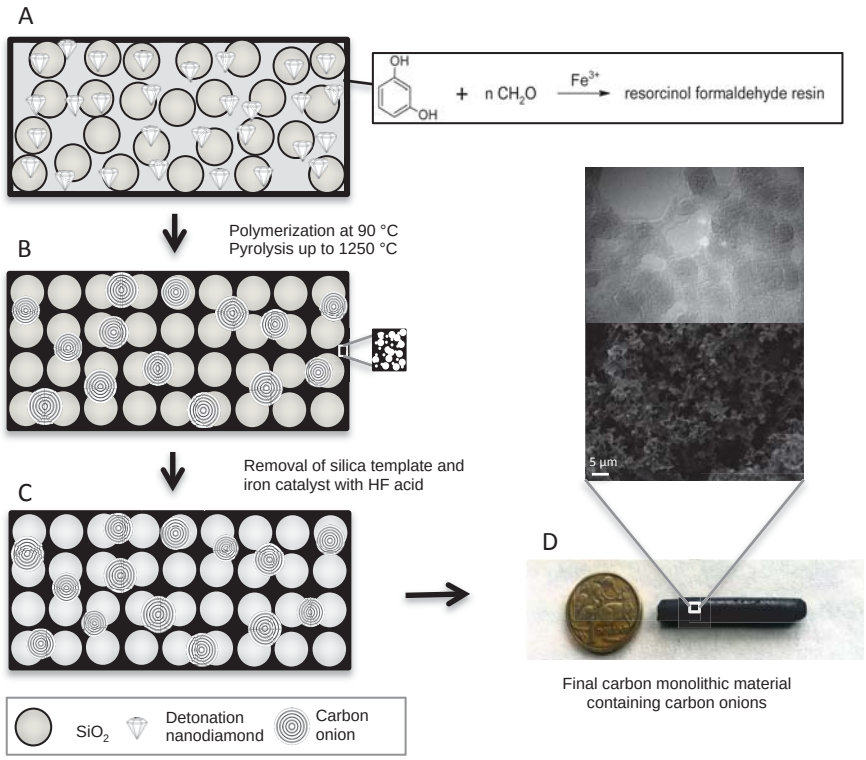

Figure 4.1 Scheme for fabrication and pyrolysis of carbon monolithic composites.

Figure 4.1(A) to 4.1(C) illustrates the steps taken in preparing the nano-composite porous graphitic carbon monoliths, and a blank carbon monolithic material (containing no additional DND). The precursor solution (A) is composed of a polymeric mixture containing a RF resin in 1-butanol. In preparation of this solution, 1 g of 5 µm silica particles, with a surface area of 359 m^2/g and a pore size of 550 Å, (Nucleosil silica beads from Macherey-Nagel, Duren, Germany) was dispersed in 1.85 mL 1-butanol and sonicated for 1 hour before adding 0.18 g of ferric chloride (99% Riedel-De Haen, Seelze, Hannover, Germany) and 0.367 g of resorcinol (99% Sigma-Aldrich, Dublin, Ireland). A 555 µL aliquot of aqueous DND suspension (Single Digit Nanodiamond, 50

mg/mL aqueous suspension, PlasmaChem GmbH Germany) was added to this RF polymeric resin, as a percentage (30%) of the total volume of 1-butanol present. The addition of 0.3 g of ice-cooled formaldehyde (37 wt.% solution, Sigma-Aldrich, Dublin, Ireland) to the mixture was made, with constant stirring. Following stirring in an ice-bath for 1 hour, the resin was transferred to a 7-mm i.d. glass tube, which was capped and sealed for polymerisation at 90 °C in a water bath (GFL water bath from Laborggerateborse GmbH, Burladingen, Germany) for 15 hours. A solid rod was formed, which was detached slightly from the walls of the tube due to shrinkage during polymerisation. A drying step (72 hours in the fume hood) to allow the slow evaporation of any remaining solvent was carried out, and materials were then dried thoroughly in a vacuum oven to ensure the removal of any remaining solvents (EHRET vacuum oven from Ehret Labor and Pharmatechnik GmbH, KG, Emmendingen, Germany). Pyrolysis of the materials was carried out in a horizontal tube furnace (model GSL1300X from MTI, Richmond, VA, U.S.A), which was purged with nitrogen. The full temperature program applied involved an initial ramp from room temperature to 800 °C at a rate of 2.5 °C/min. The temperature was held at 800 °C for 2 hours, and then further increased to either 900 °C or 1250 °C at a rate of 10 °C/min. The maximum temperature was held for 1 hour, and the furnace was subsequently allowed to cool naturally to room temperature. The carbon rods obtained showed an irregular mesoporous structure by SEM imaging (as discussed below), with the silica particles remaining intact and carbon onions present resulting from the thermal annealing of the DND (1250 °C). The rods then underwent hydrofluoric acid etching in order to remove the silica template and the Fe^{3+} catalyst. The hydrofluoric acid (HF) (38-40% Sigma-Aldrich, Dublin, Ireland) etching step involved submersion of the carbon rods for 5 hours, followed by washing with copious amounts of deionised water until a neutral pH was attained. Finally, the rods were dried in the vacuum oven at 80 °C for 16 hours and an example of the final material obtained is shown in Figure 4.1(D).

4.2.2 Material Characterisation

High-resolution images of the porous carbon materials were taken using Transmission Electron Microscopy (TEM), JEOL model JEM 2100, equipped with an Orius camera in-line (Gatan, Pleasenton, CA, U.S.A). A lanthanum hexaboride filament was used at an accelerating voltage of 200 μA. TEMCON software was used to control the instrument, and Digital Micrograph software (Gatan) was used in controlling the camera. The sample holder used was the type EM21010 single tilt holder and the preparation of samples involved the sonication of a small fragment of porous carbon monolithic material in 1-mL of *iso*-propanol in an Eppendorf tube, until a dilute suspension of the solid was formed. Then a 1-mL fine-tipped plastic pipette was used to place one drop of the suspension on to a S-160-3 carbon film mesh Cu (50) (Agar Scientific) for imaging. Samples were stored in plastic petri-dishes on filter paper to allow evaporation of the solvent prior to imaging. Scanning Electron Microscopy (SEM) imaging was performed on a Hitachi SU70 instrument (Hitachi High Technologies America, USA), and sample preparation involved placing a small cross section of the porous carbon materials on to carbon tape on an Al SEM stub. Samples were sputter coated with a thin (~4 nm) layer of platinum prior to imaging at 1.5 kV. Energy dispersive x-ray electron spectroscopy (EDX) was subsequently carried out on the same samples, where an excitation energy of 4 kV was used. Specific surface areas and pore volumes were measured using a surface area analyser (model TriStar II 3020, Micromeritics Gemini, Georgia, USA) through the nitrogen adsorption/desorption technique. Prior to measurement, crushed samples were dried overnight, at 100 °C, under vacuum. Raman spectra were measured on a LabRam800HR instrument (Horiba Jobin Yvon, Northampton, U.K). An argon laser (Innova 70-C-2 from Coherent, Santa Clara, USA) was used as the excitation source at a power output of 6 mW. The surface chemical states/electronic properties of the carbon monoliths annealed at 900 and 1250 °C were characterised by X-ray photoelectron spectroscopy (XPS), using a Kratos AXIS-165 electron spectrometer with monochromatic Al Kα (1486.6 eV) x-ray source, with a chamber pressure of 10^{-9} mbar.

Thermogravimetric analysis (TGA) was performed on a Labsys Evo (Setaram, Caluire, France) instrument under flow of argon at 50 mL/min. Samples of ~8 mg were placed in alumina crucibles for analysis. A heating rate of 2 °C/min from 30 to 900 °C was used, followed by a hold period of 2 hours at 900 °C. The temperature was then ramped from 900 to 1100 °C at a rate of 2 °C/min in order to closely replicate the pyrolysis temperature ramp conditions. A slower heating rate was employed to avoid the sudden evolution of gaseous products, which could affect the precision balance in the instrument.

4.3 Results and Discussion

4.3.1 Synthesis of Porous Graphitic Carbon Monoliths with Thermally Annealed Carbon Onions

It is known that the partial graphitisation of RF resin can be achieved through the addition of a catalyst, which reduces the temperature needed to achieve graphitisation, and also results in the formation of a mesoporous structure [24-25]. Here, ferric chloride was added as the graphitisation catalyst and to produce the desired mesoporous network. In this work, it was expected that the addition of DND should similarly promote localised graphitisation, due in part to its high thermal conductivity, and also its own graphitisation and transformation into carbon onion nano-structures.

Figure 4.2(A) shows a low magnification SEM image of a cross section of the precursor rod containing DND prior to undergoing carbonisation. The surface area of the uncarbonised material determined using nitrogen adsorption measurements was a low 55 m^2/g, with a pore volume of 0.21 cm^3/g, and an average pore diameter of 15 nm. The isotherm displayed a limiting step after the hysteresis loop suggesting that pores were completely filled during the analysis.

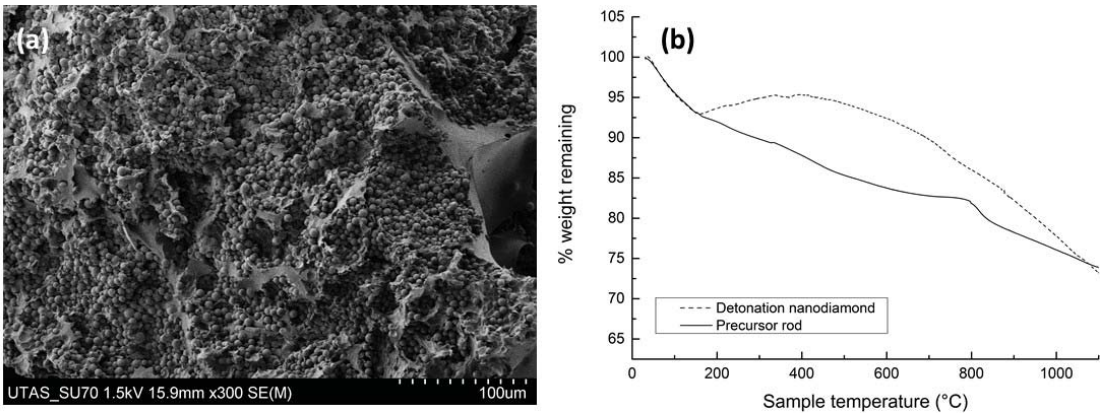

Figure 4.2 (A) SEM image taken of a cross-section of the precursor rod containing silica particles and detonation nanodiamond (DND), before carbonisation at 1250 °C. (B) Thermogravimetric analysis curves for DND, and precursor rod containing the resorcinol-formaldehyde resin with Fe^{3+} catalyst, silica particles and DND.

In prior reports on the formation of similar carbon monoliths, TGA has been used to observe the various phases of carbonisation and graphitisation [11, 14]. Here the impact of DND inclusion on these processes was also observed using TGA, under conditions similar to those used in the normal carbonisation process, although here under argon flow. The TGA curve for DND itself (Figure 4.2(B)) shows an initial weight loss of ~7 % between 30-160 °C, which is due to water losses. DND is known to be particularly hygroscopic and can contain multiple layers of water molecules on its surface, including those bound directly to the carbon surface or to the negatively charged surface functional groups. Further layers may also be bound through hydrogen bonds or other non-covalent interactions [26]. Following this initial weight loss, the TGA curve shows an unusual slight drift upwards between 200 and 350 °C, followed by a steady decline in weight between 400-900 °C, which is likely due to the removal of surface organic groups [27] and the loss of some elemental impurities, which can make up a significant amount of the DND mass (13.8 mg/g with large contributions from B, Na, Si, Ca, and Fe) [28-29]. It is known that the loss of oxygen-containing groups occurs below 900 °C in an inert atmosphere, and of CH_x groups between 900-1150 °C [30-

31]. Above ~700 °C the graphitisation of the DND normally begins. A total weight loss of 33.7% occurred between 30-1100 °C. It has been shown that DND evolves large quantities of CO_2 and CO during thermal annealing [32].

During thermal annealing, the DND will become graphitised, as the sp^3 hybrid is less energetically stable than the sp^2, and graphite is a more stable phase. Graphitisation occurs in a layer-by-layer fashion, from the more reactive surface regions inwards. Xu *et al.* have studied the thermal annealing of DND in an inert atmosphere, showing that the DND undergoes graphitisation between 670-1100 °C [33-34]. As seen in Figure 4.2(B), the precursor rod containing DND undergoes 8% weight loss below 200 °C. At lower temperatures these losses can be accounted for as the evolution of water, excess phenol or other low molecular weight compounds, as well as the release of CO, CO_2, H_2 and other gases [35]. During the pyrolysis process, the RF resin undergoes further weight losses, physical shrinkage and pore formation as the condensation of the polymer structure takes place, and the resin is gradually converted to amorphous carbon [36]. The total weight loss for the composite material between 30-1100 °C was 26.2 %, which is very similar to the total weight loss (25 %) observed for carbonisation of a composite monolith prepared with an RF precursor rod containing an Fe^{3+} catalyst, and a C_{60}-modified silica template [16]. However, these losses are both lower than those reported for a similar RF resin prepared without the addition of any nanocarbons.

4.3.2 Structure and Morphology

The porous carbon composite materials prepared exhibited a bimodal porous structure, where both macropores and mesopores were clearly evident. The interconnected macroporous network is visible in Figure 4.3(A). The ~5 μm diameter pores result from the densely packed silica template that was removed during the HF treatment. The presence of larger voids within the macroporous network was noted for the DND-containing composite materials, which were less obvious for the

bare carbon monolithic material that was prepared for comparative purposes. The addition of an aqueous suspension of DND may explain the appearance of such voids in the composite material, since 1-butanol has limited solubility in water. An increased level of porosity (compared to the bare monolithic carbon) resulted from the presence of DND, and the walls of the macropores were notably thinner, more fragile and irregular, as the DND content of the composite physically disrupts complete polymerisation of the resorcinol resin (Figure 4.3(B)).

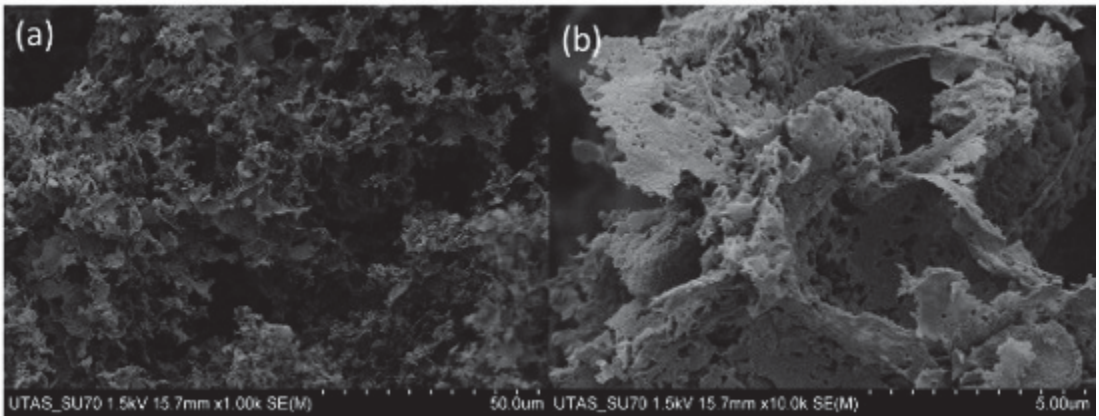

Figure 4.3 SEM images showing the porous graphitic carbon monolith with carbon onions (a) macroporous network mag. x 1 K, (b) mag. x 10 K.

Closer examination of the wall structure of the macropores revealed smooth pore walls with a low instance of raised surface features visible by low magnification SEM imaging. These regions showing irregular raised porous surfaces may be linked to some infiltration of the precursor polymerisation solution in to the 55 nm pores of the silica template. This effect is highly dependent on wetting of the silica particles, as well as the viscosity of the precursor solution. An SEM image showing such areas with irregular surface morphology is shown in Figure 4.4. Furthermore, SEM imaging was performed on cross sections of the uncarbonised monolith precursor and has revealed some instances of accumulation of polymerised resin on the surface of silica beads (highlighted in Figure 4.5).

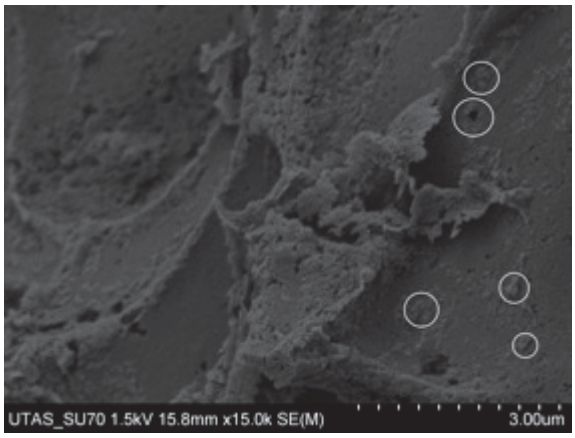

Figure 4.4 SEM image of macropore walls showing areas of irregular surface morphology (highlighted)

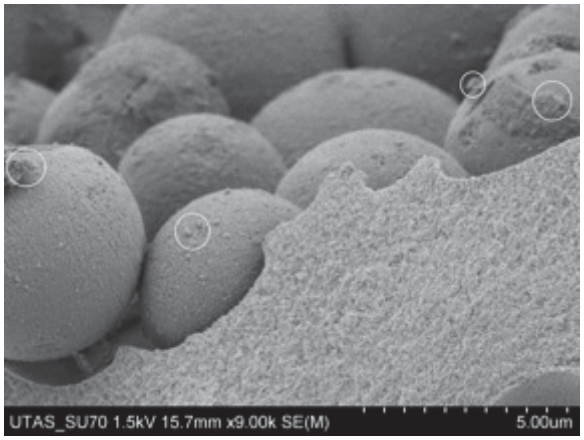

Figure 4.5 SEM image of uncarbonised precursor resin with spherical silica template and nanodiamonds, where some accumulation of polymeric resin on the silica beads is visible

Abundant mesopores were also visible by SEM imaging, and this structure was similar for materials annealed at both 900 and 1250 °C. However, examination of monoliths graphitised at the lower temperatures revealed the presence of surviving DND embedded within the mesoporous walls and attached upon the surface, both as single digit DND (< 10 nm) and clusters of up to 100 nm size (see Figure 4.6(A)). Surface EDX analysis was performed on the macroporore walls of each of the composite materials, confirming the carbon purity of the composite throughout (Figure

4.6(B)). Platinum was detected due to the thin layer of platinum coating the samples to facilitate imaging by SEM. Negligible amounts of Si were also detected in some regions of the macropore walls, although there was no evidence of the Fe^{3+} catalyst remaining.

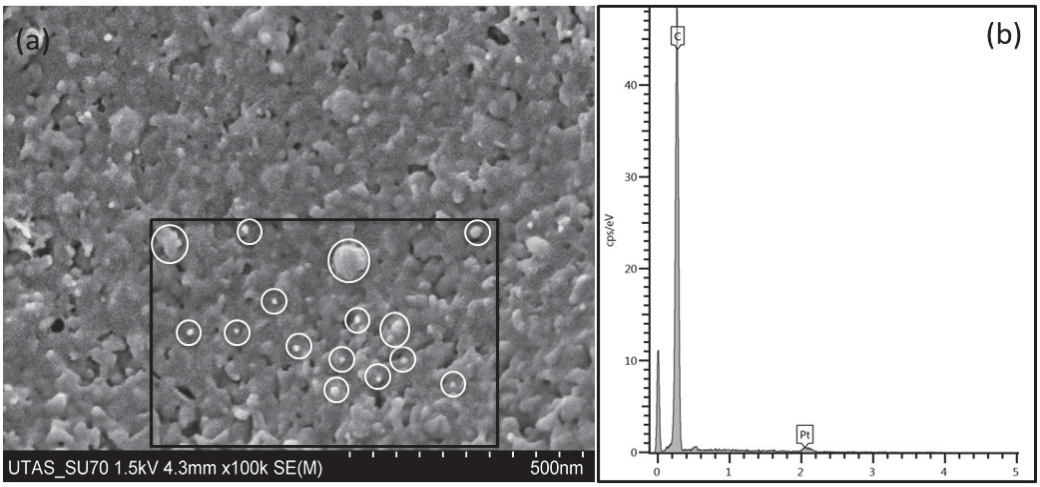

Figure 4.6 (A) High magnification (x 100 K) image of the wall of monolith macropore, showing the presence of mesoporous structure (with surviving surface detonation nanodiamonds highlighted between 10 nm and 100 nm). (B) EDX spectrum for carbon monoliths showing presence of carbon only (Pt from sputter coating).

Comparison of the carbon monoliths annealed at 900 and 1250 °C using TEM revealed the graphitic nature of the monolith, with localised graphitic structures visible. The RF resin does not undergo full graphitisation, as evidenced by the regions of amorphous carbon also visible within the TEM images. However, the thermal conversion of the DND to carbon onions within the 1250 °C monolith was confirmed. Within this sample no obvious evidence of untransformed DND particles could be seen. These TEM images are shown within Figure 4.7. It has previously been shown that carbon onions begin to form in the range of 900-1100 °C under a low vacuum [37], and in the range of 1100-1200 °C in an inert atmosphere [38]. In this case the one hour hold period at 1250 °C during pyrolysis was sufficient to quantitatively transform the DND. The carbon onions resulting

from the thermal annealing of DND within the monolithic composite are shown in Figure 4.7(B). The onions were quasi-spherical in shape, and they had an average diameter of 5.24 nm (±0.85 nm). The average interlayer spacing between the graphitic shells is 3.32 Å, which is between values previously reported for onions with five (3.35 Å) to ten (3.24 Å) shells [38].

TEM analysis confirmed that by reducing the maximum temperature of pyrolysis to 900 °C, the DND structures could actually be preserved within the composite material. Figure 4.7(C) shows a cluster of intact DND structures present within the final composite material. The DNDs shown were not graphitised at 900 °C and do not show evidence of the graphitisation of their outer layers. It is likely their structure was preserved at this temperature as a result of their being embedded within the carbon monolithic rod. The lattice fringes corresponding to the (111) planes of diamond are clearly visible, and the average interlayer spacing measured on the DND within the composite was 2.06 ± 0.28 Å. The average particle size as observed by TEM was 11.4 ± 0.9 nm, as expected based upon the specification of the commercial sample (5-15 nm particle diameter). However, some DND particles did show partial graphitisation at 900 °C, which agrees with work by Cebik *et al.,* which demonstrated that annealing DND in an inert atmosphere at 900-1000 °C can lead to the conversion of some of the surfaces of ND to layered sp^2 carbon [39]. DND present at the surface level of the composite material would not experience the same environment as those particles which were embedded in the rod during pyrolysis at 900 °C, and so partial layer-by-layer conversion to sp^2 carbon has occurred, as visible in Figure 4.7(D). Thus, careful control of temperature of pyrolysis allows control of the nature of the nano-carbons present in the final monolithic composite materials.

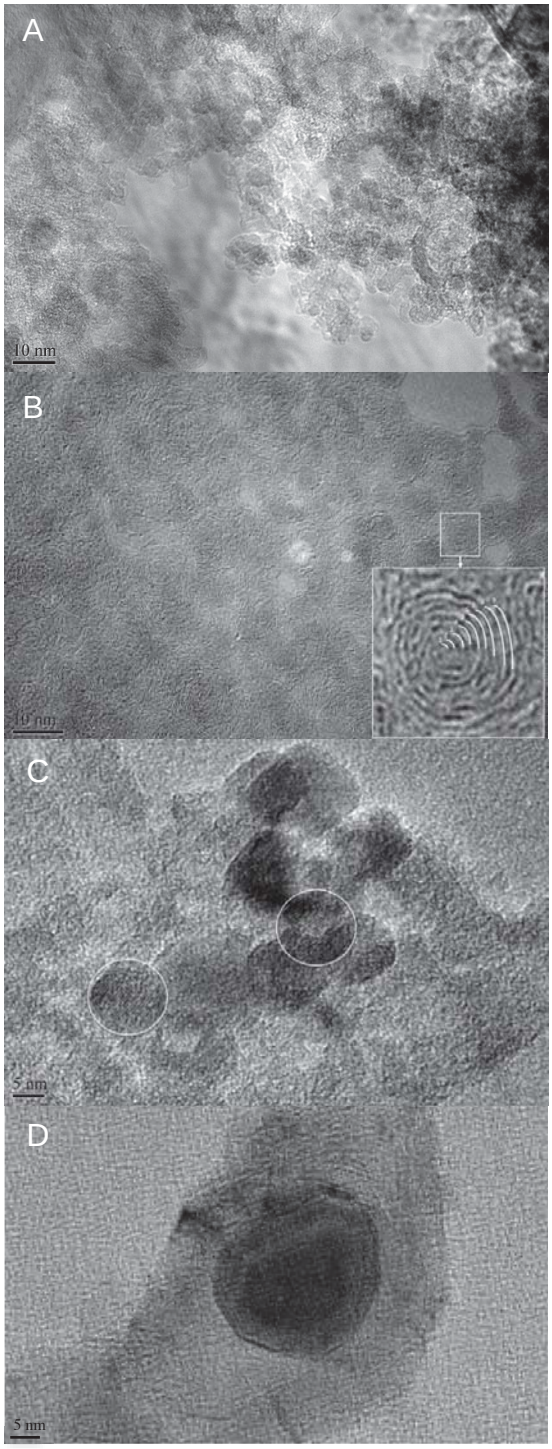

Figure 4.7 TEM images of porous graphitic carbon composites. (A) amorphous carbon, (B) carbon onions resulting from the thermal annealing of detonation nanodiamond (DND) under N_2 at 1250 °C, (C) DND remains intact within the porous graphitic carbon composite following pyrolysis up to 900 °C, (D) DND showing surface graphitisation following pyrolysis up to 900 °C.

Raman spectroscopy was applied to shed further light on the structure of the monolithic composite materials. The disorder in graphite can give rise to several characteristic Raman peaks [40]. The 800-2000 cm^{-1} region in the Raman spectrum shows common features for all carbons. The G and D peaks are typically around 1560 and 1360 cm^{-1} respectively, for visible excitation [41]. The spectrum for the blank porous carbon monolith is also shown in Figure 4.8(A). Three peaks were observed in the Raman spectrum for the monolithic composites containing carbon onions (Figure 4.8(B)). These three peaks are usually seen for carbonaceous materials with both sp^2 and sp^3 bonds present. The G band appears at ~1580 cm^{-1} and corresponds to the E_{2g} optical mode in a two-dimensional network structure, always seen for sp^2 carbon materials. The D band is visible at ~1335 cm^{-1} and it is associated with disordered carbon [42], denoting a loss of hexagonal symmetry in the material (for highly ordered pyrolytic graphite, this peak is very small or even negligible, see Figure 4.8(C) for comparison). The ratio of the intensity of the D band to the G band ($R = I_D/I_G$) can be used to illustrate the degree of graphitisation in a material. Here, the blank carbon monolithic material showed an R-value of 0.64, and the 1250 °C formed composite monolith gave a value of 0.37 (the R-value for commercial graphite was 0.14), thus confirming the greater graphitic nature of the carbon on carbon composite material. This supports the proposal that inclusion of the DND promotes localised graphitisation, both due to its inherent high thermal conductivity, and self-graphitisation during pyrolysis.

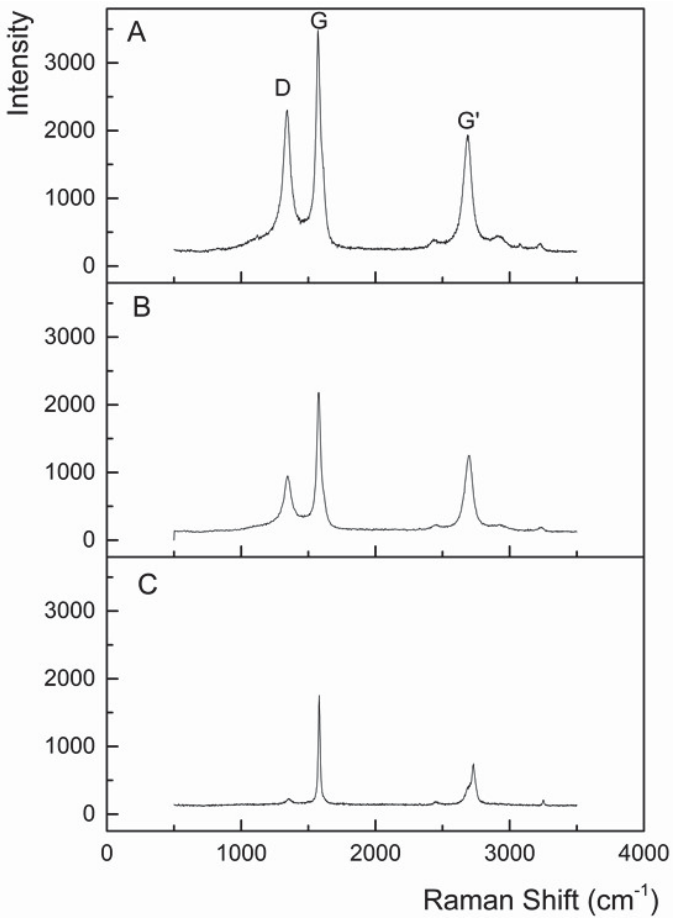

Figure 4.8 Raman spectra for (A) bare carbon monolith (prepared without the addition of carbon nanoparticles for comparative purposes), (B) carbon on carbon monolithic composite and (C) commercial graphite. Both carbon monolithic materials underwent pyrolysis at 1250 °C.

Temperature of pyrolysis is an important factor to consider here, as the composite resin remains a predominantly disordered material following its carbonisation up to 1250 °C. The G' band is seen to appear at ~2680 cm^{-1} and typically appears for sp^2 carbon materials resulting from a second order two phonon process [43]. These results confirm the presence of both graphitic and amorphous carbon in the carbon framework of the monolithic composites. Analysis by XPS further demonstrated the effect of pyrolysis temperature on partial graphitisation of the composites (Figure 4.9). A downshift in the binding energy was observed for the carbon core level (C 1s) spectral comparison of monoliths carbonised at 900 °C (285.5 ± 0.05 eV) and 1250 °C (284.5 ± 0.05 eV)

under a nitrogen atmosphere. This observation was similar to that reported by Xie *et al.* for the annealing of DND at 900 and 1500 °C [44], and within studies by Krishnamurthy and co-workers [23, 45]. This shift in binding energy relates to the material moving towards graphitisation as a function of the pyrolysis temperature. The binding energy of 284.5 eV for the composite that underwent pyrolysis at 1250 °C is slightly higher than one for graphite (284.4 eV) [30]. Also evident in the 1250 °C annealed sample, but not featured within the 900 °C sample, was the shake-up feature related to the π to π^* transition at around 290.8 ± 0.05 eV, commonly seen in more graphitised materials.

It is widely known that DND typically has a high concentration of structural defects on its surface, which increases the surface reactivity. Pyrolysis of the composites at 900 °C produced some hybrid nanocarbons combining the core properties of ND, with the surface reactivity of sp^2-based nanocarbons, as discussed above in relation to Figure 4.7(D) [46]. The production of hybrid nanocarbons is similar in effect to previous work reported by Ostrovidova *et. al.* where ND particles were bonded by a graphite-like matrix in order to produce a high surface area porous nanodiamond composite press-moulded tablet for immobilisation of biomolecules [47].

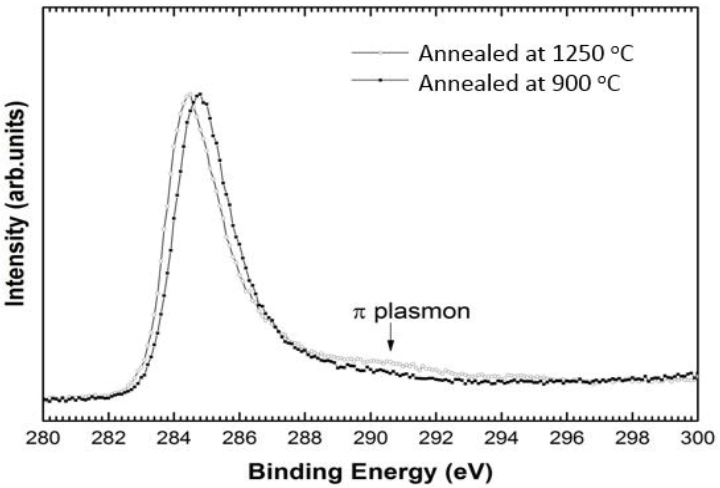

Figure 4.9 C 1s spectra of carbon monoliths containing detonation nanodiamond which underwent pyrolysis at temperatures of 900 °C and 1250 °C. Spectra were obtained in normal emission geometry at a photon energy of 1486.6 eV.

4.3.3 High-Surface Area Carbon Monoliths

The adsorption of nitrogen on the blank carbon monolith showed a type IV isotherm, which is typical of mesoporous materials (Figure 4.10(A)). Similarly, the carbon composite monolith (carbonised up to 1250 °C) also exhibited a type IV isotherm (Figure 4.10(B)). The initial region of the isotherm where an increase in adsorption followed by the knee is the point at which monolayer adsorption is preceded by multilayer adsorption. The presence of the hysteresis loop is indicative of capillary condensation within the mesopores. The hysteresis loop is type H3, which is associated with the presence of slit-like pores, and the limiting step (at high relative pressure) seen for many mesoporous sorbents of isotherm type IV is not present in a type H3 hysteresis loop. This suggests that complete pore filling may not have occurred [48]. The material does not show a sharp condensation/evaporation step, which typically characterises a narrow pore size distribution. Therefore, these materials likely exhibit a wide mesopore size distribution with irregular pore shapes.

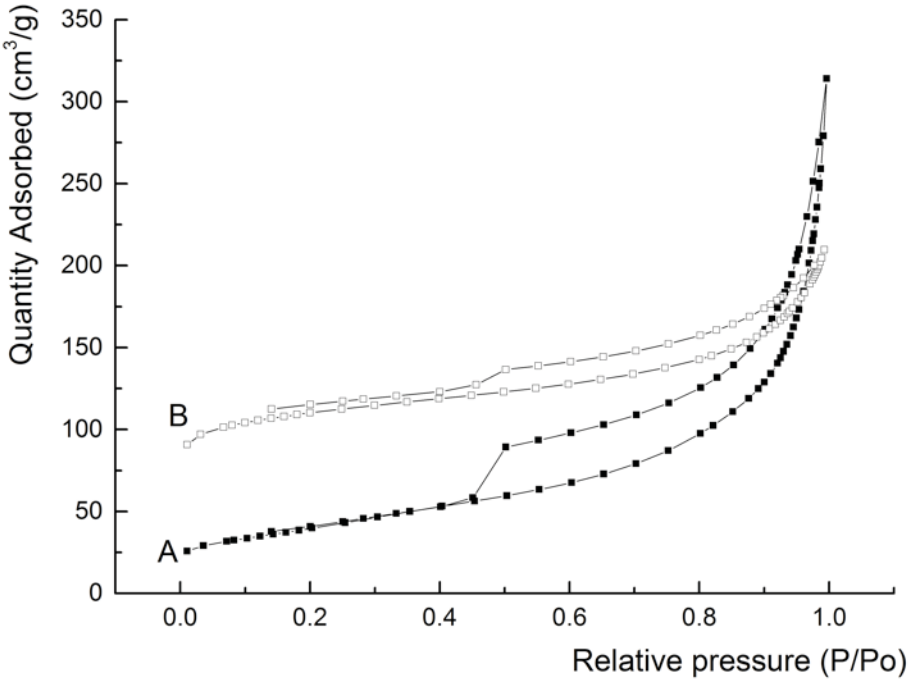

Figure 4.10 Nitrogen adsorption/desorption isotherms for (A) Bare carbon monolith (prepared without the addition of carbon nanoparticles for comparative purposes) and (B) carbon on carbon monolithic composite containing carbon onions.

The steep desorption region in the hysteresis loop (Figure 4.10) is associated with the (forced) closure of the loop due to the so-called tensile strength effect. Closure of the hysteresis loop at P/P_0 ~0.4 indicates that the mesopores were relatively small in size. The desorption branch of the isotherm for Sample B shown in Figure 4.10 did not close at the expected relative pressure of 0.4 which suggests there is a low pressure hysteresis phenomenon occurring. This commonly occurs in microporous materials and the presence of low-pressure hysteresis in the desorption branch of the isotherms of porous solids has been attributed to a number of parameters including the porosity of the adsorbent, a lack of equilibration in the adsorption isotherm and insufficient outgassing during sample preparation [49]. Both samples underwent the same outgassing and equilibration procedures, however, the carbon monolithic composite with carbon onions showed a positive y-intercept on the t-plot (shown in Appendix A, Figure A3) indicating the presence of some

microporosity in the material, unlike the blank carbon monolith. There may be kinetic restrictions for N_2 at cryogenic temperatures resulting from residual moisture in narrow micropores. Similar low-pressure hysteresis has been observed in microporous carbon materials [50]. It is also thought that there may be diffusional limitations resulting from the micropore morphology and connectivity. If there are micropores present with narrow openings their filling may be kinetically hindered [51-52].

Estimated mesopore diameters for both materials were in agreement, with the Barrett-Joyner-Halenda (BJH) method applied [53] to find mesopore diameters of 11.7 ± 0.8 nm and 10.5 ± 3.9 nm, for the blank carbon monolith and monolithic composite, respectively (see Table 4.1) (BJH pore size distribution curves are shown in Appendix A, Figure A1 and A2). The carbon monolithic composite had a slightly greater mesopore volume of 0.35 ± 0.04 cm^3/g compared to 0.33 ± 0.05 cm^3/g for the blank monolith. The addition of DND appears to have increased the prevalence of mesopores with smaller diameters. Significantly then it is clear that the addition of DND to the carbon monolith can be used to affect both the macroporous and mesoporous structure, as evidenced by both BET, and SEM images discussed previously (Figure 4.3). The average BET surface area calculated for the monolithic composite at P/P_0 from 0.05 to 0.30 was 214 m^2/g, nearly twice which obtained for the bare carbon monolith, which was 115 m^2/g. The higher surface area in the composite material is due to the increased macro and meso-porosity, and is also attributed to the formation of the 5.24 nm carbon onions within the monolithic structure. These nanomaterials are known to display high surface areas [54] and it appears that they have increased surface areas without contributing significantly to the porous structure. This represents a significant increase, which if related to the concentration of DND added, could provide a unique method for control of this important parameter.

Table 4.1 Structural characteristics of carbon monolithic composites

Monolith	S_{BET} [a] (m^2/g)	V_p [a] (cm^3/g)	Pore diameter [b] (nm)
Bare carbon monolith	115 ± 8	0.33 ± 0.05	11.7 ± 0.8
Carbon monolith with carbon onions	214 ± 17	0.35 ± 0.04	10.5 ± 3.9

[a] The Brunauer-Emmett-Teller (BET) method was used to calculate specific surface areas.
[b] The Barrett-Joyner-Halenda (BJH) method was used to calculate mesopore diameters from the adsorption branch of the isotherm.

4.4 Conclusion

New bimodal carbon on carbon monolithic composites were successfully prepared by embedding DND in a resorcinol formaldehyde precursor mixture, containing Fe^{3+} as a catalyst for localised graphitisation, and silica gel as a hard template. Pyrolysis cycles reached a maximum temperature of 1250 °C, which was sufficiently high enough to result in the full graphitisation of the DND precursor, forming quasi-spherical carbon onions within the monolith, which had an average diameter of 5.24 nm. The inclusion of DND increased the graphitisation of the composite material, which contained both sp^2 and sp^3 carbon phases following pyrolysis. Both the macroporous network and mesopores were affected by the addition of DND, and the BET surface area and pore volume were increased in comparison with a blank carbon monolith. It was also shown that the DND could be preserved within the composite by reducing the temperature of pyrolysis, thus demonstrating the ability to easily control nano-carbon synthesis within a monolithic composite. Carbon monolithic composites with carbon onions are suitable for application in a number of areas such as electrode materials, chromatographic applications and extraction processes for larger molecules including organic pollutants or biomolecules.

To the best of the authors' knowledge, this is the first report of the controlled production of carbon onions from DND within such a carbon monolithic composite. It demonstrates that the type of nano-carbons present in the final monolithic composite can be tuned, simply by controlling the temperature of pyrolysis.

References

1. Colombo, P. In Praise of Pores, *Science* 322 (2008) 381-383.
2. Wang, D-W., Li, F., Liu, M., Lu, G.Q. Cheng, H-M. 3D Aperiodic Hierarchical Porous Graphitic Carbon Material for High-Rate Electrochemical Capacitive Energy Storage, *Angew. Chem. Int. Ed.* 47 (2008) 373–376.
3. Ruo-Wen, F.U., Zheng-Hui, L.I., Ye-Ru, L., Feng, L.I., Fei X.U., Ding-Cai, W.U. Hierarchical Porous Carbons: Design, Preparation and Performance in Energy Storage, *New Carbon Materials*, 26 (2011) 171–179.
4. Sevilla, M., Fuertes, A.B. Sustainable Porous Carbons with a Superior Performance for CO_2 Capture, *Energy Environ. Sci*. 4 (2011) 1765-1771.
5. Hao, G-P., Li, W-C., Qian, D., Lu, A-H. Rapid Synthesis of Nitrogen-Doped Porous Carbon Monolith for CO_2 Capture, *Adv. Mater.* 22 (2010) 853–857.
6. Gupta V.K., Saleh, T.A. Sorption of Pollutants by Porous Carbon, Carbon Nanotubes and Fullerene – An Overview, *Environ. Sci. Pollut. Res*. 20 (2013) 2828–2843.
7. Chuenchom, L., Kraehnert, R., Smarsly, B.M. Recent Progress in Soft-Templating of Porous Carbon Materials, *Soft Matter*, 8 (2012) 10801-10812.
8. Roberts, A.D., Li, X., Zhang, H. Porous Carbon Spheres and Monoliths: Morphology, Control, Pore Size Tuning and their Applications as Li-Ion Battery Anode Materials, *Chem. Soc. Rev*., 34 (2014) 4341-4356.
9. Dutta, S., Bhaumik A., Wu, K.C-W. Hierarchically Porous Carbon Derived from Polymers and Biomass: Effect of Interconnected Pores on Energy Applications, *Energy Environ. Sci*., 7 (2014) 3574-3592.
10. Liang, C., Dai, S., Guiochon, G. A Graphitized Carbon Monolithic Column, *Anal. Chem*., 75 (2003) 4904–4912.

11. Eltmimi, A. H., Barron, L., Rafferty, A., Hanrahan, J. P., Fedyanina, O., Nesterenko, E., Nesterenko, P. N., Paull, B. Preparation, Characterisation and Modification of Carbon-Based Monolithic Rods for Chromatographic Applications, *J. Sep. Sci*. 33 (2010) 1231–1243.
12. Ruiz, V., Blanco, C., Santamaría, R., Ramos-Fernández, J. M., Martínez-Escandell, M., Sepúlveda-Escribano, A., Rodríguez-Reinoso, F. An Activated Carbon Monolith as an Electrode Material for Supercapacitors, *Carbon*, 47 (2009) 195-200.
13. He, X., Male, K.B., Nesterenko, P.N., Brabazon, D., Paull, B., Luong, J.H.T. Adsorption and Desorption of Methylene Blue on Porous Carbon Monoliths and Nanocrystalline Cellulose, *ACS Appl. Mater. Interfaces* 5 (2013) 8796-8804.
14. Wang, Z., Li, F., Ergang N.S., Stein, A. Effects of Hierarchical Architecture on Electronic and Mechanical Properties of Nanocast Monolithic Porous Carbons and Carbon-Carbon Nanocomposites, *Chem. Mater.* 18 (2006) 5543-5553.
15. Qiu, L., Liu, J.Z., Chang, S. L.Y., Wu, Y., Li, D. Biomimetic Superelastic Graphene-Based Cellular Monoliths, *Nat. Commun*. 3 (2012) 1241-1247.
16. He, X., Nesterenko, E.P., Nesterenko, P.N., Brabazon, D., Zhou, L., Glennon, J.D., Luong, J.H.T., Paull, B. Fabrication and Characterization of Nanotemplated Carbon Monolithic Material, *ACS Appl. Mater. Interfaces* 5 (2013) 8572–8580.
17. Mauter, M.S., Elimelech, M. Environmental Applications of Carbon-Based Nanomaterials, *Environ. Sci. Technol.* 42 (2008) 5843–5859.
18. Seymour, M.B., Su, C., Gao, Y., Lu, Y., Li, Y., Characterization of Carbon Nano-Onions for Heavy Metal Ion Remediation, *J. Nanopart. Res*. 14 (2012) 1087.
19. Chow, E.K., Zhang, X.-Q., Chen, M., Lam, R., Robinson, E., Huang, H., Schaffer, D., Osawa, E., Goga, A., Ho, D. Nanodiamond Therapeutic Delivery Agents Mediate Enhanced Chemoresistant Tumor Treatment, *Sci. Transl. Med.* 3 (2011) 73ra21.

20. Merkel, T.J., DeSimone, J.M. Dodging Drug-Resistant Cancer with Diamonds, *Sci. Transl. Med.* 3 (2013) 73ps8.

21. Kuznetsov, V.L., Chuvilin, A.L., Butenko, Y.V., Mal'kov, I.Y., Titov, V.M. Onion-Like Carbon from Ultra-Disperse Diamond, *Chem. Phys. Lett*. 222 (1994) 343–348.

22. Pech, D., Brunet, M., Durou, H., Huang, P., Mochalin, V., Gogotsi, Y., Taberna, P-L., Simon, P. Ultrahigh-Power Micrometre-Sized Supercapacitors Based on Onion-Like Carbon, *Nat. Nanotechnol*. 5 (2010) 651–654.

23. Butenko, Y.V., Krishnamurthy, S., Chakraborty, A.K., Kuznetsov, V.L., Dhanak, V.R., Hunt, M.R.C., Šiller, L. Photoemission Study of Onion like Carbons Produced by Annealing Nanodiamonds, *Phys. Rev. B* 71 (2005) 075420.

24. Oya, A., Marsh, H.J. Phenomena of Catalytic Graphitization, *J. Mater. Sci.* 17 (1982) 309-322.

25. Sevilla, M., Fuertes, A.B. Catalytic Graphitization of Templated Mesoporous Carbons. *Carbon* 44 (2006) 468-474.

26. Batsanov, S.S., Lesnikov, E.V., Dan'kin, D.A., Balakhanov, D.M. Water Shells of Diamond Nanoparticles in Colloidal Solutions, *Appl. Phys. Lett*. 104 (2014) 133105.

27. Zheng, W-W., Hsieh, Y-H., Chiu, Y-C., Cai, S-J., Cheng, C-L., Chen, C. Organic Functionalization of Ultradispersed Nanodiamond: Synthesis and Applications, *J. Mat. Chem*. 19 (2009) 8432-8441.

28. Mitev, D.P., Townsend, A.T., Paull, B., Nesterenko, P.N. Screening of Elemental Impurities in Commercial Detonation Nanodiamond Using Sector Field Inductively Coupled Plasma-Mass Spectrometry, *J. Mater. Sci*. 49 (2014) 3573–3591.

29. Mitev, D.P., Townsend, A.T., Paull, B., Nesterenko, P.N. Direct Sector Field ICP-MS Determination of Metal Impurities in Detonation Nanodiamond, *Carbon* 60 (2013) 326-334.

30. Butenko, Y.V., Kuznetsov, V.L., Paukshtis, E.A., Stadnichenko, A.I., Mazov, I.N., Moseenkov, S.I., Boronin, A.I., Kosheev, S.V. The Thermal Stability of Nanodiamond Surface Groups and Onset of Nanodiamond Graphitization, *Fuller. Nanotub. Car. Nanostruct*. 14 (2006) 557–564.
31. Mochalin, V., Osswald, A., Gogotsi, Y. Contribution of Functional Groups to the Raman Spectrum of Nanodiamond Powders, *Chem. Mater.* 21 (2009) 273-279.
32. Lin, K.W., Cheng, C.L., Chang, H.C. Laser-Induced Intracluster Reactions of Oxygen-Containing Nanodiamonds, *Chem. Mater*. 10 (1998) 1735-1737.
33. Xu, N.S., Chen, J., Deng, S.Z. Effect of Heat Treatment on the Properties of Nano-Diamond Under Oxygen and Argon Ambient, *Diam. Relat. Mater*. 11 (2002) 249–256.
34. Chen, J., Deng, S.Z., Chen, J., Yu, Z.X., Xu, N.S. Graphitization of Nanodiamond Powder Annealed in Argon Ambient, *Appl. Phys. Lett*. 74 (1999) 3651-3653.
35. Ko, T.H., Kuo, W.S., Lu, Y.R. The Influence of Post-Cure on Properties of Carbon/Phenolic Resin Cured Composites and Their Final Carbon/Carbon Composites, *Polym. Composite* 21 (2000) 96–103.
36. Ko, T.H., Kuo, W.S., Chang. Y.H. Microstructural Changes of Phenolic Resin During Pyrolysis, *J. Appl. Polym. Sci*. 81 (2001) 1084–1089.
37. Zou, Q., Wang, M., Li, Y., Zhao Y., Zou, L. Fabrication of Onion-Like Carbon From Nanodiamond by Annealing, *Sci. China Ser. E-Technol. Sci.* 52 (2009) 3683–3689.
38. Qiao, Z., Li, J., Zhao, N., Shi, C., Nash, P. Graphitization and Microstructure Transformation of Nanodiamond to Onion-Like Carbon, *Scr. Mater*. 54 (2006) 225–229.
39. Cebik, J., McDonough, J.K., Peerally, F. Medrano, R., Neitzel, I., Gogotsi, Y., Osswald, S. Raman Spectroscopy Study of the Nanodiamond-to-Carbon Onion Transformation, *Nanotech*. 24 (2013) 205703.
40. Tuinstra F., Koenig, J.L. Raman Spectrum of Graphite, *J. Chem. Phys.* 53 (1970) 1126-1130.

41. Ferrari A.C., Robertson J. Raman Spectroscopy of Amorphous, Nanostructured Diamond-Like Carbon, and Nanodiamond, *Phil. Trans. R. Soc. Lond. A* 362 (2004) 2477–2512.

42. Ferrari, A.C., Robertson, J. Interpretation of Raman Spectra of Disordered and Amorphous Carbon, *J. Phys. Rev. B* 61 (2000) 14095–14107.

43. He, X., Zhou, L., Nesterenko, E.P., Nesterenko, P.N., Paull, B. Omamogho, J.O., Glennon, J.D., Luong, J.H.T. Adsorption and Desorption of Methylene Blue on Porous Carbon Monoliths and Nanocrystalline Cellulose, *Anal. Chem.* 84 (2012) 2351-2357.

44. Xie, F.Y., Xie, W.G., Gong, L., Zhang, W.H., Chen, S.H., Zhang, Q.Z., Chen, J. Surface Characterization on Graphitization of Nanodiamond Powder Annealed in Nitrogen Ambient, *Surf. Interfac. Anal.*, 42 (2010) 1514-1518.

45. Krishnamurthy, S., Butenko, Y.V., Dhanak, V.R., Hunt, M.R.C., Šiller, L. In-Situ Formation of Onion-Like Carbon from the Evaporation of Ultra-Dispersed Nanodiamonds, *Carbon* 52 (2013) 145-149.

46. Petit, T., Arnault, J-C., Girard, H.A., Sennour, M., Bergonzo, P. Early Stages of Surface Graphitization on Nanodiamond probed by X-Ray Photoelectron Spectroscopy, *Phys. Rev. B* 84 (2011) 233407.

47. Ostrovidova, G.U., Makeev, A.V., Biryukov, A.V., Gordeev, S.K. Carbon Nanocomposite Materials as Medicinal Depot, *Mater. Sci. Eng. C* 23 (2003) 377-381.

48. Lowell, S., Shields, J.E., Thomas M.A., Thommes, M. *Characterization of Porous Solids and Powders: Surface Area, Pore Size and Density*, London: Kluwer Academic Publishers; 2004.

49. Silvestre-Albero, A. M., Juárez-Galán, J. M., Silvestre-Albero, J., Rodríguez-Reinoso, F. Low Pressure Hysteresis in Adsorption: An Artifact? *J. Phys. Chem. C* 116 (2012) 16652-16655.

50. Musa, M. S., Sanagi, M. M., Nur, H., Wan Ibrahim, W. A., Understanding Pore Formation and Structural Deformation in Carbon Spheres During KOH Activation, *Sains Malaysiana* 44 (2015) 613-618.
51. Jeromenok, J., Weber, J., Restricted Access: On the Nature of Adsorption/Desorption Hysteresis in Amorphous, Microporous Polymeric Materials, *Langmuir* 29 (2013) 12982-12989.
52. Rodríguez-Reinoso, F., Rouquerol, J., Sing, K. S. W., Johannes Gutenberg, K. K. U., *Characterization of Porous Solids II,* Amsterdam: Elsevier Science Publishers, 1991.
53. Barrett, E.P., Joyner, L.G., Halenda, P.P. The Determination of Pore Volume and Area Distributions in Porous Substances. I. Computations from Nitrogen Isotherms, *J. Am. Chem. Soc*. 73 (1951) 373–380.
54. McDonough, J.K., Gogotsi, Y. Carbon Onions: Synthesis and Electrochemical Applications, *Electrochem. Soc. Interface* 3 (2013) 61-66.

Chapter 5.

Hierarchical Porous Graphitic Carbon Monoliths with Detonation Nanodiamonds: Synthesis, Characterisation and Adsorptive Properties

Abstract

The addition of nano-carbons to composite materials is an area of significant research interest, when their addition results in improved properties. This work reports on the use of detonation nanodiamond (DND) in the preparation of porous carbon monoliths and an investigation of the properties of the final carbon-nanocarbon composite material. Porous carbon-nanodiamond (CND) monoliths, with macro-, meso- and micropores were prepared by carbonisation of a resorcinol-formaldehyde (RF) polymeric rod with an Fe(III) catalyst and spherical silica template. Pore characteristics and BET surface areas were determined from N_2 isotherms, with surface areas in the range 214-461 m^2/g, depending on DND content. SEM imaging further confirmed the hierarchical pore structure present, where there was a tri-modal structure for monoliths containing nanodiamond following pyrolysis up to 900 °C. The addition of DND had a stabilising effect on the RF resin, where increased DND content resulted in smaller average mesopore diameters and increased microporosity. Thermogravimetric analysis, TEM imaging, energy dispersive x-ray electron spectroscopy and Raman spectroscopy were employed to evaluate the properties of this new composite material. The adsorption of methylene blue (MB) and neutral red (NR) dyes from water onto the composite monoliths was investigated and compared with activated carbon in order to further evaluate their physical and adsorptive properties. The results showed that CND material adsorbs these two cationic dyes more effectively than activated carbon, due to a more accessible pore network. Furthermore, the DND content had a direct effect on adsorption capacities for the dye molecules. The adsorption isotherms coincided with Langmuir and Freundlich adsorption models. A maximum adsorption capacity of 599 mg/g and 284 mg/g was achieved for NR and MB, respectively, on the CND composites.

5.1 Introduction

The design and preparation of porous carbon materials with suitable structure and properties is the subject of significant research interest, due to their potential application in a wide variety of areas, including water purification, energy storage, supercapacitors [1], gas separation, and as catalyst supports [2]. Their unique properties include excellent thermal and mechanical stability, large pore volumes, high surface areas, and chemical inertness. As predominantly hydrophobic porous carbons, these materials are also highly utilised in the area of environmental remediation, adsorption and solid phase extraction (SPE) [3], offering an alternative selectivity to silica or polymer-based adsorbents. Porous carbon materials provide the advantage of chemical stability, which eliminates swelling in most organic solvents. Furthermore they have high hydrolytic stability across a wide pH range (1-14), unlike silica, which has a relatively narrow pH stability range (pH 2-8) due to the presence of polar silanol groups. Carbonaceous materials have been identified as an alternative adsorbent material for use in applications such as SPE and liquid chromatography [4-5]. Their graphitic nature results in unique retention behaviour and allows the extraction of polar (and highly soluble) species from aqueous samples based on hydrophobic interactions, π-π interactions, or weak ion exchange mechanisms when the appropriate conditions are selected [6]. The development of new selective and useful adsorbents still remains an important challenge in SPE, chromatography and other adsorption applications where sample enrichment, extraction or pollutant removal is a requirement. Carbon monoliths have emerged relatively recently for SPE and chromatographic applications [7-9], after their widespread use in other fields including catalyst supports, electrode materials and energy storage devices [10-11].

Compared to carbon powders, continuous porous carbon monoliths offer a high degree of permeability, ease of handling, lower hydraulic resistance, and improved electrolyte diffusion, all of which are advantageous for applications in separation processes, such as chromatography or filtration [7, 12]. These attributes arise from the high degree of porosity and the hierarchical

interconnected porous network within carbon monolithic materials. This enhances accessibility to the smaller pores considerably, allowing for greater ease of adsorption of larger molecules. The adsorption of larger molecules has been shown to be a kinetically unfavourable process by Weber and co-workers [13]. Enhancing the accessibility to mesopores through development of an interconnected macro-mesoporous network can improve adsorption of these larger molecules [14].

Porous hierarchical carbon monoliths have a high adsorption capability due to their chemical and thermal stability, high surface area and pore volume, as well as their accessible interconnected pore network. Porous carbon materials are highly utilised in gas and liquid separation techniques, particularly liquid chromatography (LC) and solid phase extraction (SPE), and a number of recent reviews have focused on carbonaceous materials for application in adsorption and analytical science [15-18], and the use of carbon monoliths in sample preparation and environmental adsorption applications has also been discussed in recent reviews [19-20]. Carbon monoliths can be prepared in a variety of forms, and the rod-shaped composites reported within this work are suitable for use in such applications, such as SPE for the extraction or pre-concentration of analytes in liquid samples of environmental, biological or pharmaceutical origin. The use of carbon monoliths as alternative sorbents for HPLC has been explored by Guichon and co-workers [8], and later by Eltmimi *et. al.* [7] using a method adapted from that developed by Knox and Gilbert in 1979 for production of porous graphitic carbon-based materials for HPLC [21], however separation efficiencies were relatively poor, and this research is still at the exploratory stage of development. The development of new adsorbents whether through fabrication of new compositions, or through surface modifications, is important in furthering separation and extraction technologies. These new materials require a detailed characterisation and understanding of their features, including adsorptive properties, to ensure their successful application. The adsorption of two organic dyes as model compounds, methylene blue (MB) and neutral red (NR) on CND materials was therefore investigated as a means to probe their adsorptive properties and to improve understanding of their

structural characteristics. The adsorption of aqueous dyes on porous carbon materials derived from numerous sources is a widely studied topic [22-23], and pore size plays an important role in adsorption capability. Mesoporous carbons have been shown to have a much higher adsorption capacity for larger molecules, such as dyes, than activated carbons, as they are not limited by the size exclusion effect of micropores present in activated carbons [24-26]. The interconnected macro-mesoporous network of CND materials was expected to allow for greater ease of adsorption of the large dye molecules, and carbon monoliths have been shown to outperform activated carbon and nanocrystalline cellulose in adsorption of MB [9]. The adsorption process in this case was predominantly physical, where it was shown that pH and temperature had very little effect on the dye uptake.

Carbon monoliths are typically prepared with a variety of templating methods, often using a sacrificial template to create pores, or by carbonisation of porous polymeric monoliths [26]. Templating synthesis allows for the control of carbon structure in terms of the pore size and morphology, where the synthesis conditions, and the type of template can be altered control the features of the final monolith. Often used templates include; silica (ordered mesoporous silica, silica sol, gel and opals), zeolites, clays or sol-gel derived scaffolds [27]. The use of silica monoliths as a hard template has proven an effective route for fabrication of high surface area carbon monoliths [28-29], and recently, the use of spherical silica particles as a template has proven successful in preparation of highly interconnected carbon monoliths for chromatographic and adsorption applications [7-9], where the improved accessibility to mesopores through the macro-mesoporous network has shown good adsorption of bulky organic molecules, such as dyes. These materials are suitable for electrochemical, SPE, and flow-through applications (e.g. HPLC or filtration) where the reduced pressure due to the macroporous network is advantageous. In these examples, the synthetic approach has involved the polymerisation of a RF co-polymer upon the spherical silica template (1-10 μm diameter), with the inclusion of an iron (III) catalyst for localised graphitisation, providing

the resultant monolith with a relatively high graphite index (without the use of high-temperature graphitisation).

These materials can also be surface modified, and their reaction/interaction selectivity tailored towards certain classes of compounds, or indeed to improve their structure and properties, such as pore size distributions and surface areas. An interesting new aspect of this research involves the formation of carbon-nanocarbon composite monoliths, through the modification of the carbon skeleton with carbon nanoparticles (CNPs) including fullerenes and thermally annealed carbon-onions. These CNPs were introduced into the polymerisation mixture prior to its carbonisation, and their introduction has been shown to result in significant changes to the material's properties. Improvements in surface area and pore size distributions were reported, as well as changes in the electrochemical properties and in the graphitic nature of the monoliths [30-31]. It can be assumed, provided that the CNPs can be preserved during high temperature pyrolysis cycles, that their inclusion into the carbon monolithic structures will lead to a transfer of new properties to the final composite material.

Diamond is known to have a high thermal conductivity with negligible thermal expansion at high temperatures [32]. Commercial nanodiamond produced *via* detonation synthesis and oxidative purification, also exhibits these unique thermal and mechanical properties, while retaining excellent chemical stability. These DNDs are available in commercial volumes at a low cost making DND an ideal candidate material for inclusion in carbon monolithic composites, particularly for targeted applications in electrochemical, chromatographic and/or adsorption processes [33]. It is considered a favourable type of polymer filler due to improved heat dissipation during polymerisation. To-date DND has been the focus of research in areas such as biomedicine (drug delivery, biomedical implants, bio-imaging), mechanical applications (polishing and lubrication), catalytic and electrochemical applications [34], and in adsorption and separation processes [35]. DND is also attracting significant interest in the area of composite materials, including polymer-based

composites [36-38] and carbon-carbon composites [39], and improvements in material properties have been reported as a result of DND addition [40].

Previously work within our group has focused on the preparation of carbon monoliths with CNPs, wherein the precursor monolith was carbonised up to 1250 °C, wherein CNPs present within the carbon monolith have undergone complete graphitisation, including full conversion to graphitic structures, such as DND to carbon-onions [31]. Herein the temperature of pyrolysis has been reduced to 900 °C in order to preserve DND within the monolith during this process. A detailed examination of the production and characterisation of the resulting composite monoliths is presented. The tri-modal porous monoliths (pore size distribution has three modes) exhibit a highly interconnected pore network comprising of macro-pores resulting from the silica template, and meso- and micro-pores resulting from the pyrolysis and catalytic graphitisation and embedding of DND in the precursor RF resin. Catalytic graphitisation of the RF resin is known to result in a loss of micro-porosity, and micropores must generally be formed after pyrolysis. This is commonly introduced using physical or chemical activation [41-42]. The addition of DND offered a degree of stability to the RF resin during pyrolysis, which resulted in preservation of some of the microporous structure, offering a potential route towards tailoring pore size distributions within carbon monoliths for specific applications in adsorption of single molecules e.g. CO_2, H_2, with appropriate surface treatments [43]. The adsorptive properties of the composite monoliths were also investigated in order to evaluate their potential application as an adsorbent for extraction or remediation processes. This characterisation of adsorptive properties focused on two organic dyes as model adsorbates, in order to improve understanding of the changing monolith pore networks as DND content increased, and to investigate their suitability as potential adsorbents for bulky organic molecules.

5.2 Experimental Methods

5.2.1 Preparation of Carbon-Nanodiamond Monoliths

For the preparation of carbon monoliths with DND, an aliquot of aqueous DND suspension was added to a precursor polymerisation mixture containing an RF resin in butanol. In preparation of the precursor mixture, 1 g of 5 μm silica particles with a surface area of 359 m^2/g and a pore size of 550 Å (Nucleosil silica beads from Macherey-Nagel Duren, Germany) was dispersed in 1.85 mL of 1-butanol. After sonicating the mixture for one hour, 0.367 g of resorcinol and 0.18 g of ferric (III) chloride (99% Sigma Aldrich, Dublin, Ireland) were added. At this point, the mixture was under constant stirring while an aliquot of single digit ND (50 mg/mL aqueous suspension, Plasma Chem GmbH, Berlin, Germany) was added, followed by 0.3 g of ice-cooled 37 wt % formaldehyde-water solution (Sigma Aldrich, Dublin, Ireland). DND additions were made as a percentage of the total volume of 1-butanol (1.85 mL) such that 0.0925 mL DND suspension was added for preparation of CND1, 0.185 mL DND for preparation of CND2 and 0.555 mL DND for preparation of CND3.

The mixture was then stirred for 1 hour in an ice bath, and was subsequently added to 7 mm i.d. glass tubes which were sealed for polymerisation in a water bath (Laborggerateborse GmbH, Burladingen, Germany) at 90 °C for 15 hours. The solid rods were removed from the glass tubes following polymerisation, and placed in a fume hood for 72 hours to allow for the slow evaporation of any remaining solvent. The composites were then dried in a vacuum oven (Ehret Labor and Pharmatechnik GmbH, KG, Emmendingen, Germany) overnight at 80 °C and subjected to a final curing step at 135 °C for 4 hours.

The materials were pyrolysed in a horizontal tube furnace (model GSL1300X, MTI Richmond, VA, USA) purged with nitrogen gas. The temperature was ramped from room temperature to 800 °C at a heating rate of 2.5 °C/min, and held at 800 °C for 2 hours. It was then increased to a maximum temperature of 900 °C or 1250 °C at a rate of 10 °C/min and held for 1 hour, before cooling naturally to room temperature. This method is based upon that developed by Liang *et al.,*

and further optimised by Eltmimi *et al.,* where a maximum temperature of pyrolysis of 1250 °C was applied [7-8]. Within this current work, a maximum temperature of 900 °C was selected to preserve the DND within the final composite and these materials are referred to as CND1, CND2 and CND3 herein. Preparation and properties of DND-containing composites that were pyrolysed to 1250 °C are described in detail elsewhere [31], and were used in this study for a comparison of structural and adsorptive properties, to provide a full understanding of the effects of DND on the resin. They are referred to as CND3/1250 herein and are compared with the composite pyrolysed to 900 °C which will subsequently be referred to as CND3/900 to highlight the different temperatures of pyrolysis. The final steps in material preparation involved etching with hydrofluoric acid (HF) (38-40% Sigma Aldrich, Dublin, Ireland), where the carbon composite rods were immersed in the solution for 5 hours and were then thoroughly washed with deionised water until a neutral pH was obtained. Finally, they were dried in a vacuum oven at 80 °C for 16 hours.

5.2.2 Material Characterisation

Thermogravimetric analysis (TGA) measurements were performed (Labsys Evo instrument, Setaram, Caluire, France) on fragments of the precursor rod (after polymerisation) using a similar temperature program to that applied in the actual synthesis. A heating rate of 2.5 °C/min was used to raise the temperature from 30 to 900 °C. During the analysis, the furnace was purged with argon gas at 50 mL/min. High-resolution scanning electron microscopy (SEM) imaging was performed using a JEOL JEM 2100 transmission electron microscope with an Orius camera in-line (Gatan, Pleasanton, CA, USA). A LaB_6 filament was used with 200 kV accelerating voltage. Prior to imaging, samples were suspended in *iso*-propanol and dropped on to carbon-coated copper grids (Agar Scientific, Essex, U.K.) The solvent was allowed to evaporate prior to imaging. Imaging was also carried out on a Hitachi SU70 SEM instrument. Sample preparation here involved placing a cross section of the carbon-nanocarbon monolithic composite on to carbon tape which was placed

on an Al SEM stub and sputter coated with a thin layer of platinum prior to imaging at 1.5 kV. During this analysis, energy dispersive X-ray electron spectroscopy was also performed with an excitation energy of 4 kV applied. Surface areas and pore structures were characterised using a surface area analyser (TriStar II 3020, Micromeritics, Gemini, GA, USA) by the nitrogen adsorption/desorption method. Crushed samples were dried under vacuum at 120 °C overnight prior to surface area measurements. Raman spectroscopy was performed on a LabRam800HR (Horiba Jobin Yvon, Northampton, U.K.) where an argon laser (Innova 70-C-2, Coherent, 6 mW power) was used as the excitation source.

5.2.3 Investigation of the Adsorptive Properties of Composite Carbon Monoliths

The adsorption of two aqueous dyes, neutral red (NR) and methylene blue (MB) (Aldrich, Milwaukee, WS, USA) as model compounds on carbon monolithic composites was investigated. Their performance was compared with commercial activated carbon (20-40 mesh particle size, ~600 m^2/g surface area, 0.95 mL/g pore volume, dry basis; Aldrich, Milwaukee, WS, USA). Calibration curves were established for NR (up to 200 μM) and MB (up to 20 μM) with absorbance measurements taken using a Shimadzu 1800 UV-vis spectrophotometer (Shimadzu, Tokyo, Japan) at 450 and 665 nm, respectively. The adsorption of NR and MB from aqueous solution onto carbonaceous adsorbents was studied using the batch equilibrium technique at 20 °C. Carbon-nanocarbon composite materials were crushed to powder form using a mortar and pestle and typically 10 to 20 mg of adsorbent was introduced in to polypropylene containers containing 10 to 20 mL of dye solution ranging in concentration from 100 to 2,000 μM. All solutions were then gently stirred overnight in order to reach adsorption equilibrium. Small samples (~1 mL) were taken and immediately centrifuged (10,000 rpm for 10 min). The supernatant was then collected, and diluted where necessary (x10-100 times) depending on the dye concentration, before measurement

of their absorbance. The equilibrium dye concentration was calculated from the calibration curves, and the adsorption capacity of NR or MB on the sample was calculated using Equation 5.1.

Equation 5.1 $$q_e = (C_0 - C_e).V/m$$

Where q_e is the equilibrium adsorption capacity (mg/g), C_0 is the initial concentration of dye, C_e is the equilibrium concentration of dye (mg/L), V is the volume of dye solution (L), and *m* is the mass of adsorbent used in the experiment (g). The appropriate isotherm model can then be applied to demonstrate the feasibility of adsorption of molecules on an adsorbent for particular applications and the Langmuir and Freundlich models were compared in this work. The Langmuir isotherm model assumes that the adsorption coverage is monolayer, and that all adsorption sites are equally probable, or homogeneous. The Langmuir equation is given in Equation 5.2.

Equation 5.2 $$\frac{C_e}{q_e} = \frac{C_e}{Q_{max}} + \frac{1}{Q_{max}b}$$

Where C_e is the equilibrium concentration (mg/L), q_e is the amount of dye adsorbed at equilibrium (mg/g), Q_{max} is the maximum adsorption capacity (mg/g) and *b* is the Langmuir constant (L/mg), which relates to the energy of adsorption.

The Freundlich isotherm assumes that the adsorbent is heterogeneous, and the isotherm is described using Equation 5.3.

Equation 5.3 $$\ln Q_e = \frac{1}{n} lnC_e + lnK_F$$

Where q_e is the amount of dye adsorbed (mg/g), C_e is the equilibrium concentration (mg/L), K_f and *n* are Freundlich constants that correspond to adsorption and adsorption intensity, respectively. Freundlich equilibrium constants were calculated from the plot of log q_e vs. log C_e.

MB dye was also chosen as a model compound as it is commonly used as a standard adsorbate for estimation of surface areas, where the calculation is based upon the amount of MB adsorbed [44]. The maximum adsorption capacity, Q_{max} estimated from the Langmuir adsorption isotherm, was used to estimate the specific surface area of the composite monoliths by Equation 5.4.

Equation 5.4 $$\left(\frac{Q_{max}}{M_w}\right) \propto_{MB} N_{avo}$$

Where M_w is the molecular weight of MB, α_{MB} is the area that one molecule of MB could occupy, and N_{Avo} is Avogadro's number (6.023×10^{23} mol^{-1}). The MB molecule is assumed to be lying flat on the adsorbent in this calculation, where the rectangular volume dimensions are reported to be 1.7 x 0.76 x 0.325 nm^3 with a projected area of 1.30-1.35 nm^2 [44-45]. Herein the value for α_{MB} was taken to be 1.30 nm^2 for surface area calculations.

5.3 Results and Discussion

5.3.1 Precursor Resin Characterisation

SEM imaging on a cross section of the uncarbonised monolith precursor (Figure 5.1(A)) showed the packed silica template visible with RF resin infiltrating between the particles. The macropore template particles were closely packed within the resin under gravitational force before the polymerisation step. Following this step, Brunauer-Emmett Teller (BET) surface area measurements were calculated from N_2 adsorption isotherms (Figure 5.1(B)), and revealed the solid precursor resins to have a relatively low surface area of 55 ± 3 m^2/g for each preparation, CND1, CND2 and CND3, unaffected by % DND added. Prior to polymerisation, pyrolysis and template removal, the majority of DND particles were immersed within the resin and thus did not contribute to surface area or pore volume in the precursor material.

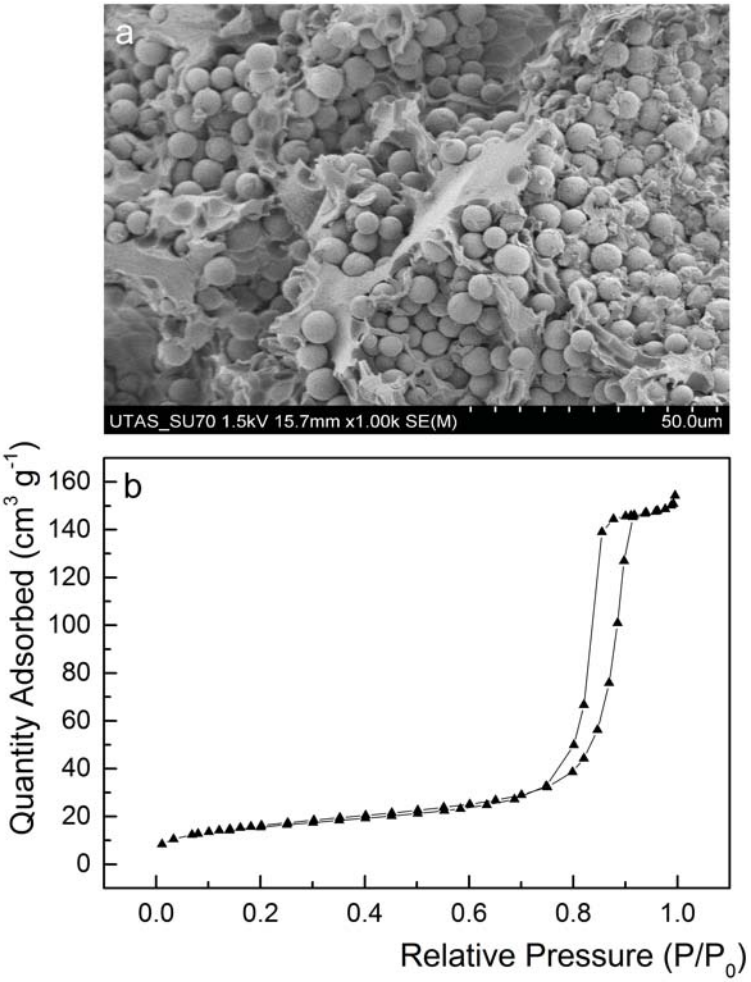

Figure 5.1 (A) SEM image (x 1K) of the carbon monolith precursor material containing detonation nanodiamond. (B) Nitrogen adsorption/desorption isotherm for the precursor phenolic resin containing nanodiamond before the pyrolysis step.

5.3.2 Structure and Morphology of Composite Monoliths

Following pyrolysis of the precursor resin, and template removal, visual inspection of the DND containing monoliths and blank carbon monoliths (prepared under the same conditions but without DND addition) saw a marked difference in material properties, notably macrostructure and light reflectance. The blank monolith surface was notably smoother upon the surface, providing a higher light reflectance, resulting in a greyer appearance compared to the blacker appearance of the DND containing monoliths. This corresponds to earlier reported observations for similar nano-composite

materials, wherein the incorporation of the CNPs (e.g. fullerenes [30]), even at relatively low concentrations, appears to disrupt the polymerisation process, resulting in a more lacy type macrostructure, compared to a more complete smooth surface structure for blank templated monoliths. Figure 5.2 shows a photograph of the two materials side by side, illustrating this difference for a blank monolith (CM), CND2 and CND3 materials.

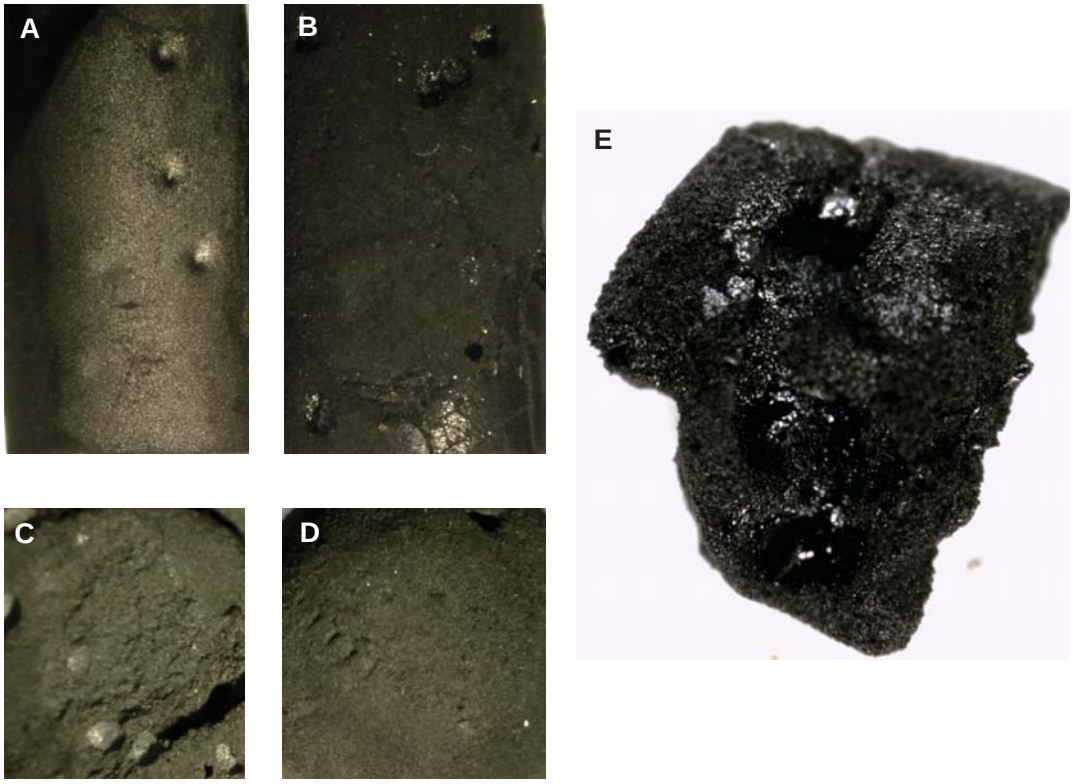

Figure 5.2 Photographs of the surface of a blank (A) and carbon-nanodiamond monolith CND2 (B), and the internal structure of the same blank (C) and CND2 composite (D). Image (E) shows a fragment of a CND3 composite monolith.

SEM imaging of the monolithic composites revealed a bimodal porous structure. The typical 3D-interconnected macroporous network can be seen in Figure 5.3(A) (showing that of CND1), resulting from the packed silica particle template that was removed by HF acid etching. Higher magnification images show the walls of these macropores to be non-uniform. Some areas were

smooth in appearance, while other regions were more porous (lace type structure), as visible in Figure 5.3(B) showing the macropore walls in CND1. Figure 5.3 (C) shows the macropore walls in CM for comparative purposes, which also displayed similar smooth and porous regions as CND materials. Higher magnification imaging also showed there to be a mesoporous structure present in the composite materials (Figure 5.3(D)). Mesopores formed as a result of the pyrolysis step during which the RF resin undergoes shrinkage and pore formation, as condensation of the polymer structure occurs. The silica spheres play a role in the textural properties of the monoliths at this level and some infiltration of the resin into the 55 nm mesopores of the template has resulted in the irregular porous surface features present on the macropore walls. The accumulation of RF resin on the surface of exposed silica beads in the precursor resin prior to carbonisation or template removal was also evident in Figure 5.1(A).

The presence of DND in the resin is expected to have affected the pore formation and if there were regions in the precursor rod where there were clusters of DND present which is expected due to its strong tendency to aggregate, the rate of pore formation throughout the rod may vary, as a result of the high thermal conductivity and low thermal expansion of DND [46-47]. The production of composites should ideally involve monodisperse “single-digit” DND particles (< 10 nm), hence a stable suspension of commercial single-digit DND particles was chosen as the additive in this study. However, it should be noted that self-assembly is a common problem for all DND particles [48], and even so-called ‘single-digit’ material has been shown to rapidly form small agglutinates (10-100+ nm) and larger aggregates (500 nm+) under certain conditions [49].

Energy dispersive X-ray (EDX) spectra were recorded for different regions on cross sections of the various pyrolysed composite monoliths containing ND to investigate elemental composition of the carbon skeleton, and the macropores, including pore walls where trace amounts of silica or iron catalyst may remain. A representative EDX spectrum taken of the carbon skeleton in CND2 is shown in Figure 5.3(E), where the carbon peak dominates. A small amount of oxygen was also

detected in all samples, due to some surface oxidation of both the carbon monolith and the embedded DND, and platinum was detected due to the thin layer of platinum coating the materials to facilitate SEM imaging. Trace levels of silica were found in some of the macropore walls, but no significant amounts were detected. There was no residual iron catalyst detected by EDX, therefore the HF acid treatment was effective for its removal.

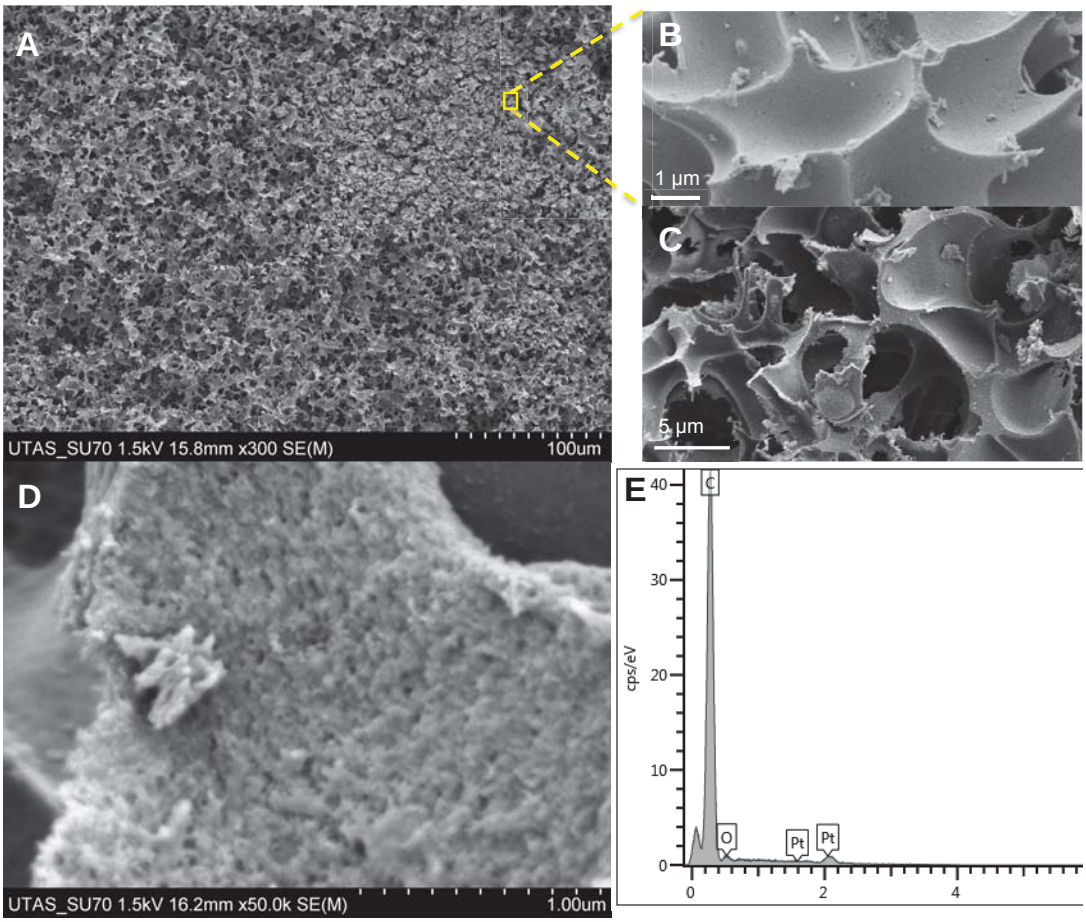

Figure 5.3 (A) Low magnification SEM image (x300) of the interconnected macroporous network in carbon monolithic composites with nanodiamond (CND). (B) Higher magnification image of the macropore walls in CND. (C) Macropore walls in blank carbon monolith for comparison. (D) High magnification (x50K) image of the macropore walls which display an irregular mesoporous structure. (E) Representatvie EDX spectrum taken on the carbon skeleton region of CND2. (Presence of Pt due to sputter coating for SEM imaging).

TEM images revealed that the carbon monolithic composites contained a mixture of amorphous and graphitic carbon. The partial graphitic nature is evidenced by structures such as the curved graphitic ribbon, highlighted in Figure 5.4(A). However, TEM imaging also revealed the preservation of the majority of DND structures following pyrolysis up to 900 °C, and confirmed the suspected aggregation of some particles. Figure 5.4(B) shows a DND agglutinate highlighted in the lower left hand corner of the image. The smaller DND cluster and single particle also visible in this image do not show any signs of surface graphitisation following pyrolysis, as was the case for the majority of DND particles imaged. It was found, however, that some particles displayed evidence of the initial steps of graphitisation. This first affects their reactive surfaces and proceeds inwards in a layer-by-layer fashion, eventually resulting in full graphitisation and conversion to onion like carbon [50]. The effects of surface graphitisation on the DND are visible in Figure 5.4(C) with typical surface-graphitised layers (sp^2 carbon) enclosing an intact ND core (sp^3 carbon) within them. It has previously been shown that graphitisation of the surface layer of bare DND when annealed in an inert atmosphere (argon) occurs between 751-800 °C. Annealing at higher temperatures results in the subsequent graphitisation of the inner layers [51]. Most DND particles embedded within the RF precursor rod, resisted conversion to sp^2 carbon, due to the fact that they were protected within the composite material.

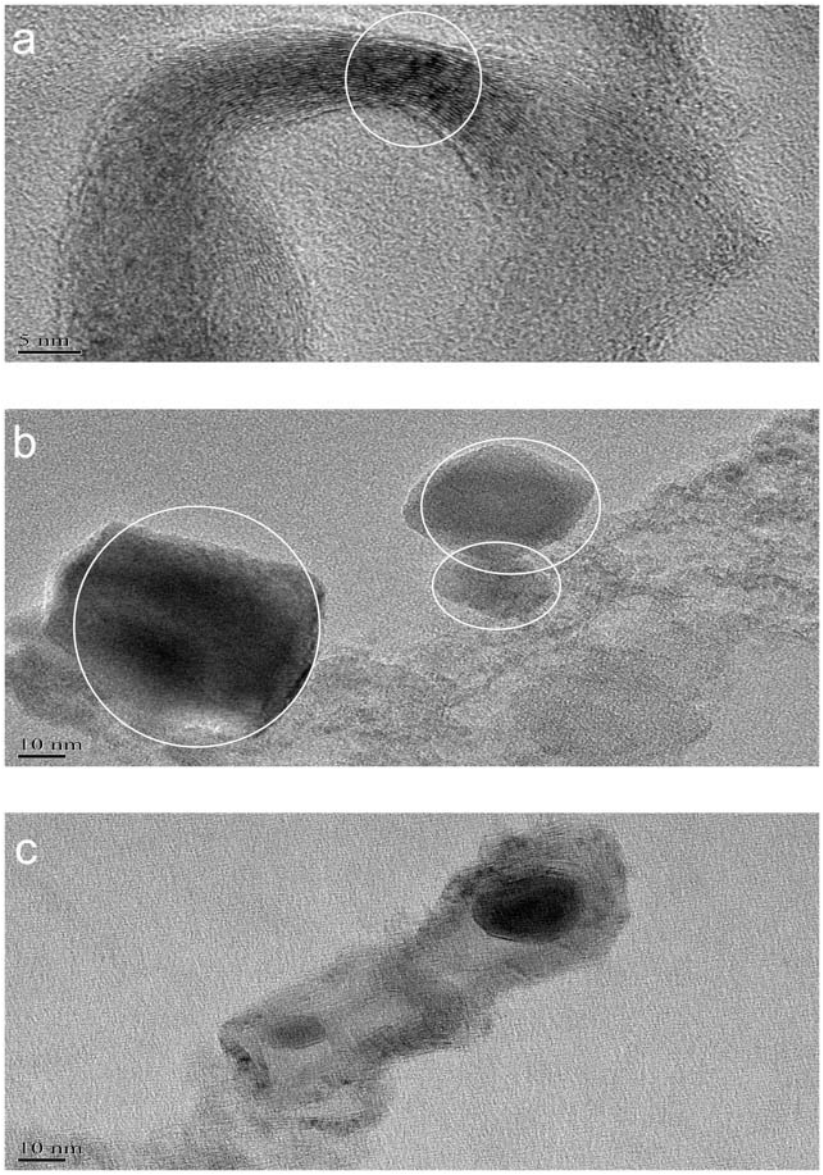

Figure 5.4 (A) TEM image of carbon monolithic composite containing graphitic ribbons (highlighted). (B) Detonation nanodiamond particles and agglutinates (highlighted) remain intact within the monolithic composite following pyrolysis up to 900 °C. (C) Some nanodiamond particles in the monolithic composite underwent surface graphitisation. The graphitic surface layers enclose the remaining nanodiamond core, forming a bucky-diamond.

5.3.3 Surface Area Measurements and Structural Characteristics

Nitrogen adsorption/desorption was used to investigate the surface areas and pore structures of the composite monoliths. The composite CND materials displayed a type IV isotherm (Figure 5.5), as commonly seen for mesoporous materials. The initial region of the isotherms for CND1 and CND2 (Figure 5.5) can be attributed to monolayer-multilayer adsorption. Both isotherms displayed a hysteresis loop, as a result of capillary condensation occurring within the mesopores. It is known that there is a relationship between the shape of the hysteresis loop, and the pore geometry, distribution, and connectivity of mesoporous sorbents [52]. These hysteresis loops can be classified as type H3, thus indicating the presence of slit-like pores in the composites. There is no limiting step in the isotherms (associated with a type H3 hysteresis loop), therefore it is likely that the pores may not have been completely filled. There is also no evidence of a sharp condensation/evaporation step, which is expected for materials with a narrow pore size distribution; therefore, the distribution of mesopore sizes in the composites is wide and likely composed of different shapes. Interestingly, the hysteresis loop here does not close between the expected relative pressures of 0.4-0.45, as was similarly seen for carbon monolithc composites containing carbon onions as described in Chapter 4. This low-pressure hysteresis phenomenon has been linked to a number of factors including the porosity of the adsorbent, a lack of equilibration in the adsorption isotherm and insufficient outgassing during sample preparation. The presence of micropores in these materials was confirmed by the t-plot (included in Appendix A, Figure A5 and A7) and there may be some kinetic hindrance or diffusional limitations depending on the micropore morphology and connectivity, as discussed in detail previously in Chapter 4.

The Barret-Joyner-Halenda (BJH) method was applied for calculation of mesopore diameters (Table 5.1) and confirmed the small size of the mesopores, with pore diameters calculated as being ~ 11 nm and 9 nm for CND1 and CND2, respectively (Pore size distribution curves are included in Appendix A, Figure A4 and A6). The trend of reductions in mesopore diameters with increased

addition of DND continued, with CND3 demonstrating mesopore diameters of only 2.4 nm. This trend was accompanied by a slight change in total pore volume, with volumes of 0.33 cm^3/g observed for CND1 and 0.35 cm^3/g for CND2. Increased DND content also resulted in significantly greater surface areas, where surface area increased from 256 to 449 m^2/g in CND1 and CND2, respectively. The change in surface area between CND2 and CND3/900 is less significant, where the addition of further amounts of DND had a stabilising effect on the resin leading to a reduction in mesopore diameter and total pore volume, without much effect on surface area. A similar stabilising effect has been observed upon the addition of fullerenes to a RF resin in fabrication of composite monolithic materials [30].

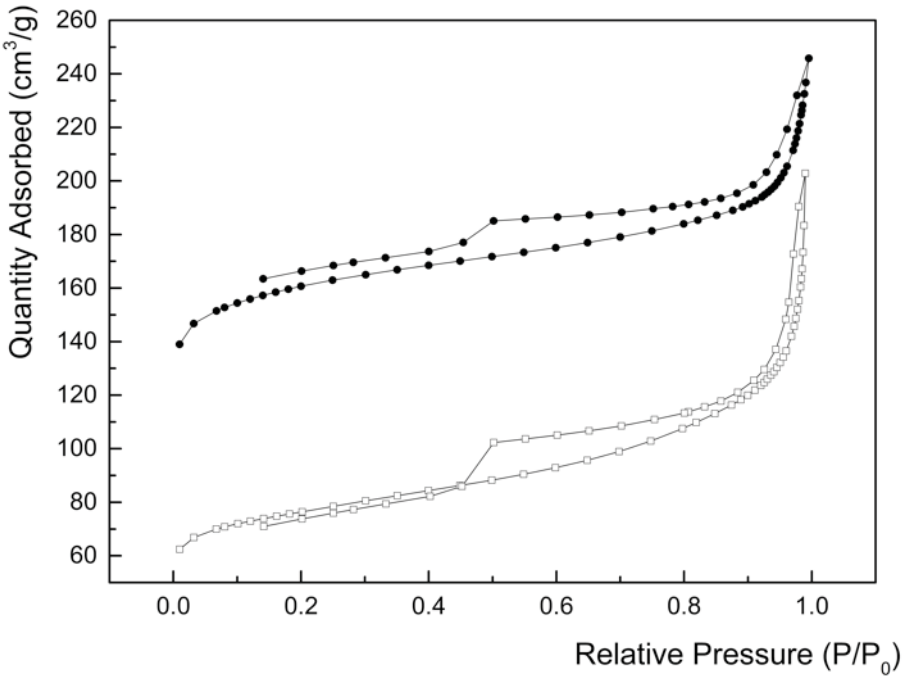

Figure 5.5 Nitrogen adsorption/desorption isotherms for carbon monoliths with nanodiamond - CND1 (□) and CND2 (●).

The initial steep adsorption at low relative pressure (P/P_0 of 0-0.1) for CND2 and the t-plot also confirms the presence of micropores, which may have formed due to the stabilising effect DND had

on the resin, allowing for more gradual pore formation during pyrolysis. Indeed the t-plot showed that there was a notable increase in micropore volume with increasing DND content. CND1 had a micropore volume of 0.08 cm^3/g, and CND2 had a micropore volume of 0.19 cm^3/g, just over 2 times greater than that of CND1. Similar to the observed surface area changes, the micropore volume of CND3 remained at a comparable level to CND2 following further addition of DND.

Interestingly, if the pyrolysis cycle is continued to a maximum temperature of 1250 °C as is often the case in synthesis of carbon monoliths from RF precursors [9, 30-31], there is a significant change to the porous structure of the DND-containing monoliths (Table 5.1, CND3/1250). The fraction of micropores was reduced to comprise only ~3.5% of the total pore volume, with mesopores dominating the porous structure at this level. This effect was also observed for CND1 and CND2 materials carbonised to 1250 °C where mesopores in the range ~6-8 nm were present, and mesopore width decreased slightly with increased DND content. Furthermore the DND itself underwent graphitisation within these composites, resulting in a more graphitic composite monolith overall [31].

Clearly, the DND plays an important role during the pyrolysis step, where it strongly affects the surface area, macro-, meso-, and micro-porous structures. However, the surface area of the DND particles did not contribute significantly to the changing surface areas between CND materials, based on the small change between CND2 and CND3, where DND content was 3 times higher. The DND particles used had a BET surface area of 362 m^2/g, however, the particles were embedded within the resin, thus their surface area was not additive to that of the composites.

Table 5.1 Structural characteristics of carbon monoliths with nanodiamond (CND) and a bare carbon monolith (CM) (n=3)

Material	T_P (° C) [a]	S_{BET} (m^2/g) [b]	V_{total} (cm^3/g)	Pore diameter (nm) [c]	V_{micro} (cm^3/g)
CND1	900	256 ± 20	0.33 ± 0.02	10.6 ± 3.2	0.08 ± 0.01
CND2	900	449 ± 63	0.35 ± 0.04	8.7 ± 2.1	0.19 ± 0.01
CND3	900	461 ± 50	0.30 ± 0.03	2.4 ± 0.1	0.18 ± 0.01
CND3	1250	214 ± 17	0.36 ± 0.04	5.9 ± 0.07	0.01 ± 0.01
CM	900	347 ± 3	0.33 ± 0.01	6.4 ± 0.6	0.10 ± 0.01

[a] Temperature of pyrolysis

[b] Specific surface areas were calculated using the Brunauer-Emmet-Teller (BET) method

[c] Mesopore diameters were calculated using the Barrett-Joyner-Halenda (BJH) method (from the adsorption branch of the isotherm)

5.3.4 Thermogravimetric Analysis

TGA can offer further insight into the effect DND inclusion on the pyrolysis and carbonisation phases of such monoliths. The pyrolysis of RF resins in the preparation of carbon-carbon composites is relatively well documented. Ko *et al.* have reported detailed findings on this topic, where they observed a weight loss of ~32% of the total material mass below 900 °C [53]. Similar findings have recently been reported for pyrolysis of RF/Fe(III) systems in the synthesis of templated carbon monolithic materials, where the total weight loss below 900 °C varied from 25% to ~50% for the different composites [30].

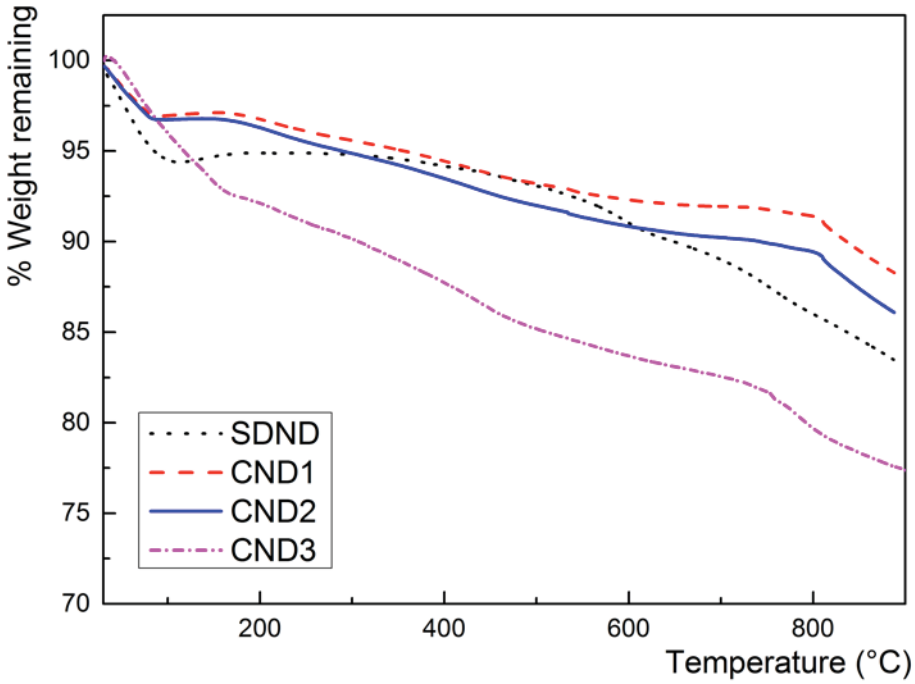

Figure 5.6 Thermogravimetric curves for single digit nanodiamond (SDND), and carbon monoliths with nanodiamonds (CND1, CND2 and CND3). Samples were heated to 900 °C at a rate of 2.5 °C/min in an atmosphere of argon (50 mL/min).

Figure 5.6 shows the multi-step decomposition resulting from pyrolysis of bare DND and CND materials. The SDND experienced a significant weight loss of 7.1% up to 160 °C due to the presence of water and other volatiles on its surface. DND is known to be a highly hygroscopic material [54-55]. The carbon monoliths underwent 3 main stages of weight loss. The initial steady decline in weight was the first point of maximum weight loss rate (Figure 5.8) up to 100 °C, where CND2 containing more DND experienced a slightly higher weight loss compared to CND1. This rapid initial loss was greater for CND3 and continued to ~170 °C. It is likely due to the release of O_2, CO, and CO_2, or other gases, as well as water and excess phenol, any residual solvent remaining in the pores of the monoliths, or any remaining unreacted monomers [56]. The difference in weight losses supports the BET data discussed above (Table 5.1) in relation to the impact of thermal properties of ND on the pyrolysis process and pore formation. The microporosity and decreasing

mesopore diameters could also account for greater reductions in sample mass within this lower temperature range as smaller pores retain more moisture from the atmosphere. The trend of increased weight loss with increased DND content observed by TGA continued up to 900 °C, and as well as being linked to pore formation (total pore volume increased between CND1 and CND2), could also be due to the high oxygen content (up to 16 wt.%) typically present on the surface of DND as a result of oxidising purification treatments [57]. This could react to produce CO or CO_2 during pyrolysis and account for a significant weight loss.

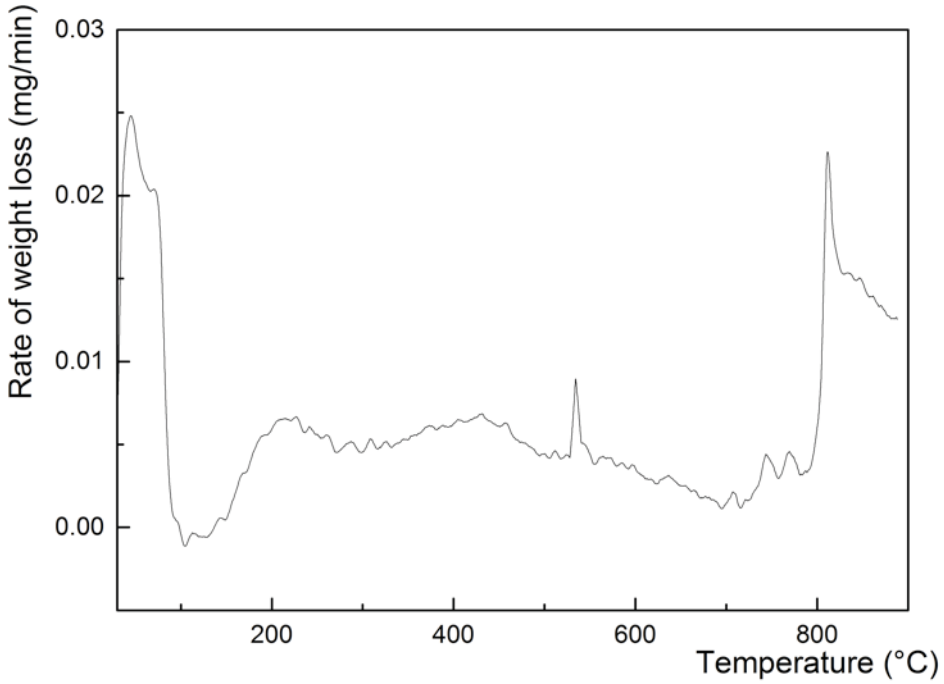

Figure 5.7 Rate of weight loss (mg/min) observed for carbon monolith with nanodiamond (CND2) during thermogravimetric analysis with temperature ramp to 900 °C at a rate of 2.5 °C/min under argon (50 mL/min).

Two further stages of weight loss occurred between 200 and 900 °C. The rate of weight loss slowed down for this significant reduction in mass (up to 6 % for CND3) which occurred between 300 and 700 °C, as similarly reported by Ko *et al.* for pyrolysis of RF resins, where there is physical

shrinkage and pore formation in the material as cross-linking of the polymer structures and condensation reactions occur [53]. The catalytic graphitisation of these resins typically occurs around 600 to 800 °C, and CND underwent further weight loss within this temperature range. The third stage of weight loss (800-900 °C) was another point of maximum for rate of weight loss (Figure 5.7), where there was a reduction of ~2.5% of the mass. During this period it is expected that further pore formation occurred, with continued graphitisation of the resin and some potential surface graphitisation of the ND, which can occur at temperatures of 751-800 °C in an inert atmosphere [58].

The total weight loss incurred by CND1 and CND2 up to 900 °C was less than 12%. This is lower than values previously reported for similar carbon monolithic materials in the literature [9, 30]. Comparing the published data on the nanotemplated carbon monolith material (~25% weight loss) and the blank monolith (~28% weight loss), composites CND1 and CND2 experienced less than half of this weight loss under the same conditions. CND3 actually underwent a ~25% weight loss, similar to the nanotemplated carbon monolith. These results are in agreement with He *et al.,* who observed the stabilisation effect of adding CNPs to the RF resin [9].

5.3.5 Raman Spectroscopy

The graphitic nature of the monoliths was further investigated by Raman spectroscopy. The Raman spectra for CND materials displayed three major peaks as shown in Figure 5.8, similar to those typically seen for samples containing both sp^2 and sp^3 carbon. The disorder in graphite has been shown to produce several Raman peaks [59]. For CND, the D band was present at 1337 cm^{-1} and is associated with imperfections in graphite, or disordered carbon [60]. The D band is usually negligible for highly ordered pyrolytic graphite, and the Raman spectrum of commercial graphite is shown in Figure 5.8 for comparison. The G band, seen at 1574 cm^{-1} for CND, is always present for sp^2 carbon materials and corresponds to the C-C bond-stretching mode in graphitic materials. The

G' band appears at 2687 cm^{-1} and is associated with sp^2 carbon. These results are in agreement with observations discussed above (Figure 5.4) and confirm the presence of a heterogeneous mixture of graphitic and amorphous carbon within in carbon framework of the composite monoliths. R-values can indicate the degree of graphitisation in a material and they are calculated from the ratio of the intensity of the D band to the G band ($R = I_D/I_G$). Taking commercial graphite with an R-value of 0.14, it can be concluded that the addition of ND to the composite monolith has resulted in a more graphitic material, as R = 0.37 for CND3, and R=0.39 for CND1. The blank CM material was less graphitic by comparison, with a calculated R-value of 0.64.

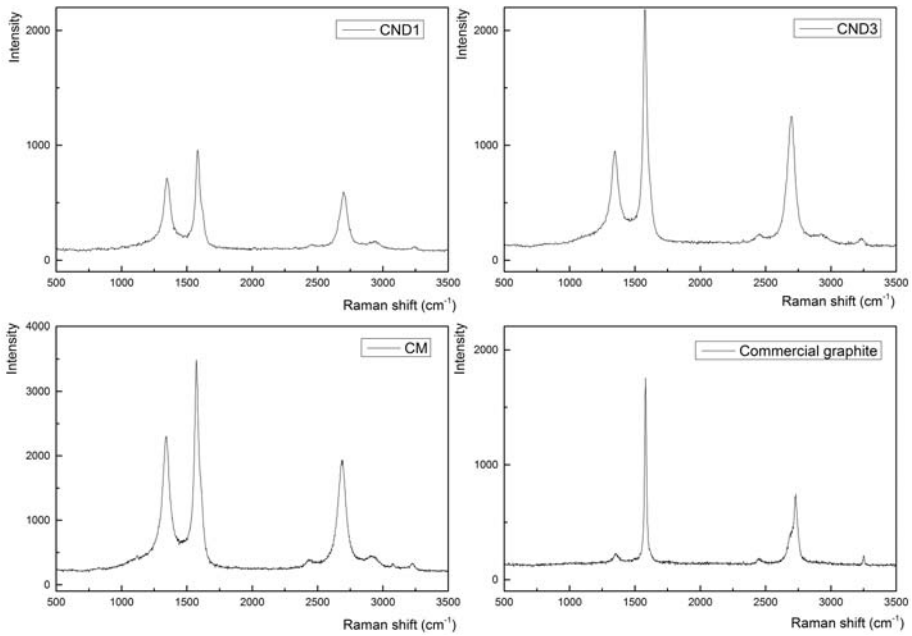

Figure 5.8 Raman spectra for composite carbon monolith with nanodiamonds (CND1, CND3), blank carbon monolith (CM) and commercial graphite.

5.3.6 Investigation of the Adsorptive Properties of Composite Monoliths

The Langmuir adsorption isotherms for both NR and MB dye on activated carbon; CND1 and CND2 are shown in Figure 5.9 and 5.10, respectively. The general trend shows an increase in the

equilibrium adsorption capacity as the equilibrium concentration is increased. The composite CND2 displayed the highest adsorption capacities for both NR and MB, and at high equilibrium concentrations these were 599 mg/g and 278 mg/g, respectively. In comparison, CND1 demonstrated a maximum adsorption capacity of 426 mg/g for NR and 132 mg/g for MB. This difference is attributed to the difference in total pore volumes, where CND2 has a greater total pore volume and a larger surface area than CND1, as discussed above in relation to Table 5.1. The presence of oxygen (as previously discussed for EDX analysis, Figure 5.3(E)) was expected to promote hydrogen bonding between the analytes and the adsorbent, which was similarly reported in previous studies on porous graphitic carbon monoliths where the uptake of MB on CND1 is comparable to that of a blank carbon monolith (no additional nano-carbons) with 128 mg/g adsorbed [9].

In comparison to the CND monoliths, activated carbon demonstrated a lower adsorption capacity for both of the dye molecules despite its higher surface area, due to its highly microporous nature. The tri-modal CND materials have a much more accessible surface area for adsorption of molecules with the macro-mesoporous network providing more accessible surface sites for adsorption. MB, with a pK_a of 3.8 exhibits a positive charge under the experimental conditions used herein, and has the potential to undergo dipole-dipole or van der Waals interactions with the oxygenated surface of CND materials. NR, on the other hand, is uncharged under the same conditions (pK_a = 6.7) and can undergo π-π stacking or hydrophobic interactions with CND. Due to the combined sp^2/sp^3 hybridisation in CND composites confirmed by TEM and Raman characterisation, and the limited evidence for the presence of functional species on the surface of CND (Figure 5.8) thus eliminating ionic interactions, the mechanism of adsorption is most likely to be due to π-π stacking or hydrophobic interactions. The molecular size of NR and MB is another factor to consider here. The molecular size of MB is known to be 1.41 x 0.55 x 0.16 nm^3, and of NR is 1.26 x 0.56 x 0.16 nm^3 [61]. The smaller NR molecule would have larger packing density in pore

channels also explaining higher NR adsorption values, and can be the reason for higher NR adsorption on activated carbon than MB. It is not likely that the molecules can fully diffuse into the micropores of CND, but the -$N(CH_3)_2$ groups of MB and NR could project into the smaller pores and undergo hydrophobic interactions or hydrogen bonding within the micropore walls. Attractive interactions between the dye molecules, as well as the fluid wall attractions can lead to multilayer adsorption occurring within the macro- and mesopores. It is worth considering that chemically activated microporous carbons have been shown to facilitate good adsorption of aqueous dye molecules, including MB. Their "honeycomb" structure and some mesoporosity provided a more accessible area for dye adsorption [62], and their varied surface chemistry allowed for many different types of solute-adsorbent interactions, which played an important role in the high adsorption capacities demonstrated.

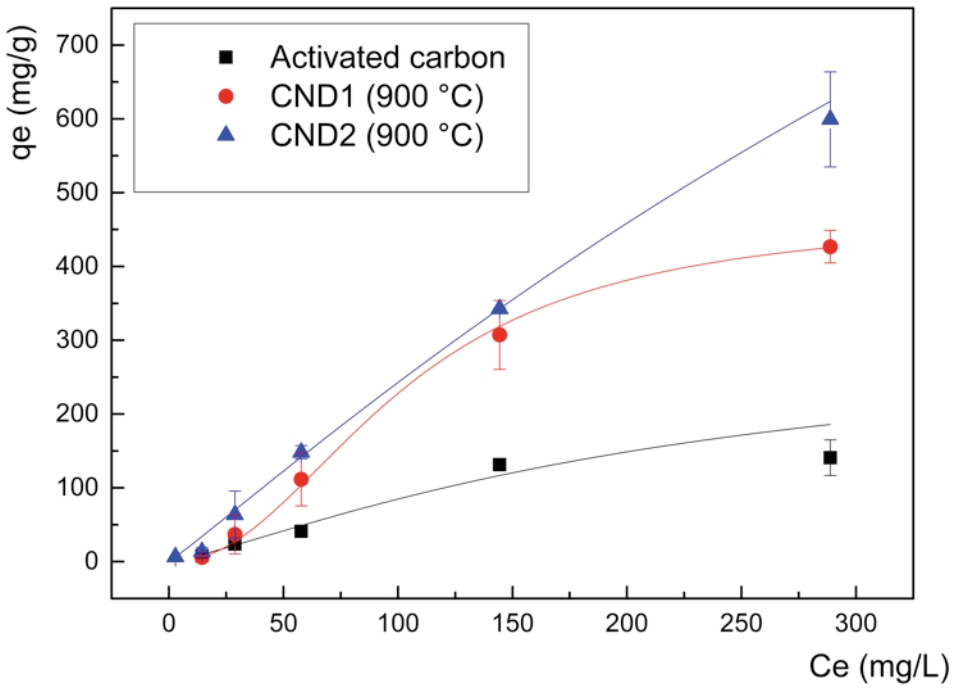

Figure 5.9 Langmuir adsorption isotherms of neutral red dye over carbon monolithic composites with nanodiamond (CND1 ▲ and CND2 ●), and activated carbon ■ showing increased dye uptake with increasing nanodiamond content in composite monoliths.

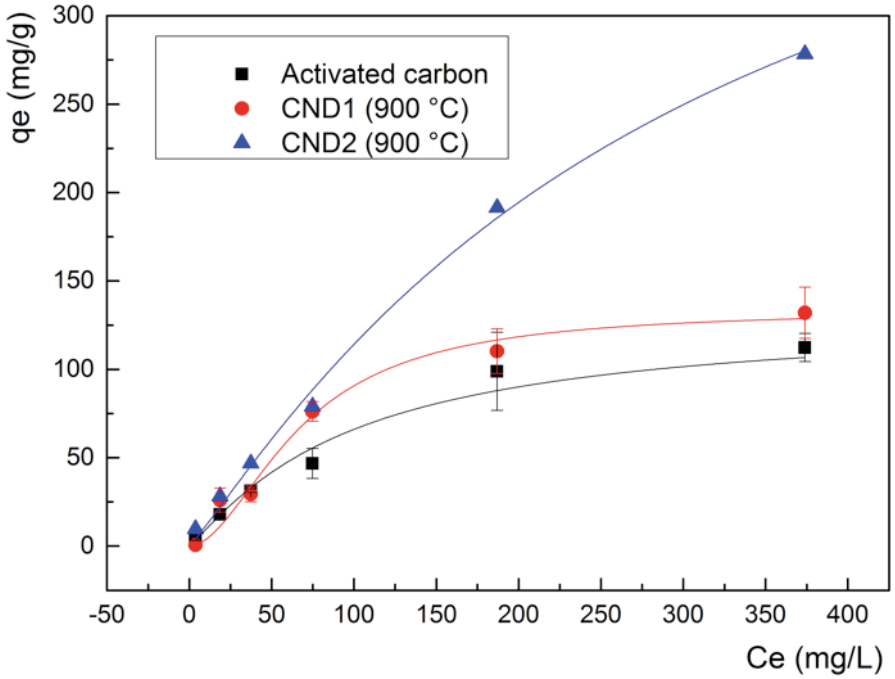

Figure 5.10 Adsorption isotherms of methylene blue dye over carbon monolithic composites with nanodiamond (CND1 ▲ and CND2 ●), and activated carbon ■ showing increased dye uptake with increasing nanodiamond content in composite monoliths.

In order to better understand the role of micropores in adsorption of dyes by these composites, the adsorption of MB on CND3 was also investigated. The composite prepared at 900 °C was selected as it displayed a very similar BET surface area and micropore volume to CND2, with a reduction in mesopore diameters (~3.5 times smaller). The performance of CND3/900 (Figure 5.11)

was actually similar to that of activated carbon for uptake of MB from solution, where the maximum adsorption capacity at high equilibrium concentrations was 112 mg/g, the same as for the activated carbon which was also 112 mg/g. CND3/900 had the lowest total pore volume of all the monoliths prepared, as shown in Table 5.1. The stabilising effect of the DND on the resin during pyrolysis has resulted in a reduction of mesopore diameters to only 2.4 nm. With the mesopores approaching micropore dimensions, there is little accessible pore space for high levels of adsorption of the bulky dye molecules. It is expected that at high equilibrium concentrations, the mesopores in CND3/900 are almost completely filled with dye molecules.

When the temperature of pyrolysis was increased to 1250 °C in CND3 the microporosity was essentially lost (Table 5.1) and small mesopores (5.9 nm) dominated the monolith at this level, which were expected to result in an improved performance for adsorption of such molecules. This composite had a lower surface area than any of the other DND-containing monoliths, however, it demonstrated a superior performance in adsorption of MB (226 mg/g) (Figure 5.11), and one comparable to that of CND1. This high capacity demonstrated by CND3/1250 is a result of the higher degree of mesoporosity in this monolith as compared to the other composite monoliths. This particular composite has the highest total pore volume (0.36 cm^3/g) and the lowest fraction of micropores (0.01 cm^3/g) of all the monoliths prepared. It is also worth considering the more graphitic nature of the CND3/1250 material in terms of adsorption performance, as it has been pyrolysed at a higher temperature than the other composites. This has given the lower surface area material a preferential selectivity to adsorption of MB molecules through π-π stacking or hydrophobic interactions. Pore volume had an important effect on adsorption capacities for all composites investigated in this study, thus suggesting that MB molecules have filled the pores of CND materials.

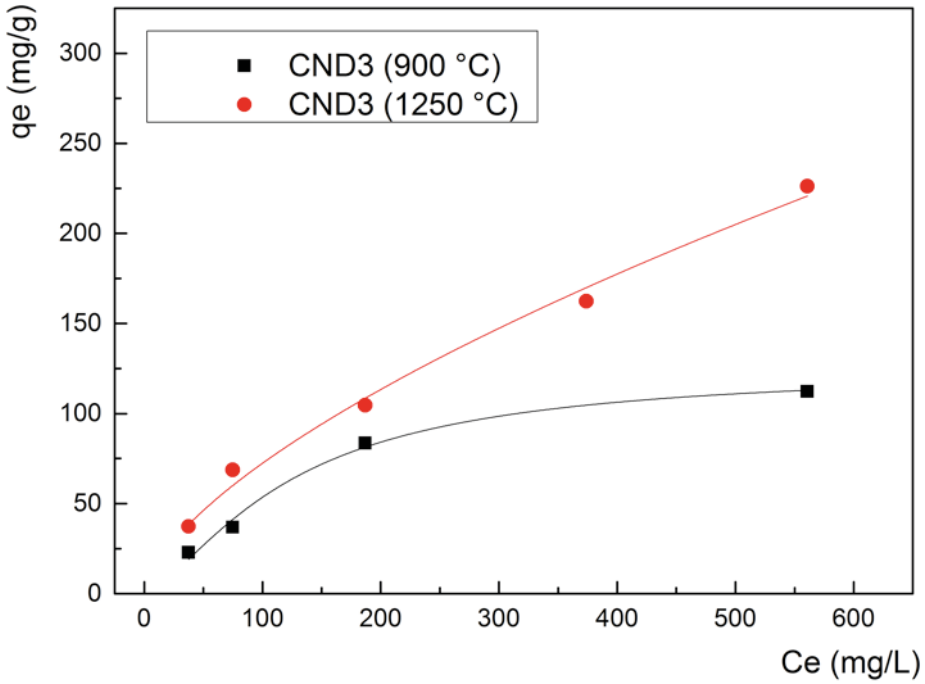

Figure 5.11 Langmuir adsorption isotherms of methylene blue dye over carbon monolithic composites with nanodiamond (CND3/900 ■ and CND3/1250 ●) showing increased dye uptake with increased temperature of pyrolysis in composite monoliths.

The appropriate isotherm model can demonstrate the feasibility of adsorption of molecules on an adsorbent for particular applications. Both the Langmuir and Freundlich isotherms were selected for consideration in this work [63]. The calculated parameters for both Langmuir and Freundlich isotherms, and the correlation coefficients (r^2) are shown in Table 5.2. The coefficients are generally higher for Langmuir than Freundlich isotherms; therefore the Langmuir isotherm is generally better for describing the adsorption of MB and NR on CND/900 materials. CND2 displayed higher Q_{max} values for both dyes than CND1 did, and this is in agreement with the discussion on Figures 5.9 and 5.10, where the larger surface area and pore volume in CND2 allowed for increased adsorption of dye molecules compared with CND1. However, CND3/1250 had a Q_{max} value that was larger than anticipated and the linear correlation coefficient for the relationship between C_e and C_e/q_e was lower at 0.979. On the basis of Q_{max} estimated from the

Langmuir model, the wet state surface areas of CND1 and CND2 were estimated to be 338 and 567 m^2/g, which was higher than those calculated by the BET method (Table 5.2), however this method of surface area estimation assumed the MB molecules were all lying flat on the adsorbent surface. It is worth considering that in both macro- and mesopores, the sorption depends on the fluid wall attraction and also on the attractive interactions between MB molecules themselves, leading to possible multilayer adsorption.

In terms of the Freundlich model, The n value indicates the degree of non-linearity between solution and adsorption concentration, and if $n > 1$, (as in this case where n = 1.24 - 1.94 and 1.62 - 2.5 shown in Table 5.2 for MB and NR, respectively) the adsorption is a physical process, as was expected based on previous MB adsorption studies on carbon monoliths [9]. A value of n within 1-10 is known to represent good adsorption, and $n > 1$ is typically the most common outcome [64-65].

Table 5.2 Langmuir and Freundlich adsorption isotherm parameters of methylene blue and neutral red dyes on carbon monolithic composites with nanodiamonds (CND)

	Langmuir Model			Freundlich Model		
Material	Q_{max} (mg g^{-1})	*b* (L mg^{-1})	r^2	K_F (mg g^{-1})	*n*	r^2
			Methylene Blue			
CND1	161.3	1.19	0.952	70.2	1.37	0.988
CND2	322.6	2.38	0.981	142.2	1.71	0.89
CND3/900	135.1	1.25	0.958	66.02	1.94	0.737
CND3/1250	555.5	0.21	0.979	91.6	1.24	0.991
			Neutral Red			
CND1	555.5	1.06	0.982	234.5	1.61	0.939
CND2	625	1.23	0.997	251.2	2.5	0.956

The effect of isotherm shape can be used to predict whether an adsorption system is favourable or unfavourable in batch processes [66]. As shown by Hall *et al.* the essential features of the Langmuir isotherm can be expressed in terms of a dimensionless constant equilibrium factor referred to as K_R, which is given in Equation 5.5 [67].

Equation 5.5 $$K_R = \frac{1}{1 + b.C_0}$$

Where K_R is a dimensionless separation factor, *b* is the Langmuir constant (L/mg) and C_0 is the initial dye concentration (mg/L) used in the adsorption studies. K_R indicates the shape of the isotherm where $0 < K_R < 1$ represents a favourable isotherm. Based on values calculated for K_R, the isotherms generated for CND were all in the favourable range with $0 < K_R < 1$, and a plot of C_0

versus K_R showed that adsorption was most favourable on CND2, corresponding well with the highest adsorption capacity achieved for this material.

5.4 Conclusion

Carbon monolithic composites containing DND were successfully prepared by pyrolysis of a RF resin with iron (III) as a localised graphitisation catalyst, and a spherical silica template for fabrication of macropores. The composite monoliths contained macro- meso- and micropores, with both sp^2 and sp^3 carbon phases co-existent in the sample. The effect of DND content on the pyrolysis process and structural characteristics of the final monolith were evaluated. For the first time, it has been demonstrated that the use of DND additives allows for the controlled modification of porous structure in a carbon monolith. Increased DND content saw improved resin stability during pyrolysis, which led to increased microporosity in the final material. By changing temperature of pyrolysis from 900 °C to 1250 °C, microporosity was essentially removed from CND composites, and the monolithic structure became predominantly mesoporous with a high degree of accessibility for target analytes through the macroporous network. These composites demonstrated good adsorption capacities for bulky dye molecules due to their accessible macro-mesoporous network, and are suitable for application in areas such as SPE and adsorption. With surface modifications or activation, they could be tailored to adsorb biomolecules, or to capture small molecules such as CO_2.

References

1. Ruo-wen, F.U., Zheng-hui, L.I., Ye-ru, L., Eng, L.I., Eei, X.U., Ding-cai, W. U. Hierarchical Porous Carbons: Design, Preparation and Performance in Energy Storage, *New Carbon Materials* 26 (2011) 171-179.
2. Upare, D.P., Yoon, S., Lee, C.W. Nano-Structured Porous Carbon Materials for Catalysis and Energy Storage, *Korean J. Chem. Eng.* 28 (2011) 731-743.
3. Gupta, V.K., Saleh, T.A. Sorption of Pollutants by Porous Carbon, Carbon Nanotubes and Fullerene – An Overview, *Environ. Sci. Pollut. Res.* 20 (2013) 2828-2843.
4. Pereira, L., Porous Graphitic Carbon as a Stationary Phase in HPLC: Theory and Applications, *Journal of Liquid Chromatography & Related Technologies,* 31 (2008) 1687-1731.
5. Carneiro, M.C., Puignou, L., Galceran, M.T., Comparison of Silica and Porous Graphitic Carbon as Solid Phase Extraction Materials for the Analysis of Cationic Herbicides in Water by Liquid Chromatography and Capillary Electrophoresis, *Anal. Chim. Acta* 408 (2000) 263-269.
6. Hennion, M.C., Graphitized Carbons for Solid Phase Extraction, *J. Chromatogr. A.* 885 (2000) 73-95.
7. Eltmimi, A.H., Barron, L., Rafferty, A., Hanrahan, J.P., Fedyanina, O., Nesterenko, E., Nesterenko, P.N., Paull, B. Preparation, Characterisation and Modification of Carbon-Based Monolithic Rods For Chromatographic Applications, *J. Sep. Sci.* 33 (2010) 1231-1243.
8. Liang, C., Dai, S., Guichon, G.A Graphitized Carbon Monolithic Column, *Anal. Chem*. 75 (2003) 4904-4912.
9. He, X., Male, K.B., Nesterenko, P.N., Brabazon, D., Paull, B., Luong, J.H.T. Adsorption and Desorption of Methylene Blue on Porous Carbon Monoliths and Nanocrystalline Cellulose, ACS *Appl. Mater. Interfaces* 5 (2013) 8796-8804.

10. Kim, Y.S., Guo, X.F., Kim, G.J., Synthesis of Carbon Monolith with Bimodal Meso/Macroscopic Pore Structure and its Application in Asymmetric Catalysis, *Catalysis Today* 150 (2010) 91-99.
11. Garcia-Gomez, A., Miles, P., Centeno, T.A., Rojo, J.M., Why Carbon Monoliths are Better Supercapacitor Electrodes than Compacted Pellets, *Electrochem. Solid State Lett.* 13 (2010) 112-114.
12. Guichon, G., Monolithic Columns in High-Performance Liquid Chromatography, *J. Chromatogr. A*. 1168 (2007) 101-168.).
13. Kilduff, J.E., Karanfil, T., Chin, Y.-P., Weber, W.J., Adsorption of Natural Organic Polyelectrolytes by Activated Carbon: A Size-Exclusion Chromatography Study, *Environ. Sci. Technol.* 30 (1996) 1336-1343.
14. Taguchi, A., Smått, J.H., Lindén, M. Carbon Monoliths Possessing a Hierarchical Fully Interconnected Porosity, *Adv. Mater.* 15 (2003) 1209-1211.
15. Nesterenko, E.P., Nesterenko, P.N., Connolly, D., He, X., Floris, P., Duffy, E., Paull, B., Nano-particle Modified Stationary Phases for High-Performance Liquid Chromatography, *Analyst* 138 (2013) 4229-4254.
16. Herrera-Herrera, A.V., Gonzalez-Curbelo, M.A., Hernández-Borges, J., Rodríguez-Delgado, M.A., Carbon Nanotubes Applications in Separation Science: A Review, *Anal. Chim. Acta* 734 (2012) 1-30.
17. Scida, K., Stege, P.W., Haby, G., Messina, G.A., Garcia, C.D., Recent Applications of Carbon-Based Nanomaterials in Analytical Chemistry: Critical Review, *Anal. Chim. Acta* 691 (2011) 6-17.
18. Valcarel, M., Cardenas, S., Simonet, B.M., Moliner-Martinez, Y., Lucena, R., Carbon Nanostructures as Sorbent Materials in Analytical Processes, *TrAC* 27 (2008) 34-43.

19. Namera, A., Nakamoto, A., Saito, T., Miyazaki, S., Monolith as a New Sample Preparation Material: Recent Devices and Applications, *J. Sep. Sci.* 34 (2011) 901-924.
20. Moreno-Castilla, C., Perez-Cadenas, A.F., Carbon-Based Honeycomb Monoliths for Environmental Gas-Phase Applications, *Materials* 3 (2010) 1203-1227.
21. Knox, J.H., Gilbert, M.T. US Patent 4263268, 1979.
22. Saleh, T.A., Gupta, V.K., Processing Methods, Characteristics and Adsorption Behaviour of Tire Derived Carbons: A Review, *Adv. Coll. Interface Sci.* 211 (2014) 93-101.
23. Yagub, M.T., Sen, T.K., Afroze, S., Ang, H.M., Dye and Its Removal from Aqueous Solution by Adsorption: A Review, *Adv. Coll. Interface Sci.* 209 (2014) 172-184.
24. Liu, F., Xu, Z., Wan, H., Wan, Y., Zheng, S., Zhu, D. Enhanced Adsorption of Humic Acids on Ordered Mesoporous Carbon Compared With Microporous Activated Carbon, *Environ. Toxicol. Chem.* 30 (2011) 793–800.
25. Han, S., Sohn, K., Hyeon, T. Fabrication of New Nanoporous Carbons Through Silica Templates and Their Application to the Adsorption of Bulky Dyes, *Chem. Mater.* 12 (2000) 3337–3341.
26. Sevilla, M., Fuertes, A.B. Fabrication of Porous Carbon Monoliths With a Graphitic Framework, *Carbon* 56 (2013) 155-166.
27. Sakintuna, B., Yürüm, Y. Templated Porous Carbons: A Review Article, *Ind. Eng. Chem. Res.* 44 (2005) 2893-2902.
28. Alvarez, S., Fuertes, A.B. Synthesis of Macro/Mesoporous Silica and Carbon Monoliths By Using a Commercial Polyurethane Foam as Sacrificial Template, *Mater. Lett.* 61 (2007) 2378-2381.
29. Tao, S., Wang, Y., Shi, D., An, Y., Qiu, J., Zhao, Y., Cao, Y., Zhang, X. Facile Synthesis of Highly Graphitized Porous Carbon Monoliths With a Balance on Crystallization and Pore-Structure, *J. Mater. Chem. A* 2 (2014) 12785-12791.

30. He, X., Nesterenko, E.P., Nesterenko, P.N., Brabazon, D., Zhou, L., Glennon, J.D., Luong, J.H.T., Paull, B. Fabrication and Characterization of Nanotemplated Carbon Monolithic Material, *ACS Appl. Mater. Interfaces* 5 (2013) 8572-8580.
31. Duffy, E., He, X., Nesterenko E.P., Dey, A., Krishnamurthy, S., Brabazon, D.; Nesterenko, P.N., Paull, B. Thermally Controlled Growth of Carbon Onions Within Porous Graphitic Carbon-Detonation Nanodiamond Monolithic Composites, *RSC Advances* 5 (2015) 22906-22915.
32. Nesterenko, P.N., Haddad, P.R. Diamond-Related Materials as Potential New Media in Separation Science, *Anal. Bioanal. Chem.* 396 (2010) 205-211.
33. Mochalin, V.M., Shenderova, O., Ho, D., Gogotsi, Y. The Properties and Applications of Nanodiamonds, *Nature Nanotechnology*, 7 (2012) 11-23.
34. Krueger, A. Diamond Nanoparticles: Jewels for Chemistry and Physics, *Adv. Mater.* 20 (2008) 2445-2449.
35. Peristyy, A.A., Fedyanina, O., Paull, B., Nesterenko, P.N. Diamond Based Adsorbents and Their Application in Chromatography, *J. Chromatogr. A* 1357 (2014) 68-86.
36. Wang, D.H., Tan, L.-S., Huang, H., Dai, L., Osawa, E. In-Situ Nanocomposite Synthesis: Arylcarbonylation and Grafting of Primary Diamond Nanoparticles with a Poly(ether-ketone) in Polyphosphoric Acid, *Macromolecules* 42 (2009) 114-124.
37. Shenderova, O., Jones, C., Borjanovic, V., Hens, S., Cunningham, G., Moseenkov, S., Kuznetsov, V., McGuire, G. Detonation Nanodiamond and Onion-Line Carbon: Applications in Composites, *Phys. Stat. Sol. (a)* 205 (2008) 2245-2251.
38. Manandhar, S., Roder, P.B., Hanson, J.L., Lim, M., Smith, B.E., Mann, A., Pauzauskie, P.J. Rapid Sol-Gel Synthesis of Nanodiamond Aerogel, *J. Mater. Res.* 29 (2014) 2905-2911.
39. Ostrovidova, G.U., Makeev, A.V., Biryukov, A.V., Gordeev, S.K. Carbon Nanocomposite Materials As Medicinal Depot, *Mater. Sci. Eng. C* 23 (2003) 377-381.

40. Shenderova, O.A., Zhirnov, V.V., Brenner, D.W. Carbon Nanostructures, *Crit. Rev. Solid State Mater. Sci.* 27 (2002) 227-356.

41. Choma, J., Jedynak, K., Fahrenholz, W., Ludwinowicz, J., Jaroniec, M. Microporosity Development in Phenolic Resin-Based Mesoporous Carbons for Enhancing CO_2 Adsorption at Ambient Conditions, *App. Surf. Sci.* 289 (2014) 592-600.

42. Sajad , M., Kazemzad, M., Hosseinnia, A., Preparation of Activated Carbon Monolith by Application of Phenolic Resins as Carbon Precursors, *Funct. Mater. Lett.* 7 (2014) 1450035.

43. Robertson, C., Mokaya, R., Microporous Activated Carbon Aerogels Via a Simple Subcritical Drying Route for CO_2 Capture and Hydrogen Storage, *Microporous Mesoporous Mat.* 179 (2013) 151-156.

44. Kipling, J.J., Wilson, R.B. Adsorption of Methylene Blue in the Determination of Surface Areas, *J. Appl. Chem.* 10 (1960) 109−113.

45. Los, J.M., Tompkins, C.K. Adsorption of Methylene Blue on A Positively Charged Mercury Surface, *J. Chem. Phys.* 24 (1956) 630.

46. Taha-Tijerina, J.J., Narayanan, T.N., Tiwary, C.S., Lozano, K., Chipara, M., Ajayan, P.M. Nanodiamond-Based Thermal Fluids, *ACS Appl. Mater. Interfaces* 6 (2014) 4778–4785.

47. Branson, B.T., Beauchamp, P.S., Beam, J.C., Lukehart, C.M., Davidson, J.L. Nanodiamond Nanofluids for Enhanced Thermal Conductivity, *ACS Nano* 7 (2013) 3183–3189.

48. Barnard, A.S. Self-Assembly in Nanodiamond Agglutinates, *J. Mater. Chem.* 18 (2008) 4038-4041.

49. Duffy, E., Mitev, D., Kazarian, A.A., Nesterenko, P.N., Paull, B. Separation and Characterisation of Detonation Nanodiamond by Capillary Zone Electrophoresis, *Electrophoresis* 35 (2014) 1864-1872.

50. Kuznetsov, V.L., Chuvilin, A.L., Butenko, Y.V., Mal'kov, I.Y., Titov, V.M. Onion-Like Carbon from Ultra-Disperse Diamond, *Chem. Phys. Lett.* 222 (1994) 343–348.

51. Chen, J., Deng, S.Z., Chen, J., Yu, Z.X., Xu, N.S. Graphitization of Nanodiamond Powder Annealed in Argon Ambient, *App. Phys. Lett.* 74 (1994) 3651-3653.

52. Lowell, S., Shields, J.E., Thomas, M.A., Thommes, M. *Characterization of Porous Solids and Powders: Surface Area, Pore Size and Density,* Kluwer Academic Publishers, London, 2004.

53. Ko, T.-H., Kuo, W.-S., Chang, Y.-H. Microstructural Changes of Phenolic Resin During Pyrolysis, *J. Appl. Polym. Sci.* 81 (2001) 1084-1089.

54. Batsanov, S.S., Lesnikov, E.V., Dan'kin, D.A., Balakhanov, D.M. Water Shells of Diamond Nanoparticles in Colloidal Solutions, *App. Phys. Lett.* 104 (2014) 133105.

55. Fang, X.W., Mao, J.D., Levin, E.M., Schmidt-Rohr, K. Nonaromatic Core-Shell Structure of Nanodiamond from Solid-State NMR Spectroscopy, *J. Am. Chem. Soc.* 131 (2009) 1426-1435.

56. Ko, T.H., Kuo, W.S., Lu, Y.R. The Influence of Post-Cure on Properties of Carbon/Phenolic Resin Cured Composites and Their Final Carbon/Carbon Composites, *Polym. Composite* 21 (2000) 96–103.

57. Mitev, D.M., Townsend, A.T., Paull, B., Nesterenko, P.N. Microwave-Assisted Purification of Detonation Nanodiamond, *Diam. Relat. Mater.* 48 (2014) 37-46.

58. Xu, N.S., Chen, J., Deng, S.Z. Effect of Heat Treatment on the Properties of Nano-Diamond Under Oxygen and Argon Ambient, *Diam. Relat. Mater.* 11 (2002) 249-256.

59. Tuinstra, F.; Koenig, J.L. Raman Spectrum of Graphite, *J. Chem. Phys.* 53 (1970) 1126-1130.

60. Ferrari, A.C., Robertson, J. Interpretation of Raman Spectra of Disordered and Amorphous Carbon, *Phys. Rev. B* 61 (2000) 14095–14107.

61. Yuan, X., Shu-Ping, Z., Wei, X., Hong-You, C., Xiao-Dong, D., Xin-Mei, L., Zi-Feng, Y. Aqueous Dye Adsorption on Ordered Mesoporous Carbons, *J. Colloid Interface Sci.* 310 (2007) 83-89.

62. Wu, F.-C., Tseng, R.-L., Juang, R.-S. Preparation of Highly Microporous Carbons From Fir Wood by KOH Activation for Adsorption of Dyes and Phenols From Water, *Sep. Purif. Technol.* 47 (2005) 10-19.

63. Dabrowski, A. Adsorption - From Theory To Practice, *Adv. Colloid Interface Sci.* 93 (2001) 135-224.

64. Wang, S., Wei J., Lv, S., Guo, Z., Jiang, F. Removal of Organic Dyes in Environmental Water Onto Magnetic-Sulfonic Graphene Nanocomposite, *CLEAN* 41 (2013) 751-764.

65. Desta, M.B. Batch Sorption Experiments: Langmuir and Freundlich Isotherm Studies for the Adsorption of Textile Metal Ions Onto Teff Straw *(Eragrostis Tef)* Agricultural Waste, *J. Thermodyn.* **(**2013) 375830.

66. Poots, V.J.P., McKay, G., Healy, J.J. Removal of Basic Dye From Effluent Using Wood as an Adsorbent, *J. Water Pollut. Con. F.* 50 (1978) 926-035.

67. Hall, K.R., Eagleton, L.C., Acrivos, A., Vermeulen, T. Pore- and Solid-Diffusion Kinetics in Fixed-Bed Adsorption Under Constant-Pattern Conditions, *Ind. Eng. Chem. Fundamen.* 5 (1966) 212-223.

Chapter 6.

Final Conclusions and Future Work

6.1 Final conclusions and future work

This thesis presented a systematic study of the development of a novel carbon monolithic composite material containing detonation nanodiamond (DND), followed by a detailed characterisation of its properties and suitability as an adsorbent. This first involved studying the properties of DND from different sources and purification routes (including silane-functionalised DND) in order to address some of the challenges associated with these variable nanomaterials prior to their incorporation within monolithic composites.

Capillary electrophoresis (CE) was shown to offer some unique capabilities in the characterisation of DND materials, providing valuable information on particle charge, size, stability, onset of aggregation, and showing potential for use in sample fractionation. The effects of purification, storage and functionalisation of DND by silylation were quantified using a direct inductively coupled plasma-mass spectrometry approach. This analysis was coupled with Fourier transform infrared spectroscopy, thermogravimetric analysis and CE among other techniques, for a detailed comparison of efficiency of different functionalisation procedures and provided a valuable insight into the effect everyday handling procedures can have on the impurity levels of DND.

Composite carbon monoliths with nanodiamond (CND) were then prepared by embedding DND in a resorcinol formaldehyde precursor mixture, containing iron as a catalyst for localised graphitisation, and silica gel as a hard template. The influence of pyrolysis temperature and DND content on the graphitisation process and structural characteristics of the final composites were evaluated and compared with a blank carbon monolith. For the first time it has been shown that altering the content of DND allows for facile tuning of graphitic nature, pore sizes and surface areas of carbon monoliths. The first controlled production of carbon onions from DND within such a carbon monolithic composite was also demonstrated. These materials have shown promise for application in adsorption, demonstrating higher capacities for methylene blue and neutral red compared with activated carbon and previously reported values for blank carbon monoliths. Further

evaluation of their adsorptive performance is required beyond the preliminary studies herein, which were limited by time constraints. These monoliths have the flexibility to be used in rod-format, or in the form of a powder or disc shape by cutting with a blade, and grinding with a pestle and mortar, thus offering a variety of potential routes for their incorporation in adsorption applications. They could be clad within a column for liquid chromatography, or within the barrel of a solid phase microextraction syringe for analyte pre-concentration, or used in a larger-scale batch adsorption process for removal of pollutants. CND materials embody an interesting new group of carbon on carbon composite materials that may also find their application in areas such as gas adsorption or storage, catalysis, and electrode materials.

Suggested future work will focus on improving the aggregation and distribution of the DND nano-filler within CND materials, since aggregates can affect the pyrolysis process differently to well dispersed particles. In order to ensure a more well distributed and de-agglomerated nano-filler, routes for incorporation of the stable silylated DND materials within CND will be investigated. Instead of adding an aqueous suspension of DND to the precursor polymerisation mixture, the silica template can easily be modified with DND using silane linkers. A similar principle was applied to the incorporation of fullerenes within a carbon monolithic composite material, where the silica template was first modified with 3-aminopropyltriethoxysilane prior to reaction with C_{60} fullerene [1]. With the grafting of DND to the surface of the silica template, a better distribution of DND within the composite can be expected, and the porous structure will likely be affected as a result of the thermal properties of DND. The silylation of porous and non-porous silica has been widely studied, including trimethylsilylation of mesoporous silicas [2-4], and it has also been demonstrated for hexadimethylsilazane (HDMS) and trimethylchlorosilane (TMCS) by Fierro and co-workers [5], thus providing a straightforward strategy for grafting DND to the silica surface. The resultant CND materials may show improved structural characteristics such as more uniform micro- and mesopore formation and size distributions, as well as improved surface areas, due to the

uniform infiltration of nano-fllller. Further tuning of pore characteristics and nano-carbons within CND can still be achieved simply by altering the temperature of pyrolysis. With the new strategy for DND incorporation and anticipated improvements in structural characteristics, CND should demonstrate superior adsorption performance. Further investigation into adsorption of environmental pollutants including dyes and phenols will be the focus of future work, and the suitability of CND as an adsorbent for CO_2 capture will be explored.

References

1. He, X., Nesterenko, E.P., Nesterenko, P.N., Brabazon, D., Zhou, L., Glennon, J.D., Luong, J.H.T., Paull, B. Fabrication and Characterization of a Nanotemplated Carbon Monolithic Material, *ACS Appl. Mater. Interfaces* 5 (2013) 8572-8580.
2. Koyano, K.A., Tatsumi, T., Tanaka, Y., Nakata, S. Stabilization of Mesoporous Molecular Sieves by Trimethylsilylation, *J. Phys. Chem.* 101 (1997) 9436-9440.
3. Bu, J., Rhee, H.-K., Silylation of Ti-MCM-41 by Trimethylsilyl-imidazole and its Effect on the Olefin Epoxidation with Aqueous H_2O, *Catal. Lett.* 66 (2000) 245-249.
4. Bu, J., Rhee, H.-K. Improvement in Hydrophobicity of Ti-MCM-41 Using a New Silylation Agent MSTFA, *Catal. Lett.* 65 (2000) 141-145.
5. Chapel-Sanchez, M.C., Barrio, L., Campos-Martin, J.M., Fierro, J.L.G. Silylation and Surface Properties of Chemically Grafted Hydrophobic Silica, *J. Colloid Interfac. Sci.* 227 (2004) 146-153.

Appendix A

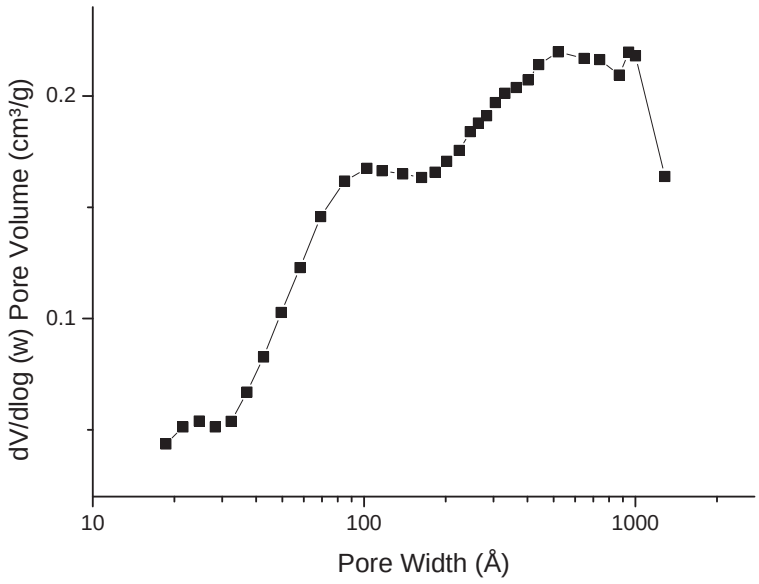

Figure A1. BJH pore size distribution data for blank carbon monolith, pyrolysed to 1250 °C. Data was obtained from the adsorption branch of the isotherm.

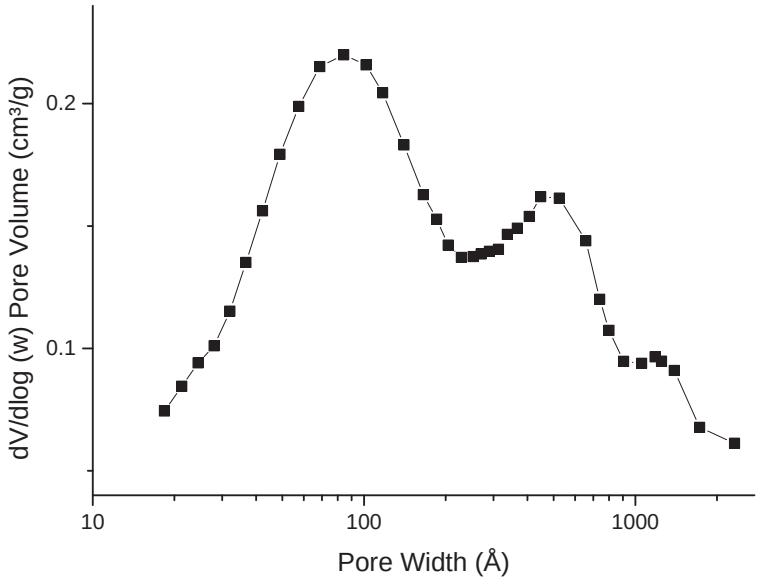

Figure A2. BJH pore size distribution data for carbon monolithic composite with carbon onions, pyrolysed to 1250 °C. Data was obtained from the adsorption branch of the isotherm.

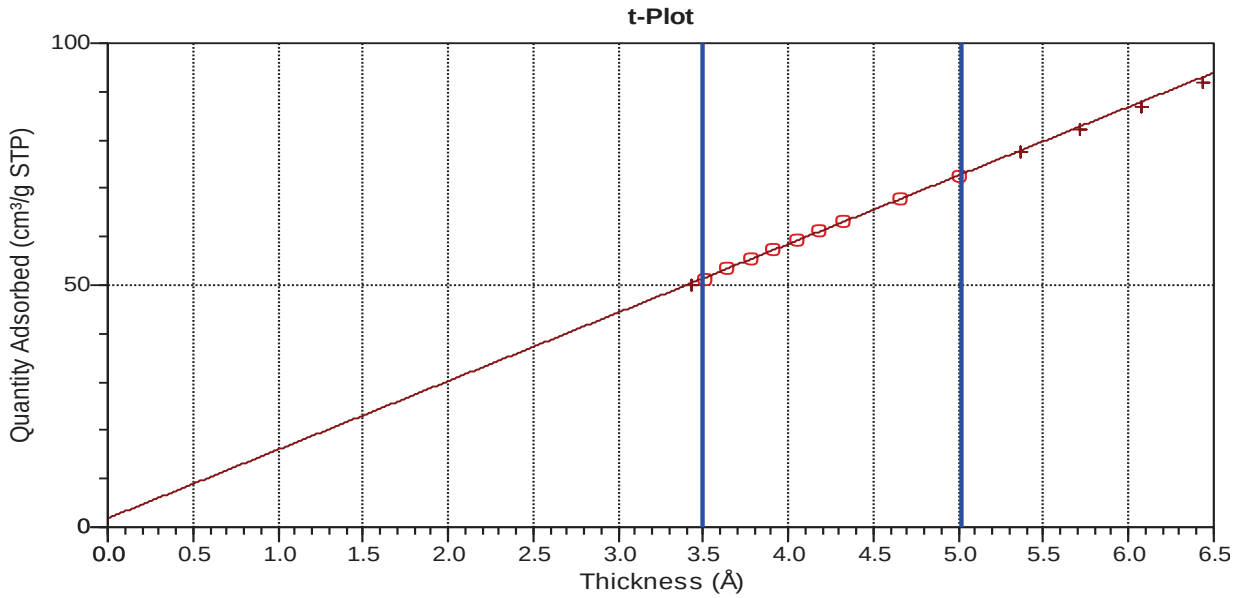

Figure A3. T-plot for carbon monolithic composite with carbon onions, pyrolysed to 1250 °C.

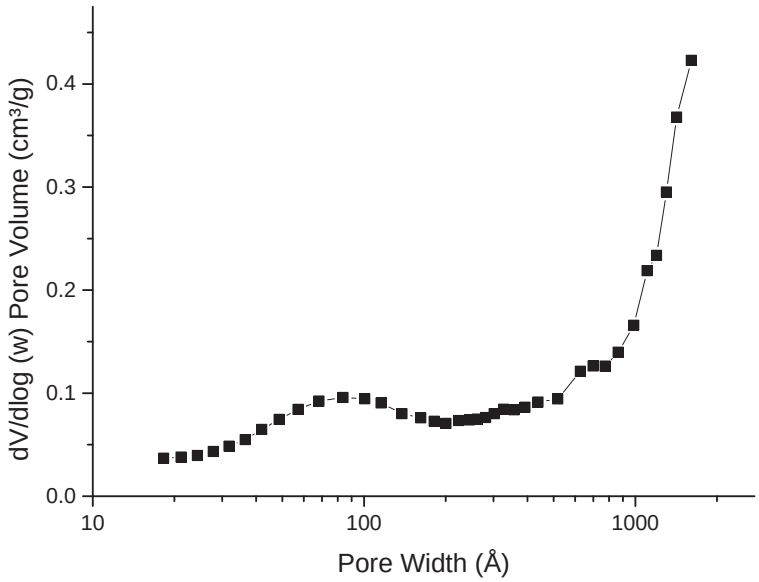

Figure A4. BJH pore size distribution data for carbon monolithic composite CND1 with detonation nanodiamonds, pyrolysed to 900 °C. Data was obtained from the adsorption branch of the isotherm.

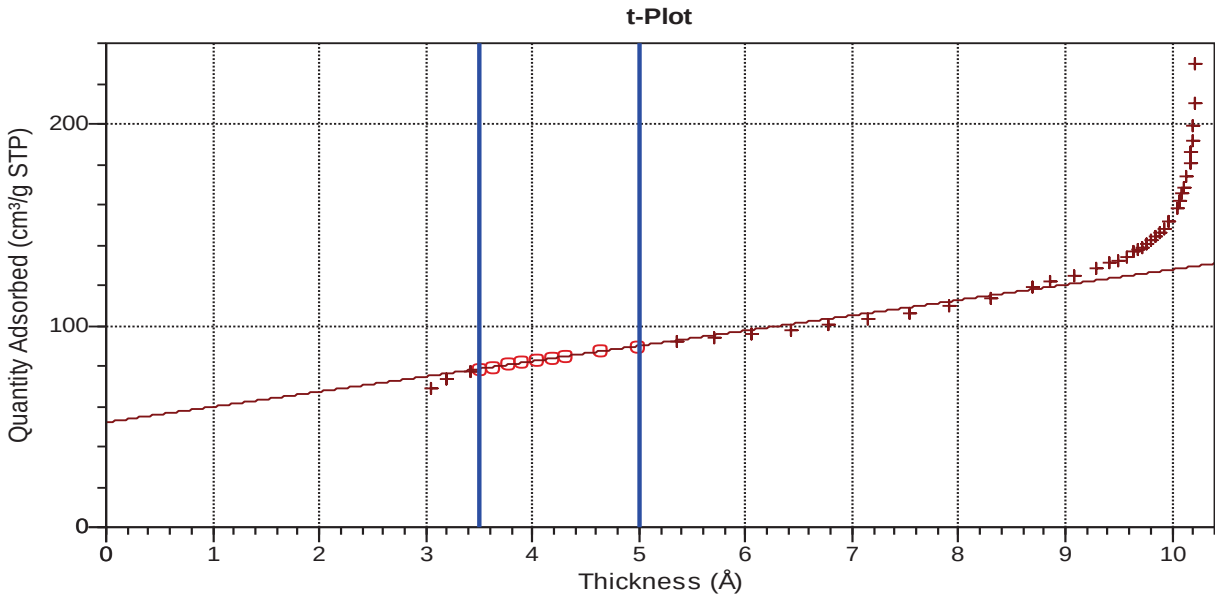

Figure A5. T-plot for carbon monolithic composite CND1 with detonation nanodiamonds, pyrolysed to 900 °C.

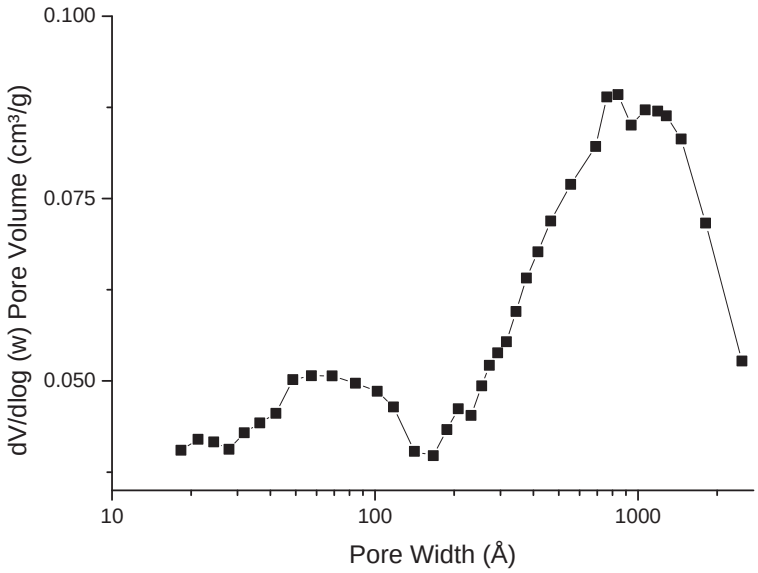

Figure A6. BJH pore size distribution data for carbon monolithic composite CND2 with detonation nanodiamonds, pyrolysed to 900 °C. Data was obtained from the adsorption branch of the isotherm.

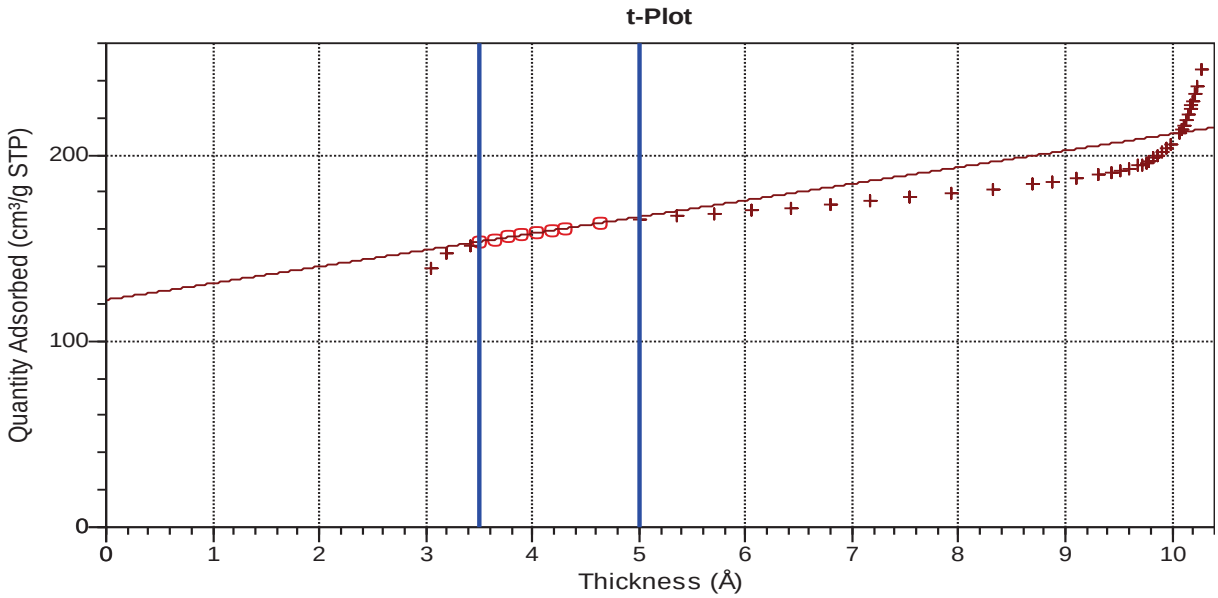

Figure A7. T-plot for carbon monolithic composite CND2 with detonation nanodiamonds, pyrolysed to 900 °C.

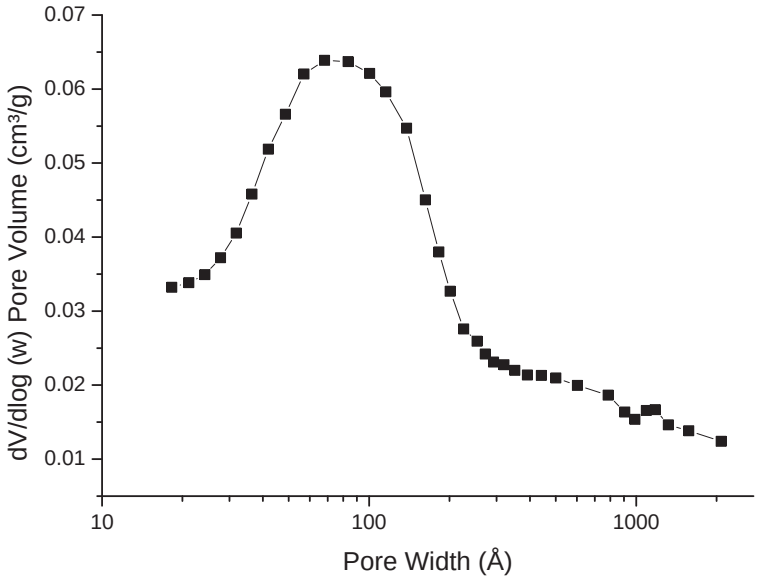

Figure A8. BJH pore size distribution data for carbon monolithic composite CND3 with detonation nanodiamonds, pyrolysed to 900 °C. Data was obtained from the adsorption branch of the isotherm.

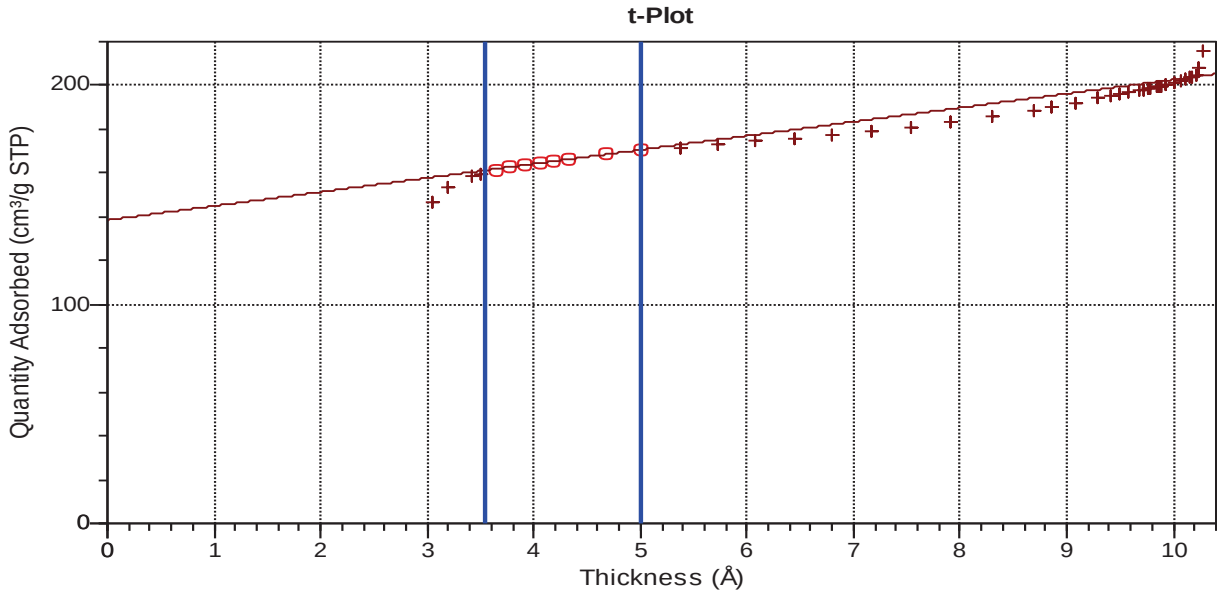

Figure A9. T-plot for carbon monolithic composite CND3 with detonation nanodiamonds, pyrolysed to 900 °C.